Single-Source-Precursor Synthesis of SiC-Based Ceramic Nanocomposites for Energy-Related Applications

A Dissertation Approved by the Department of Materials Science in Fulfillment of the Requirements for the Degree of Dr.rer.nat.

M.Sc. Sarabjeet Kaur
Born on 02.02.1982 in Umaria, M.P., India
July 2016-Darmstadt-D17

TECHNISCHE
UNIVERSITÄT
DARMSTADT

Single-Source-Precursor Synthesis of SiC-Based Ceramic Nanocomposites for Energy-Related Applications

Approved dissertation submitted by M.Sc. Sarabjeet Kaur, born in Umaria, M.P., India

1. Referee: Prof. Dr. Ralf Riedel

2. Co-referee: Prof. Dr. Sanjay Mathur

Fachbereich Material-und Geowissenschaften, Technische Universität Darmstadt

Date of submission: 24 March 2016

Date of oral examination: 14 July 2016

Darmstadt D-17

Acknowledgment:

Foremost, I would like to express my sincere gratitude to my supervisor Prof. Ralf Riedel for the continuous support during my Ph.D. study and related research. His guidance, patience, constant motivation, and encouragement have helped me to make progress in my research career.

Thanks to advisor Dr. Emanuel Ionescu for his supervision and encouragements to develop my research work. It was a great pleasure for me to work with him. He has been actively interested in my work and has always been available to advise me. I really appreciate all his contributions of time, ideas, and suggestion to make my Ph.D. experience productive and stimulating.

I would like to extend my thanks to Prof. Hans-Joachim Kleebe to help me for TEM measurements. I will keep on record my sincere thanks to all the Professors and colleagues in Materialwissenschaft for all their help and support during my stay.

I express my deeply thanks to Prof. Clara Viñas for accepting the request to be as a host for SIPs programme and allow me to be a part of her group, Institut de Ciència de Materials de Barcelona. I am using this opportunity to express my gratitude to everyone who supported me throughout the stay in Barcelona. I am thankful for their aspiring guidance, and friendly advice during the research work. I would like to thanks Dr. Rosario Nuñez for her support and guidance during my stay in Barcelona. I would also like to thanks Justo Cabrera for his kind support and help while working in the laboratory.

I would like to thanks Dipl.-Ing. Claudia Fasel for TG/MS measurements and for a lot of technical help in routine lab work. Thanks to Jean-Christophe Jaud and Jian Yuan for the XRD measurements, Cristina Schitco for BET measurement and lot of discussion related to research, Markus Motzko for XPS measurement, and Stefania Hapis for TEM measurements.

I would like to thanks all the DF members who gave me good and friendly working atmosphere. I could not even think to accomplish my target without DF members.

I would like to thank the Xycarb Ceramic, Deutsche Forschungsgemeinschaft (DFG, Germany), and COST Action SIPs programme for financial help.

Last but not the least, I would specially like to thank my family: my parent and to my brother for supporting me spiritually throughout writing this thesis and my life in general.

Dedicated to My Grand Father

Table of Contents:

List of Figures

List of Table

Abstract

The present work deals with the synthesis, characterization, and fabrication of Si-M-C-based ceramic nanocomposites (M = B and V). These were produced by the thermal transformation of tailor-made single-source-precursors, which were synthesized by the chemical modification of an allyl-hydrido polycarbosilane with suitable precursors (i.e., borane dimethylsulfide, allyl-functionalized carboranes, vanadium acetylacetonate and vanadium oxytriisopropoxide). The typical approach to this synthesis consists of a pyrolytic ceramization of the precursors, which converted into amorphous single-phase SiMC(O)-based materials. They are further subjected to high temperature treatment for phase separation and crystallization processes to furnish SiC-based ceramic nanocomposites.

The preceramic polymer allyl-hydrido polycarbosilane (commercial name SMP-10) and derived SiC-based ceramics were thorougly investigated with respect to cross-linking behavior, polymer-to-ceramic transformation as well as high-temperature phase composition and microstructure. This knowledge served to optimize the processing of the preceramic polymeric precursor to produce dense and crack-free SiC-based monolithic ceramics by pressureless technique. The obtained ceramic monoliths have been shown to exhibits residual porosity of 15-25 vol%, which however can further be reduced by the use of polymer-infiltration and pyrolysis (PIP) to about 0.5 vol%.

Boron-containing single-source-precursors were synthesized upon reactions of SMP-10 with borane dimethylsulfide complex (BMS) or with allyl-functionalized carboranes (AFC). In case of BMS-modified SMP-10 (BMS-SiBC), a detailed structural characterization has been done by means of various spectroscopic techniques. The main aspects addressed in case of BMS-modified SMP-10 (BMS-SiBC) are the fate of boron in the prepared SiBC ceramics, which was not been clarified unambiguously so far, and the role of boron in terms of densification of SiC. X-ray diffraction data, corroborated with X-ray photoelectron spectrocopy, Attenuated total reflectance-Fourier transform infrared spectroscopy, and Raman spectroscopic results indicate that in the SiBC ceramic prepared from the BMS-SiBC, boron preferably gets incorporated within the segregated carbon phase. Moreover, it was shown that the incorporation of boron has a positive effect on the densification behavior of SiC; so monolithic SiC ceramics with residual porosity below 5 vol% could be produced with pressureless processing. The SiBC material prepared from the AFC-modified SMP-10 shows a different phase composition, indicating the presence of

a boron-rich boron carbide phase, which was not detected in BMS-SiBC. The results shows the crucial effect of the molecular architecture and chemism of the single-source-precursors on the phase composition and consequently properties of the resulting ceramic materials.

Vanadium-containing single-source-precursors were obtained upon chemical modification of SMP-10 with vanadyl acetylacetonate or vanadium oxytriisopropoxide. High temperature treatment of the resulting single-source-precursors in argon atmosphere initially led to an amorphous single-phase ceramic (SiVCO) which was then converts into ceramic nanocomposites consisting of a non-stoichiometric vanadium carbide phase (V_8C_7) finely dispersed in a polycrystalline β-SiC matrix. In this context, the first investigation was carried out on biomorphic and the template-assisted processing of single-source-precursor to form porous monolithic samples. In addition, preliminary results of the catalytic activity of SiVC(O) show that the nanocomposites are active for the decomposition of the ammonia. The maximum ammonia conversion efficiency was found to be 35 % at around 650 °C which is higher than that of pure V_8C_7 reported in the literature (13 %).

The results of this study show that the processing of ceramics starting from suitable preceramic polymer is a versatile technique for the production of SiC-based ceramic nanocomposites with tailored phase composition, microstructure, and property profiles. Moreover, the single-source-precursor technique used for the preparation of ceramic nanocomposites allows flexibility with respect to processing. Thus it is possible, starting from preceramic precursors to prepare ceramic powder, crack-free and dense monoliths as well as materials/components with tailored porosity which can be used flexibly for different applications.

Zusammenfassung

Vorliegende Arbeit behandelt die Synthese, Charakterisierung und Verarbeitung Si-M-C-basierter keramischer Nanokomposite (M = B und V). Diese wurden durch thermische Umwandlung von maßgefertigten Single-Source-Precursoren erhalten, welche durch die chemische Modifikation eines Allyl-Hydrido-Polycarbosilans mit geeigneten Precursoren (z.B. Boran-Dimethylsulfidkomplex, Allyl-funktionalisierte Carborane, Vanadylacetylacetonat und Vanadiumisopropoxid) synthetisiert wurden. Der typische Syntheseansatz hierzu besteht aus einer pyrolytischen Keramisierung der Precursoren, die in amorphe, einphasige SiMC(O)-basierte Materialien umgewandelt werden. Diese werden mittels Hochtemperaturauslagerungen Phasenseparations- und Kristallisationsvorgängen unterzogen und somit in SiC-basierten Keramik-Nanokomposite überführt.

Das präkeramische Polymer Allyl-Hydrido-Polycarbosilan (kommerzieller Name SMP-10) und die daraus erhaltene SiC-basierte Keramik wurden ausführlich auf das Vernetzungsverhalten, die Polymer-zur-Keramik-Umwandlung sowie die Hochtemperaturentwicklung der Phasenzusammensetzung und Mikrostruktur hin untersucht. Die hierzu gewonnen Erkenntnisse dienten dazu, die Verarbeitung des präkeramischen Polymers in dichte und rissfreie SiC-basierte monolithische Keramiken zu optimieren, die in einem drucklosen Verfahren erhalten wurden. Die hergestellten keramischen Monolithe zeigen eine Restporosität von 15-25 vol%, welche jedoch durch den Einsatz von Polymerinfiltration und Pyrolyse (PIP) auf ca. 0,5 vol% reduziert werden konnte.

Borhaltige Single-Source-Precursoren wurden durch Reaktionen von SMP-10 mit Boran-Dimethylsulfidkomplex (BMS) oder mit Allyl-funktionalisierten Carboranen (AFC) synthetisiert. Im Fall der aus dem BMS-modifizierten SMP-10 hergestellten SiBC-Keramik (BMS-SIBC) wurde eine eingehende strukturelle Charakterisierung mittels unterschiedlicher spektroskopischer Methoden durchgeführt. Die primären Zielsetzungen hierbei waren die Aufklärung der Phase(n), die das mittels des Boran-Dimethylsulfidkomplexes eingebaute Bor im Material beherbergt, sowie die Rolle des Bors hinsichtlich der Verdichtung von SiC zu erläutern. Die Ergebnisse der Röntgenbeugung, zusammen mit denen der Röntgenphotoelektronenspektroskopie, ATR-FTIR und Ramanspektroskopie deuten darauf hin, dass das Bor bevorzugt in der segregierten Kohlenstoffphase von BMS-SiBC vorhanden ist. Darüber hinaus wurde gezeigt, dass sich

der Einbau von Bor positiv auf das Verdichtungsverhalten des SiC auswirkt; so konnten monolithische SiC-Keramiken mit Restporositätswerte unter 5 vol% drucklos hergestellt werden. Das aus dem AFC-modifiziertem SMP-10 synthetisierte SiBC zeigt eine andere Phasenzusammensetzung, welche die Anwesenheit einer borreichen Borkarbidphase andeutet, die im BMS-SiBC nicht detektiert wurde. Die Ergebnisse zeigen den maßgeblichen Einfluss des molekularen Aufbaus und des Chemismus des Single-Source-Precursors auf die Phasenzusammensetzung und infolgedessen auf die Eigenschaften der daraus resultierenden keramischen Materialien.

Vanadiumhaltige Polycarbosilan-basierte Single-Source-Precursoren wurden durch eine chemische Modifizierung von SMP-10 mit Vanadylacetylacetonat oder Vanadiumpxytriisopropoxid erhalten. Die Hochtemperaturbehandlung der erhaltenen Single-Source-Precursoren unter Argonatmosphäre führte zunächst zu einer amorphen, einphasigen Keramik (SiVCO), welche anschließend mittels Hochtemperaturauslagerung in Keramik-Nanokomposite, bestehend aus einer nicht-stöchiometrischen Vanadiumkarbid-Phase (V_8C_7) fein dispergiert in einer polykristallinen β-SiC-Matrix, überführt wurde. In diesem Zusammenhang wurden erste Untersuchungen zur biomorphen sowie zur Templat-assistietren Verarbeitung des Single-Source-Precursors in Form poröser monolithischer Proben durchgeführt. Darüber hinaus zeigten vorläufige Ergebnisse über die katalytische Aktivität einiger der hergestellten Proben, dass V_8C_7/SiC-Nanokomposite aktiv hinsichtlich der katalytischen Zersetzung von Ammoniak sind. Die maximale Effizienz der Ammoniakzersetzung betrug 35 % bei rund 650 °C, was höher als die mit 13 % in der Literatur angegebene Effizienz von reinem V_8C_7 ist.

Die Ergebnisse der vorliegenden Arbeit zeigen, dass die Verarbeitung von Keramiken ausgehend von geeigneten präkeramischen Polymeren eine vielseitige Technik zur Herstellung von SiC-basierten keramischen Nanokompositen mit maßgeschneiderter Phasenzusammensetzung, Mikrostruktur und Eigenschaftsprofilen ist. Darüber hinaus ermöglicht diese Single-Source-Precursor-Technik eine einzigartige Flexibilität hinsichtlich deren Verarbeitung. Somit ist es möglich ausgehend von präkeramischen Precursoren keramische Pulver, rissfreie und dichte Monolithe als auch Materialien/Bauteile mit maßgeschneiderter Porosität zu gewährleisten, die flexibel für unterschiedliche Anwendungen einsetzbar sind.

Motivation and Aim of the Thesis

Silicon Carbide (SiC) is a promising candidate as structural and functional ceramic for various industrial applications such as electronic and optic devices, catalyst support, nuclear fuel cladding, and so forth. This relies on its excellent thermal stability, high mechanical strength and hardness, chemical inertness, wide band gap, and unique optical properties [1-5].

SiC is an attractive material for high temperature applications, however, it is susceptible to fast fracture upon loading due to its brittle nature. Moreover due to the highly covalent nature of the Si-C bond, it exhibits very low self-diffusion, which restricts its densification even at high temperatures. Within this context, numerous studies have been performed with respect to the development of SiC-based nanocomposites by incorporation of additional favorable phase(s) in order to improve their properties. For instance, incorporation of metal particles helps to solve the problem of brittleness whereas the addition of metal borides such as ZrB_2, TaB_2, or TiB_2, promote the densification of SiC powder as well as improve hardness and other mechanical properties of the material [6].

Additionally, the incorporation of functionally active phases into the SiC matrix, enables the facile generation of SiC-based nanocomposites for functional applications [7-9]. For example, Ni/SiC catalyst nanocomposites were used for the direct oxidation of H_2S into S. SiC is a suitable catalyst support in heterogeneous catalysis owing to its high thermal conductivity, high oxidation resistance, high mechanical strength, low specific weight, and chemical inertness [10].

The synthesis of SiC-based nanocomposites suffers from the inhomogeneous distribution of the additional desired phases within the SiC matrix [11]. Additionally, the difficulty also lies in their processing, i.e., their fabrication with desired shapes or tunable (micro)porosity, which in turn limits its application spectrum. The powder technology used to fabricate SiC-based monoliths requires high sintering temperatures and hot pressing techniques, which increases the fabrication costs.

Polymer-derived ceramics (PDCs) have been widely investigated in the last decades and were shown to possess intriguing properties which make them excellent candidates as structural and (multi)functional materials. They can be synthesized by controlled crosslinking and pyrolysis of suitable preceramic polymeric precursors. The molecular structure and the type of preceramic polymeric precursors influence the composition, the

amount of phases, phase distribution, and microstructure of the final ceramic. In this way, the chemical and physical properties of PDCs can be tailored by the proper design of the starting molecular precursor [12].

Furthermore, suitable chemical modification of the preceramic precursor leads to the formation of single-source-precursors (SSPs) for multi-element ceramics. The high temperature treatment of SSPs first leads to an amorphous single-phase materials, which subsequently undergo phase separation and crystallization process to furnish homogeneously distributed bi-or multi-phase ceramic nanocomposites. Polymer-processing of ceramics has also been shown to be a highly promising alternative towards processing of dense ceramic parts [13-19]; also ceramic films, fibers as well as miniaturized, complex-shaped parts. This was also shown to be applicable for processing of SiC-based materials [20-25].

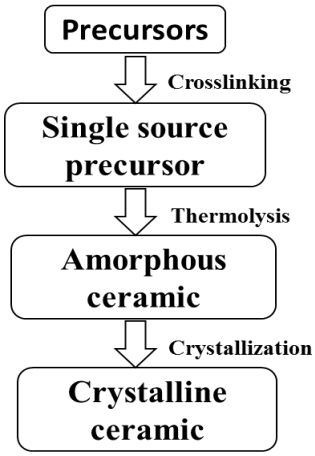

Figure 1-1. Scheme showing the polymer processing route of ceramics.

The principle objective of this work was to demonstrate the feasibility of the SSPs route for the preparation of metal modified SiC-based nanocomposites (metal = B and V). In addition to the synthesis of the nanocomposites, two case studies has been done. It involved development and optimization of the processing technique to produce dense and porous SiC-based monoliths as per the targeted application.

Allyl-hydrido polycarbosilane (SMP-10) is considered as a very prominent polymeric preceramic precursor for the production of near stoichiometric SiC [26]. The allyl- and hydrido-substituents at silicon in the SMP-10 help to adjust its chemistry and network architecture. This work begins with the feasibility study of polymer-processing route using SMP-10 as preceramic precursor for preparing dense, crack-free, and near stoichiometric SiC monoliths. Thus, the overall process for the fabrication of dense SiC-based ceramic

parts involved four major steps: (i) Curing/pre cross-linking of the liquid preceramic polymeric precursor (SMP-10) at moderate temperatures to obtain a polycarbosilane-based powder; (ii) Shaping with warm-pressing techniques; (iii) Ceramization process (pyrolysis) of the shaped green-bodies, which are converted into SiC-based monoliths by means of heat treatment at temperatures ranging from 1100 to 1700 °C and (iv) Polymer-infiltration and pyrolysis (PIP). The prepared green bodies and the ceramic monoliths were investigated with respect to their porosity, shrinkage, phase and chemical composition, as well as concerning their evolution at high temperatures.

The work continues with the synthesis of metal modified SiC-based nanocomposites (metal = B and V). The addition of boron has been done to promote the densification of SiC. For this, chemical modification of SMP-10 has been performed with a boron precursor to produce SSPs (polyborocarbosilanes). For this, two different boron precursors have been used: 1) Borane dimethyl sulfide (BMS) and 2) allyl-functionalized carboranes (AFC). The main question addressed in case of BMS-modified samples, is the fate of boron in the SiBC ceramics, which has not been clarified unambiguously so far in the literature. Thus, spectroscopic and diffraction studies were performed in order to understand how and where boron is present in the SiBC ceramic prepared from polyborocarbosilanes and how their phase composition evolves at high temperatures (1100 to 1900 °C). Moreover, effect of the molecular architecture of the starting boron precursor (BMS; elemental boron attached to SMP-10, AFC; "pre-organized" molecular $B_{10}C_2$ clusters attached to SMP-10) onto the microstructure and phase composition of the SiBC-nanocomposites has also been investigated.

In addition, the processing of the selected and promising polyborocarbosilanes has been carried out. The thermoplastic processing of BMS-modified SMP-10 (BMS-SiBC) and its pressureless conversion into boron-containing SiC monoliths with minimum residual porosity is discussed. Comparable studies of the results obtained from SMP-10 with those achieved with the BMS-SiBC are considered. Thus, the overall process for the fabrication of dense SiBC-based ceramic parts involved three major steps: (i) Synthesis of the single-source-precursor from SMP-10 and BMS; (ii) Shaping using warm-pressing and (iii) Ceramization process (pyrolysis) of the shaped green-bodies upon heat treatment at temperatures ranging from 1100 to 1900 °C. The prepared green bodies and the ceramic monoliths were investigated with respect to their porosity, shrinkage, phase and chemical composition, as well as concerning their evolution at high temperatures.

Pure vanadium carbide (V_8C_7) was shown to be an active catalyst for the decomposition of ammonia [27] and SiC as a catalyst support. The feasibility study of the SSPs route for the preparation of V_8C_7/SiC ceramic nanocomposites has been addressed. Detailed studies have been performed related to the thermal conversion of the obtained single-source-precursor with respect to phase composition and microstructure. Vanadium modified SSPs have been synthesized by using two different vanadium precursors (vanadium acetyl acetonate and vanadium oxytriisopropoxide). The prepared precursors and ceramic nanocomposites obtained after thermal treatment were investigated with respect to their chemical and phase composition as well as microstructure. The preliminary investigation of the catalytical activity of V_8C_7/SiC(O) nanocomposite for the decomposition of ammonia was also performed and is briefly introduced in the present study.

Further, a feasibility study for the fabrication of porous SiC-based ceramic nanocomposites via polymer-processing route using bio-and sacrificial-templates is introduced. The steps involved in the fabrication of porous monoliths includes (i) Shaping of SSPs using a bio-template, prepared by the infiltration of single-source-precursor into the templates (wood and paper) whereas the sacrifial template has been processed by warm-pressing of cured SSPs (ii) Ceramization process (pyrolysis) of the shaped green-bodies, which are converted into SiC-based monoliths by heat treatment at temperatures ranging from 1100 to 1700 ^{o}C (iii) Preliminary investigation of the catalytic activity for the selected samples.

1. Introduction

1. Introduction

1.1. Silicon carbide-based engineering ceramics

Silicon Carbide (SiC) is one of the most widely used materials in industrial applications such as aerospace, electronics, nuclear, industrial furnaces, and production of wear-resistant mechanical parts among others [28]. This is primarily due to its excellent thermal stability, high mechanical strength and hardness, chemical inertness, wide band gap, and unique optical properties [1-5]. Important properties of SiC are listed in Table 1-1.

SiC typically exhibits three types of crystal structures, namely: cubic, hexagonal and rhombohedral. The cubic crystal structure known as β-SiC, whereas all non-cubic structures are collectively known as α-SiC. The cubic crystal structure refers to a single polytype called 3C-SiC. However, the hexagonal crystal structure is associated with a wider range of polytypes such as 2H-SiC, 4H-SiC, and 6H-SiC. The least common polytype is rhombohedral, which refers to polytypes such as 15R-SiC, 21R-SiC, and 33R-SiC. The cubic crystal of SiC transforms into one of the α-polytypes at higher temperatures [29].

Table 1-1. Properties of Silicon Carbide [30-33]

SiC Properties	Values
Density	3.21 g/cm^3 (all polytypes)
Electronic mobility	~ 900 cm^2/V.s (all polytypes)
Refractive index	2.55 (all polytypes)
Oxidation resistance	upto 1600 ^{o}C
Dissociation temperature	2850 ^{o}C
Hardness	21-25 GPa (solid state sintered) 19-22 GPa (Liquid state sintered)
Fracture toughness	3-4 MPa m$^{1/2}$ (solid state sintered) 7-9 MPa m$^{1/2}$ (liquid phase sintered)
Thermal conductivity	3.6 W cm^{-1}K^{-1} (β-SiC) 4.9 W cm^{-1}K^{-1} (α-SiC)
Thermal expansion	4.5 X 10^{-6}/ ^{o}C - 5.9 X 10^{-6}/ ^{o}C at 20-2000 ^{o}C

1.1.1. Synthesis approaches of SiC powder

Edward Goodrich Acheson accidentally developed a new crystal during his research work, focused on the synthesis of diamond-like crystal from carbon and alundum, coined as carborundum, which later has been known by the name of silicon carbide. Thereafter, the process has been known by his name as the Acheson process. This is a well established method to synthesize SiC, via the carbothermal reduction of silica (SiO_2) sand in the presence of petroleum coke (C) at very high temperatures (more than 2500 °C). The process consists of a high temperature solid-state reaction between pure SiO_2 sand and C which leads to the formation of SiC. Conventionally, such high temperatures are reached using an electrical resistance furnace. The chemical reaction for the manufacture of SiC is [34]:

$$SiO_2(s) + 3C(s) \rightleftharpoons SiC(s) + 2CO_2(g)$$

Initially, it was assumed that the reaction of SiO_2 and carbon occurs in a condensed phase. Even if one assumes this fact, such a direct reaction can only occur efficiently above the fusion point of SiO_2 (1750 °C). Moreover, extensive diffusion must occur in order to increase the proximity of silicon atoms with respect to the carbon atom. This is not reasonable explanation as the large size particle used in commercial SiC production phase. Later on, more reasonable formation pathway had been suggested which incorporates the reaction of SiO_2 with carbon to obtain SiC. The path consists of four subreactions, where each reaction involves the mass transfer in the gas phase [34].

$$SiO_2(s) + C(s) \longrightarrow SiO(g) + CO(g)$$

$$SiO_2(s) + CO(g) \longrightarrow SiO(g) + CO(g)$$

$$C(s) + CO_2(g) \longrightarrow 2CO(g)$$

$$SiO(g) + 2C(s) \longrightarrow SiC(s) + CO(g)$$

The main drawbacks of the Acheson approach are the use of high temperature and long reaction time which leads to a large thermal and economical footprint of the process. Furthermore, the SiC powders derived from this method display large particle size and require an extended milling process for further utilization. Recently, microwave heating has replaced the use of an electrical resistance furnace which offers many advantages such as rapid, selective, and volumetric heating. This, in turn, increases the reaction rates

and dramatically reduces reaction times [35-38] but the problem related to the controlled particle size still exist.

An alternative to the Acheson process is the self-propagating high-temperature synthesis (SHS) method or combustion synthesis (CS) for producing inorganic compounds by exothermic reactions. The CS method has several advantages over traditional powder metallurgical technologies. These advantages include: (i) Short synthesis time; (ii) Energy saving, since the internal system chemical energy is primarily used for material production; (iii) Ability to produce high purity products, (extremely high-temperature conditions (up to 3726 °C), which take place in the combustion wave, burn off most of the impurities) and (iv) Possibilities for nanomaterials production.

However major disadvantage with this method is that it includes the reaction of elemental silicon and carbon with an insufficient exothermic reaction [39].

$$Si + C \longrightarrow SiC + 73\ kJ/mol$$

Therefore, the self-propagating high-temperature synthesis of SiC needs to be “activated”. It can be done by various ways, typically via preliminary heating of the initial mixture, by addition of chemical activators, by long term mixing of the initial components (more than 6h), or through SHS synthesis in Si-C-air/nitrogen systems [39-42].

Properties of many conventional materials get enhanced when the particle size of the resultant material is reduced to the nanoscale. This is typically because nanoparticles exhibit a greater specific surface area as compared to its bulk counterparts which in turn increases the availability of the surface of the particles for the participation in its respective application/reaction. Nanosized SiC particles can be obtained by several advanced techniques for example rice husk conversion, chemical vapor deposition (CVD), sol-gel processes, and laser gas phase pyrolysis or laser evaporation processes [43-47]. Bulk SiC as well as one-dimensional (1-D) nanostructured SiC such as nanorods, nanotubes, nanobelts, and nanowires have been extensively investigated during the past decade [48-51].

Rice husk (RH) is a low-cost and abundant agricultural byproduct in rice-producing countries. There is an increasing demand for eco-friendly disposal and utilization of RH which contains high amounts of SiO_2 and exhibits high activity and intimate contact with C, making it a good candidate for carbothermal synthesis of SiC [52].

Fine amorphous SiC powders have been prepared via the chemical vapour deposition from silane in the temperature range 900–1250 °C [45, 53]. A new method for preparation of high-specific-surface (60-400 m^2/g) SiC has been described which consists of the attack of high-specific-surface activated carbon by SiO vapor, generated by the high-temperature reaction of Si and SiO_2 [1].

The sol-gel method is a highly explored chemical approach for nanomaterials synthesis at relatively low temperatures. The basic advantages of using the sol-gel synthesis approach are the lower temperatures, the production of high purity products with extremely uniform and disperse microstructures, not achievable using conventional processing techniques. The sol-gel method involves the preparation of a colloidal sol which subsequently converts into a gel upon hydrolysis and polycondensation reactions [54]. The process starts with the formation of solution by mixing of an appropriate alkoxide as precursor, using water and a mutual solvent. Hydrolysis leads to the formation of silanol groups (Si-OH), subsequently condensed to produce siloxane bonds (Si-O-Si). The resultant silica gel formed by this process leads to a rigid, interconnected three dimensional network consisting of submicrometer pores and polymeric chains [55]. The obtained silica gel is used for carbothermal reduction in order to form SiC.

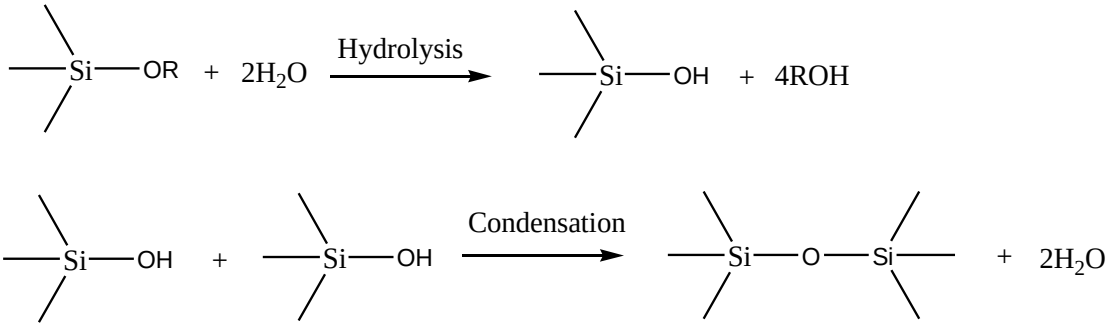

Pure silicon carbide can also be prepared by the thermal decomposition of a preceramic polymer (e.g., polycarbosilane), in an inert atmosphere at relatively low temperatures. This preceramic polymeric route to SiC manufacturing has been extensively investigated during the last 40 years, since the pioneering work of Yajima in 1975 (discussed in details later serves as a basis of the present study) [56].

1.1.2. Synthesis of SiC powder from preceramic polymeric route

1.1.2.1. General overview: Polymer-derived ceramics

To meet the different challenges in the new millennium, development of materials with unique properties for broad application spectrum is of crucial importance. Advanced ceramic materials possessing a combination of characteristics, such as thermal stability, resistance to corrosion, erosion, oxidation, and wear etc., are being developed from a range of materials. They are broadly categorized as oxide or non-oxide ceramics. This class of materials are also termed as engineered, fine, or technical ceramics, and have found application in the past 3 to 4 decades to improve yields, reproducibility, sustainability and efficiencies of many industrial processes [57, 58].

In the last four decades, Polymer-derived ceramics (PDCs), have been intensively studied. PDCs can be synthesized by the solid-state thermolysis of a suitable preceramic polymeric precursor. It involves the conversion of the polymer to ceramics with tailored structures, chemical composition and properties. The composition, microstructure and phase distribution of the final ceramic can be influenced to a great extent by the molecular structure and chemistry of preceramic polymer [59].

Following requirements should be fulfilled by the preceramic polymer, in order to be used as a precursor for ceramics: 1) The polymer should possess a sufficiently high molecular weight in order to avoid volatilization of low molecular components, 2) It should have appropriate rheological properties and solubility for the shaping process and 3) Should have reactive functional groups for the curing and cross-linking step [60].

PDCs have shown to possess outstanding stability at extremely high temperatures (up to 2000 ^{o}C) with respect to decomposition, crystallization, phase separation, and creep. Also additive-free ceramics can be produced with excellent oxidation and chemical resistance up to very high temperature [61, 62]. These outstanding and unique properties of the PDCs are mainly attributed to their unique structure: amorphous at large scale (determined by XRD) but heterogeneous at the nanometer scale. Their extraordinary thermal stability is governed largely by kinetic rather than thermodynamic reasons [63].

The conventional method to prepare ceramics involves powder based technologies which are hard to be processed further, especially in form of fibers and coatings. The use of preceramic polymer was shown to be highly promising alternative towards processing of

dense ceramic parts [13, 15-19], also ceramic films, fibers as well as miniaturized and complex-shaped parts [20-25]. The polymeric precursors can be processed into different forms by using simple polymeric processing techniques such as polymer-infiltration and pyrolysis (PIP), injection molding, resin transfer molding, dip coatings etc [64].

Processing parameters such as the precursor rheology, reactivity, crosslinking degree, presence and types of filler, pyrolysis environment (inert or reactive) as well as pyrolysis parameters (heating rate/temperature and dwelling time) strongly affect the yield, microstructure, chemical composition and functional-structural properties of the final ceramic [65] .

The overall process for fabrication of PDCs involves three major steps: (i) Synthesis of preceramic polymers starting from suitable monomers; (ii) Polymer crosslinking at moderated temperatures (100 to 400 °C; this step can be useful for the processing of preceramic polymer); and (iii) ceramization process (pyrolysis) of the crosslinked and shaped green bodies, which are converted into inorganic materials by heat treatment (1100 to 1500 °C).

The unique properties of the PDCs, such as excellent creep resistance (zero steady-state creep up to high temperatures) and environmental robustness, make them promising materials for applications in harsh environments They are suitable for applications as high temperature resistance materials (automotive, aerospace etc), hard and functional materials [64, 65].

The advantages of the production of ceramic using PDCs route than the traditional powder technologies can be summarized as:1) Production of additive free ceramics, 2) Possibility to modify the preceramic polymer by chemical reactions, in order to enhance the structural and functional properties of the final ceramic, 3) Easy shaping of the green body into different shapes with tunable porosity, and 4) Relatively low synthesis temperature used.

Silicon-based polymer-derived ceramics (SiC, SiCO, SiCN) are well-studied among all PDCs. A simplified structure of silicon containing preceramic polymers is shown in the Figure 1-1. Here X represents the backbone of the polymer whereas R and R´ represent the functional groups. The chemical and thermal stability as well as the solubility of the polymer depends on the attached functional group. General classes of silicon-based polymers, those are used as precursors for ceramics, are thus polycarbosilanes,

polysiloxanes, polysilazanes, and polysilylcarbodiimides [65]. Controlled thermal decomposition of silicon-based polymers provides nanosized silicon-based ceramics.

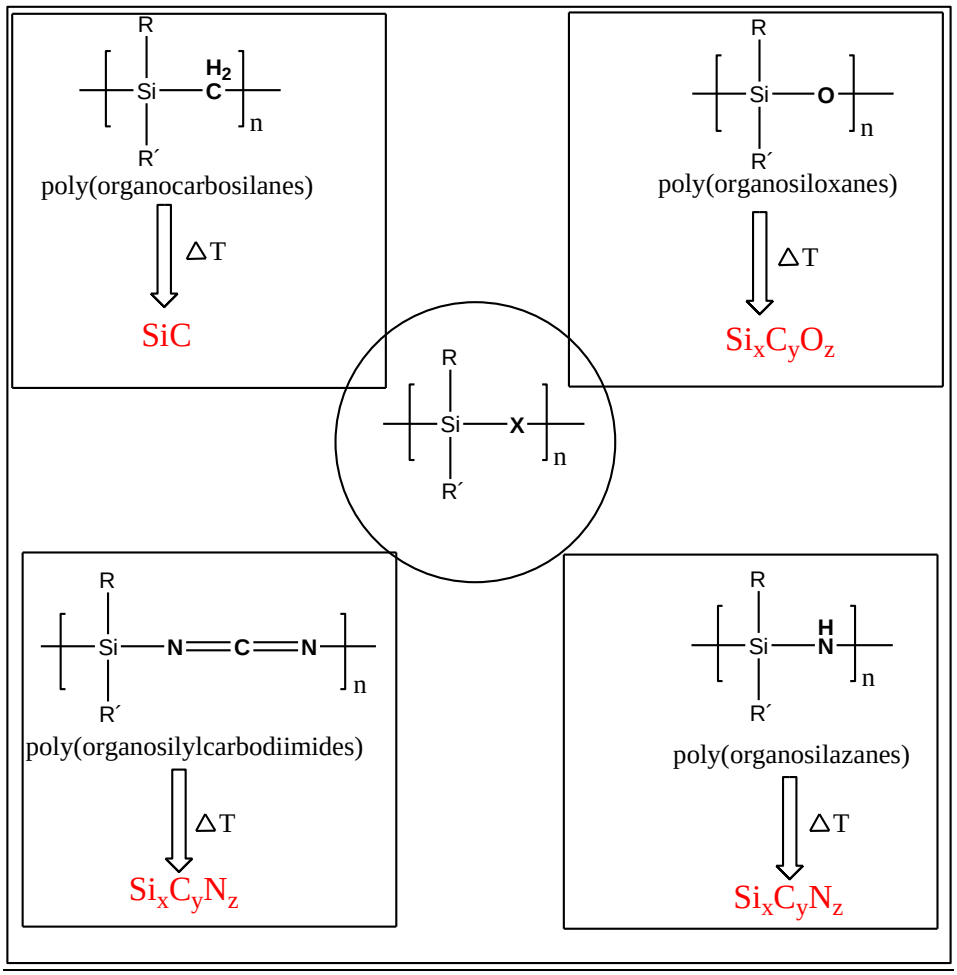

Figure 1-1. A simplified structure of the silicon-containing preceramic polymers and their derived ceramics.

Polymer-derived silicon-based ceramics exhibit enhanced thermo-mechanical properties with respect to creep and oxidation, crystallization, or phase separation (T >>1000 °C). Excellent creep resistance up to 1550 °C and high thermal stability in terms of decomposition to 2200 °C has been shown by polymer derived boron containing SiCN. PDCs resist crystallization at high temperatures (SiC (Tc~1000 °C), Si_3N_4 (Tc~1200 °C) and as well as SiCN (Tc~1400 °C)). In addition to this advanced properties, they can be synthesized at considerable lower temperatures (1100-1300 °C) than compared to those used to prepare conventional ceramics (i.e., 1700-2000 °C) [65].

Commercially available preceramic polymers and their applications [66, 67]

Polymer	Derived Ceramics	Company	Applications
Polysilazane	SiC or Si_3N_4-containing ceramics	KiON Defense Technologies, Inc	Ceramic Matrix Composites (CMCs), Metal Matrix Composites (MMCs), Ceramic MEMS, Ceramic Joining, SiC/ Si_3N_4 coatings for C/C composites and SiC/ Si_3N_4 ceramic nanocomposites.
Polycarbosilane	SiC	StarFire System	CMCs, high-temperature coatings, and joined SiC materials
Polysiloxane	SiOC	StarFire System	Oxidation protective coatings, CMCs

Commercially available polymer derived ceramics and its applications [65, 68]

Company	Application
Starfire Systems Inc	Brake rotors fitted on a motorcycle
Bosch GmBH Germany	Glow plugs (available for short period of time)
Nippon Carbon Co., Ltd.	Fibers

1.1.2.2. Polycarbosilane, as a precursor for SiC

Polymer-derived nonoxide ceramics were firstly reported in 1956 by Fritz and Raabe in Germany. They demonstrated that small organic precursors such as tetramethylsilane and tetraethylsilane can yield SiC ceramics after thermal decomposition in an inert atmosphere. Few years later, Yajima and co-workers presented the possibility to produce SiC fibers from polycarbosilanes. Figure 1-2 shows the Yajima's process for the synthesis of SiC-based ceramic from the thermolysis of a polycarbosilane. Earlier reports on nonoxidic PDCs by Ainger and Herbert were published in 1960, followed by Chantrell and Popper in 1965. In the early 1970's, the first practical transformation of Si-containing polymers (polysilane, polycarbosilane, polysilazane, polysiloxane) to ceramic materials had been done by Verbeek, Winter and Mansmann. Now almost half a century later, research on PDCs still is in the upswing [64, 65].

Polycarbosilanes (PCS) is the promising preceramic polymeric precursor for the synthesis of SiC. PCS is the general term for organosilicon polymers containing a -Si-C- backbone with a general formula of $(\text{-RSiH-CH}_2\text{-})_n$ where R is alkyl group. The PCS has some crosslinking points and ring structures are composed of $\text{Si-CH}_2\text{-Si}$ bonds. In these bonds the crosslinking reaction proceeds in the early stages of the pyrolysis [69, 70]. It is the most typical polymeric precursor for SiC-based ceramics and has been widely used since the pioneering work done by Yajima et al. on SiC fibers [56, 71-73]. It may be linear, cyclic or polycylic in nature. It may be a good candidates for the preparation of SiC films, fibers, and monoliths [20, 74-76].

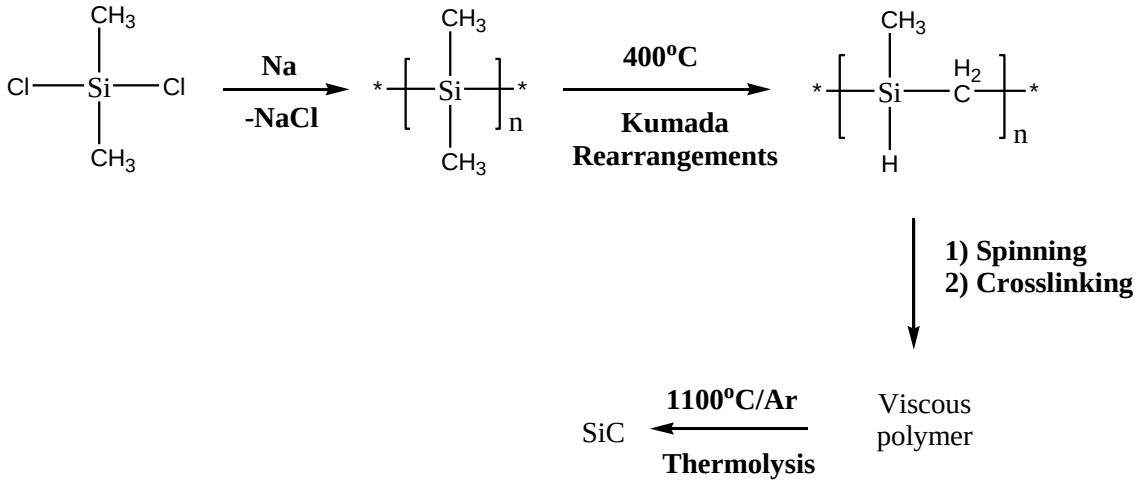

Figure 1-2. Yajima's process for the synthesis of SiC-based ceramic fibers.

The crosslinking of the preceramic polymer, prior to the pyrolysis, is required to increase the ceramic yield. Initially, crosslinking of PCS occurs in air, which in turn, inserts the oxygen and affects the properties of the SiC. Many methods have been used, in order to reduce the oxygen content in the final ceramic e.g., electron beam irradiation and chemical vapor curing with halogenated and unsaturated hydrocarbons. Thermal treatment at 400 °C in inert environment replaces the crosslinking in air and finally helps to avoid the incorporation of the oxygen into the ceramic. The use of crosslinking agents like divinyl benzene, *p*-diethynylbenzene have also been investigated [77].

Whitmarsh et al. first reported the synthesis of hydrido polycarbosilane (HPCS) by Grignard coupling of (chloromethyl)trichlorosilane, followed by reduction with lithium aluminium hydride (Figure 1-3) [78]. The chemistry of the PCS can be tailored by the type of the substituents attached at the silicon atom. For example, replacement of alkyl-group by allyl-group enhances the reactivity and crosslinking degree of PCS. There are at least two possible pathways capable of facilitating the attachment of allyl-pendant groups onto the intermediate polymer end-branches. One approach involves a mechanism of free radical substitution directly utilizing propene to incorporate the allyl-groups. The other possible scenario for attaching allyl-groups to polymer end-branches within the reaction mixture calls for utilizing the allyl-Grignard reagent [79].

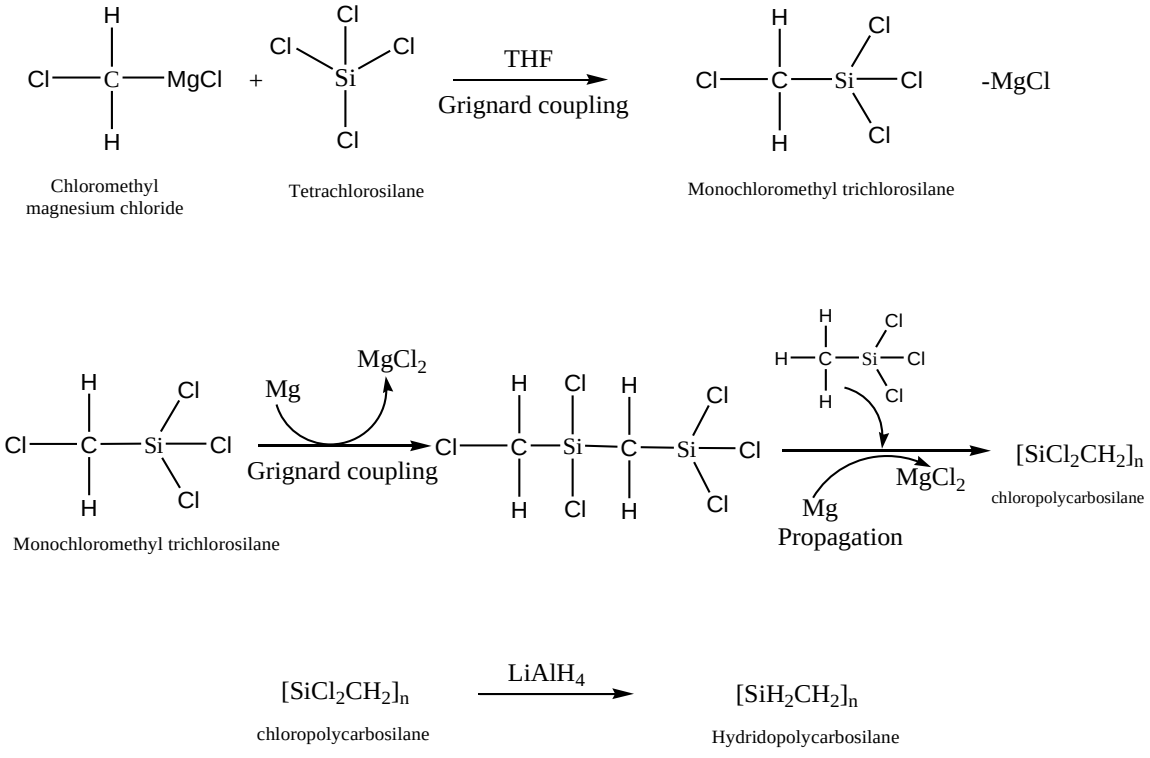

Figure 1-3. Reaction mechanism for the formation of HPCS.

Allyl-hydrido polycarbosilane (AHPCS) is a liquid polymer precursor that has a nominal structure of $[Si(CH_2CH{=}CH_2)_2CH_2]_{0.1}[SiH_2CH_2]_{0.9}$. AHPCS is commercially available (Starfire Systems Co. Malta, New York, USA) and commonly known by the name SMP-10. It is a clear, amber-colored, viscous liquid and requires no solvents for processing. The material has been used as a matrix source in the fabrication of SiC-based ceramic matrix composites (CMCs), to produce SiC coatings, and to join monolithic and composite ceramic parts. According to the supplier, SMP-10 can be green cured at low temperature 180-400 °C, depending on the degree of hardness required. On further heating at 850-1200 °C, amorphous (glassy) SiC forms with 72-78% ceramic yield which on further heating at 1250-1700 °C converts into nano-crystalline β-SiC. The ceramics formed are stable up to 1800 °C in air and up to 2200 °C in inert gases, making them ideal for high temperature applications [66].

Detailed study on cross-linking mechanism of polycarbosilane reveals that the mechanism involves the dehydrocoupling and hydrosilylation reactions. The liquid SMP-10 can be thermally cured at moderate temperatures ($T \leq 200$ °C) via a hydrosilylation reaction (a reaction between Si-H and vinyl groups) and provides cured polycarbosilane-based powder. Further cross-linking of the polymer occurs by means of dehydrocoupling reactions and involves the 1,1-elimination of molecular hydrogen from SiH_n groups at higher temperatures ($T \leq 300$ °C) [77].

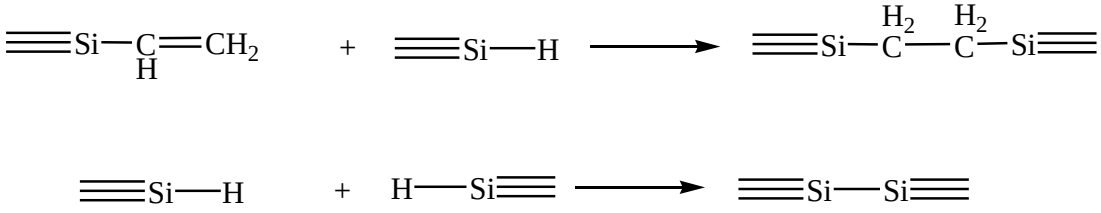

Figure 1-4. Hydrosilylation (a) and dehydrocoupling (b) reactions occuring upon thermal cross-linking of SMP-10.

The selection of this particular polymer has been favoured due to the fact that it is the only commercially available one-component liquid precursor to provide near stoichiometric upon annealing at high temperatures ($T>>1500$ °C), high purity with high ceramic yield SiC. And this polymer exhibits relatively low shrinkage as compared to other polymers [80]. Further importance of this polymer is the presence of Si-H and allyl-functional groups in its network which help to adjust its chemistry and network architecture [81].

1.2. SiC-based ceramic nanocomposites

During the 1970ies, polymeric precursor polycarbosilane was used to prepare SiC ceramic fibers (Yajima process, discussed above). The SiC ceramic fibers prepared by using the Yajima process were shown to exhibit excellent high-temperature stability and promising mechanical properties. However its limited oxidation resistance and poor mechanical properties, at temperatures exceeding 1300 °C, restricts their use at high temperature. Within this context numerous studies have been performed with respect to the development of SiC-based nanocomposites by modification with metal (metal = Ti, Zr, Al, etc) to improve their properties.

Additionally, SiC-based ceramics (which are typical attributes as structural material) can also be used as a functional material by the incorporation of functionally active phase. Thus, it can be designed to possess incorporated magnetic, electric, catalytic, or other functionalities, by the incorporation of additional phase which work in synergistic manner.

1.2.1. Fundamental concepts about nanocomposites

Nanocomposites materials can be defined as a combination of two or more phases, one of them being nanoscale. The nanocomposites are capable of providing two or more primary functions, either in a simultaneous manner or sequentially. The basic motivation for the development of nanocomposites relies on their ability to address several objectives with only one structure e.g., a materials exhibits electrical, magnetic, optical, sensing, power generative or other functionalities, in addition to their basic mechanical strength or stiffness (which are typical attributes of structural materials) [82].

Roy and Komarneni recognized the potential of sol-gel preparative method to synthesize nano-heterogeneous materials i.e., combination of different phases with atleast one nano-sized phase and called them nanocomposites. Gleiter, brought attention on the nanosized materials. It has been observed that by reducing the size of the components within the composites materials towards nanoscale range, an enormous improvement in their properties (mechanical, electrical, optical etc) can be achieved. Thus nanocomposites can be defined as a multiphase materials consisting of one of the phases in the nanosized regime. Over the last decades, a large number of nanocomposite materials classes have been developed, e.g., polymer-based nanocomposites (such as polymer/glass,

polymer/metal, polymer/ceramic), metal-based nanocomposites (metal/metal, metal/glass, or metal/ceramic), ceramic-based nanocomposites [59].

Various techniques have been used to prepare ceramic nanocomposites, such as gas-phase (chemical vapor deposition or sputtering methods), liquid-state methods (sol-gel processes, intercalation techniques, pyrolysis of organometallic and polymeric precursors, combustion synthesis, spray conversion), or solid-state processes (e.g., mechanical alloying). The focus of the present work will be on polymeric precursors for ceramic nanocomposites.

Polymer-derived ceramic nanocomposites (PDC-NCs) are usually composites of several distinct phases derived from tailored polymeric precursor. Common preceramic polymers for the preparation PDC-NCs include polysilanes, polycarbosilanes, polysiloxanes, as well as polysilazanes and polysilylcarbodimides. For the synthesis of the PDC-NCs, different methods have been used which include the chemical modification of the polymer with the desired metal-containing complex in order to get a single-source-precursor, blending of polymer with the desired metal/metal complex, or modification of a suitable monomer [83].

The obtained polymeric precursors, regardless of employing any of the above mentioned methods can be heat treated in order to be converted into a ceramic (polymer-to-ceramic transformation). The polymer-to-ceramic transformation consists of three steps: 1) First step occurs at low temperature (100-400 ^{o}C) that includes the crosslinking of the polymer, leading to an infusible organic/inorganic network (the fabrication of precursor has been done by using this step). This process prevents the loss of the low molecular weight components within the precursor during ceramization and thus helps to increase the ceramic yield. 2) The pyrolysis of the crosslinked precursors at temperature up to 1000-1400 ^{o}C leads to the formation of amorphous ceramics, 3) Subsequently it is annealed at high temperatures leads to the formation of polycrystalline nanocomposites materials [59].

1.2.2. Synthesis of SiC-based nanocomposites from single-source-precursors

Three general approaches utilizing molecular and polymeric preceramics have been used for preparing SiC-based nanocomposites: 1) In a first approach polymeric precursor is combined with reactive fillers (e.g., metals, alloys, metal hydrides etc.); 2) A second approach employs the blending of two or more polymeric precursors; and 3) A third approach involves the synthesis of single-source-precursor that contain all the necessary elements of the desired composite. The precursors synthesized by the above mentioned methods can further thermally treated to produce SiC-based nanocomposites [83].

The first approach involves the blending process. It involves the mixing of polymer with metal (Ti, Ni, Zr, B, V etc), or intermetallic compound ($MoSi_2$, $CrSi_2$), or metallic compound (e.g., Cerium oxide were *in situ* prepared using reverse microemulsion method in the blend of polycarbosilane by cerium nitrate) [84] which finally lead to the formation of PDC-NCs. The phase composition of the final ceramic composites strongly depends on the type of the Si-containing polymer, metal used and pyrolysis temperature. For instance, Ti- and Zr-blended polysilazanes were shown to convert into metal-nitrides/SiC nanocomposites whereas the pyrolysis of the blend of metals with polycarbosilane give rises to the metal-carbide/SiC nanocomposites.

The second synthesis approach involves the blending of two or more polymeric precursors. The best example to understand this approach is the work done by Interrante and coworker. It involves the pyrolysis of blends from an aluminum organometallic precursor with different polycarbosilane provides AlN/SiC nanocomposies [85].

The third approach involves pyrolysis of pure SSPs to get ceramic nanocomposites. This method have attracted attention due to improved homogeneity of the resulting ceramic. Several studies in literature focus on synthesis of SSP, which is mainly achieved by using silicon-based preceramic precursors (polycarbosilanes, polysiloxanes, or polysilazanes) and their chemical modification with element-organic or organometallic compounds (metal alkoxides, metal amido complexes, boranes, or borazines). The obtained SSPs are subsequently converted into PDC-NCs upon pyrolysis [59].

Polycarbosilane was modified with metal alkoxides or acetyl acetonates (metal=Ti, Zr, Al, etc) to get SiC-based nanocomposites in order to improve their properties. Depending on the metal precursor used for the modification, different reaction pathways have been reported. Thus metal alkoxide (metal = Al, Ti, and Zr) react with PCS with the formation

of Si-O-M units; whereas metal acetonates were assumed to react upon Si-M bond formation. However the formation of the Si-O-M has been proved by some spectroscopic data (such as FTIR and NMR spectroscopy) in some cases whereas with regards to the Si-M no direct proof has been reported yet [59].

Boron-doping of PDCs result in enhanced densification as well as electrical conductivity and thermoelectric power. Boron-containing SSPs are mainly synthesized by using hydroboration reactions. The process was developed by Brown and involves the addition of a compound with a B-H bond to an unsaturated hydrocarbon. A new polymeric ceramic precursors has been synthesized by the hydroboration of silylcarbodiimides which on further pyrolysis leads to the production of Si-BCN ceramic [86]. Later on hydroboration of unsaturated groups on polycarbosilanes, polysilanes, polysiloxanes and polysilazane was explored to generate such single-source-precursors for silicon-based ceramics [81, 87].

Single-source-precursor route has also been used to produce SiFeC-based ceramic nanocomposites. In this aspect iron-containing polycarbosilane has prepared by the reaction of polydimethylsilane with dicyclopentadienyl iron [88]. Ferric acetylacetonate has also been used as the source of iron and similar results like dicyclopentadienyl iron have been obtained [89]. SiC/C/Fe nanocomposites were obtained from a single-source-precursor polyferrocenylcarbosilane (PFCS) with high ceramic yield. PFCS was obtained by the hydrosilylation reaction of vinyl ferrocene with allyl-hydrido polycarbosilane [90].

1.3. Processing of dense SiC-based monoliths

The commercialization of the ceramics depend on the fact that it should be easily processable with tunable morphology and porosity. There are several known methods in order to processes advanced ceramics into desired shapes. Some of these processes include die pressing (uniaxial or isostatic pressure), slip casting, tape casting, injection-molding etc. Due to the high melting point of the raw materials, the green compact requires an additional heat treatment step in order to get a dense ceramic, commonly reffered to as “sintering”. During the sintering process densification of the green microstructure occurs due to the diffusion of the atoms in the materials across the boundaries of the particles, fusing the particles together and creating one solid piece. During diffusion, the pores in the compact will diminish and eventually produce dense compacts.

Sintering is broadly classified into four categories, depending on the composition being fired and the extent to which the second phase formed during the heat treatment; 1) Solid-state sintering (SSS) (no liquid is formed), 2) Liquid-state sintering (LPS) (a small amount of liquid is formed), and 3) Viscous sintering (viscous flow of glass). But technical or advanced ceramics are usually produced using either SSS or LPS. In solid-state sintering, the shaped green compact is heated upto temperature that is typically 0.5-0.9% of the melting point. No liquid is formed during the heating and atomic diffusion takes place in the solid state, whereby the densification causes the shrinkage, shape change and growth of grain. Solid-state sintering can be defined via three steps 1) adhesion 2) neck formation and growth 3) grain growth and pores elimination. Whereas, the LPS process has been characterized by rapid densification in which liquid phase is formed during the process, which helps in particle diffusion and in turn results in densification. Liquid-phase sintering involves three sequential stages 1) a rearrangement stage 2) a solution precipitation process 3) a coalescence stage [57].

For enhanced densification of ceramic powder, pressure-assisted methods are generally used e.g., hot pressing, hot-isostatic pressing, or hot extrusion. Besides these methods, a number of conventional techniques have been applied to ceramic powder sintering, including microwave sintering, shock or dynamic sintering and field assisted sintering [57].

Dense SiC can be used for the production of abrasives, turbine components, suction box covers, seals, bearings, ball valve parts, hot gas flow liners, heat exchangers etc. However,

due to the highly covalent nature of the Si-C bond, SiC exhibits a very low self-diffusion coefficient, which restricts its densification, even when subjected to high temperatures. Additives are frequently used in order to enhance the sintering to get dense SiC. Consequently, the production of dense SiC parts is rather challenging. In order to understand, the effect of additives on densification of SiC, Alliegro *et.al* (1956) studied the effect of different metals (e.g., magnesium, tantalum, cobalt, barium, molybdenum, tungsten, strontium, copper, manganese, zirconium, boron, nickel, lithium, calcium, chromium, iron, and aluminum) on the densification of hot pressed SiC. It was found that SiC could be hot pressed to relative densities of the order of 98% of the theoretical density with slight additions (approximately 1%) of aluminum. Whereas other elements, such as lithium, calcium, chromium, boron, and iron, facilitate additional densification [91].

In 1982, SiC was modified by the combination of additive Al_2O_3 + Y_2O_3 to get dense monoliths at 2150 °C without pressure [92, 93]. Numerous studies have been done on modification of SiC using sintering additive with various combinations e.g., yttria+alumina, magnesia+alumina, other rare-earth metal oxides + alumina, alumina, sialon or yttria + aluminium nitride, ytterbium + aluminium nitride, lanthanum oxide + aluminium nitride in order to process fully dense SiC [94-96].

Prochazka *et. al* disclosed the method to produce dense SiC ceramic, which was prepared by forming a homogeneous dispersion of submicron SiC powder and a boron containing additive (elemental boron or boron carbide), wherein the amount of boron additive was equivalent to 0.5-3.0 wt % of elemental boron at a temperature and pressure of about 1900-2000 °C and 35-70 MPa, respectively [97]. It has been observed that the improved chemical homogeneity of the additives within the SiC matrix results in enhanced densification and significant reduction in grain growth [98].

Different methodologies have been used to produce dense SiC using different densifying agents which can be categorized as: i) pressureless solid-state sintering using sintering aids like boron and carbon, which delivers SiC parts with good high-temperature creep and oxidation resistance, but at the same time with poor fracture toughness [99, 100], ii) infiltration of reaction bonded (porous) SiC by molten silicon, which leads to ceramic parts having limited thermal stability, due to the relatively low melting point of excess silicon, and iii) hot-pressing, which however requires also additives as well as high pressures (>2000 MPa without additives [101] and 25-70 MPa with additives [91, 102]) and very high temperatures (i.e., beyond 2000 °C, [25]).

Liquid phase sintering (LPS) has also been used to prepare dense SiC, using additives such as Al_2O_3 or Al_2O_3+Y_2O_3 [103, 104]. The strength of the obtained ceramics is however, affected and limited by the presence of additives, which in turn restricts its use at high temperatures. Thus, there is an obvious and urgent need to find new processing techniques allowing the production of dense SiC parts without/minimum amount of additives with pressureless assisted technique at considerable low temperature. In this context, polymer-processing of ceramics has been shown to be a highly promising alternative towards dense ceramic parts [13-19].

In order to obtain dense bulk ceramics via polymer processing route, many methods have been used e.g., pressing, extrusion, and injection molding. The major problem for the processing of fully dense monolithic ceramic from liquid polymeric precursor is the evolution of gaseous by-products during the pyrolysis which in turn is the reason for pores with crack formation and significant material shrinkage. In order to minimize the shrinkage during the pyrolysis, fillers are often used. Two types of fillers are generally considered based on its reactivity i.e., passive and active fillers. Passive fillers include metal carbides or nitrides that occupy space, but do not react with polymeric precursors during pyrolysis, and reduce the volume fraction of polymer. Active fillers are usually metals or intermetallics powder, e.g., Al, Ti, Zr, B, or Si which react during pyrolysis, with the decomposition products generated during heating, or the heating atmosphere to form new phases that expand in volume. In order to produce pure systems, self fillers (produced from the same precursor as the matrix material) have been used. Fillers can constitute a volume fraction of the majority of the final ceramic part, and assist in achieving higher densities [105].

An additional technique which involves polymer-infiltration and pyrolysis cycles of pressureless monoliths have been shown to lead to the formation of materials with less residual porosity. Also pressure-assisted cross-linking step which was further followed by the pressureless pyrolysis was shown to be a promising approach. Uniaxial warm press is an effective technique for bulk shaping, and is correlated to the polymer crosslinking process and accompanied under an optimized temperature-pressure program, yielding a green body with controlled porosity. The advantage of using warm pressing is that it avoids the loss of oligomers during pyrolysis, and increases the ceramic yield. Optimal processing parameters depend on the type of precursor used. Pressing temperatures usually vary from 120 ^{o}C to 320 ^{o}C, and the applied pressure can range between 20 to 710 MPa. The obtained green body is pyrolyzed at elevated temperatures to obtain a

monolithic ceramic body with residual porosity, produced by the escape of gaseous pyrolysis by-products [16, 106, 107]. Beside pressureless techniques, dense PDC-based parts can be prepared by using pressure-assisted methods, such as uniaxial hot pressing (HP), hot isostatic pressing (HIP), or spark plasma sintering (SPS), etc [105].

1.4. Processing of porous SiC-based monoliths

The application spectrum of SiC is not limited as in the form of dense monoliths, but also extends towards porous SiC-based ceramics. Intensive fundamental studies related to the porous SiC have been done in the past which seeks attention of current research. Porous SiC ceramics are ideal candidates for thermoelectric energy conversion [108], porous burners [109-111], grinding materials, diesel particulate filter [112, 113], catalytic supports [114-117], separation membranes [118-120], power electronics [121], gas turbine combustor [122], or reinforcement of composites [123].

Macroporous SiC is widely used in various industrial applications owing to its unique properties such as excellent mechanical strength, good chemical resistance, high thermal conductivity, low thermal coefficient and high thermal shock resistance. The properties of the macroporous SiC strongly depend on the porosity and its existing microstructure. Extensive work has been reported on its morphological control and connectivity of distributed pores. The production of porous SiC has been done by using wide range of processing techniques such as : (i) partial sintering, (ii) replica, (iii) sacrificial template, (iv) direct foaming, and (v) bonding technique [124].

Partial sintering is the simplest, frequently used and most conventional method to fabricate porous SiC ceramics. The method involves retardation or prohibition of full densification by reducing the sintering potential. Reduced sintering potential is achieved by low sintering temperature, sintering without additives, and recrystallization. For instance, Lin and Tsai processed macroporous SiC ceramics with tailored porosity and pore within a range of 29-39% and 0.10-2.33 μm, respectively. This was achieved by varying both sintering temperature (1450-1800 ^{o}C) and alumina content (used as additive; 3-8 wt%) [125].

The replica method is based on the copy of the porous templates with respect to its pores and structure. The method based on the impregnation of the porous templates with the ceramic suspension, or precursor solution etc and conversion into template-assisted ceramic with subsequently heat treatment. Various synthetic and natural cellular structures can be used as templates. The most frequently used synthetic templates are porous polymeric sponges such as polyurethane [126].

Recently, the characteristics and advantages arising from the imitation of natural structures to ceramics have diversified into numerous technical applications. Natural structures which can be used as templates are woods, coral, cotton, or sea sponges. Due to the unique hierarchical architecture of the cellular microstructure, wood exhibits excellent strength at low density, high hardness and elasticity, and tolerance to the damage equally on the micro and macro-scale. The fact that the trees are able to remain upright as beams during hundreds of years is due to their outstanding mechanical properties. Heating wood in non-oxidizing atmosphere at temperatures above 600 °C results in decomposition to form a carbonaceous residue which reproduces the originial cellular structure. Generally, wood templates are fabricated through three steps: 1) Formation of carbon-preform template by pyrolyzing the wood materials; 2) Infiltration of the carbon-preform template with ceramic precursors; 3) Calcination to form ceramics and remove organic materials [127, 128].

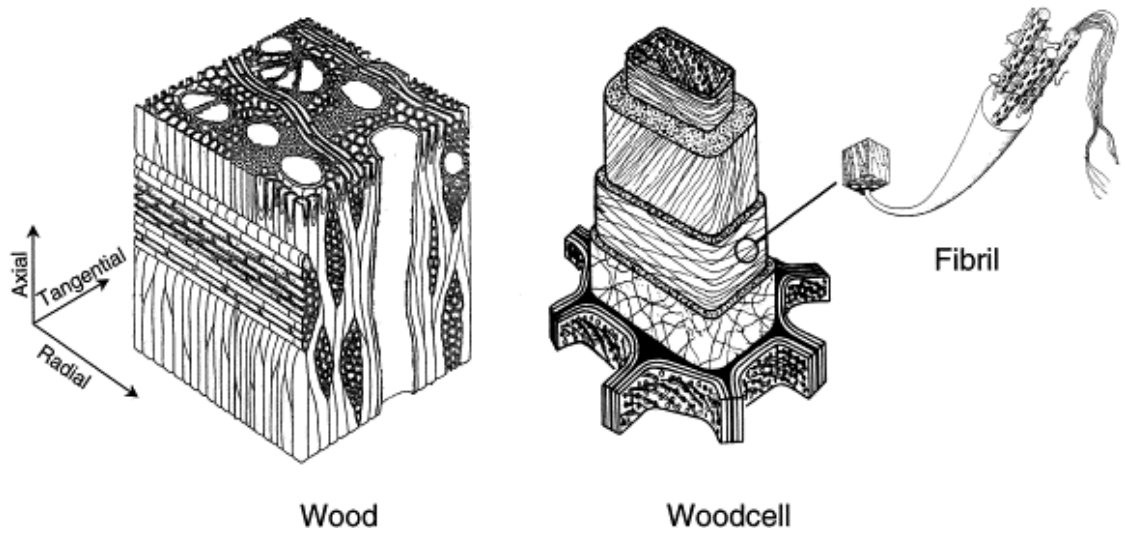

Figure 1-5. Hierarchical microstructure of wood; (a) macroscopic and (b) microscopic cell structure [128]

A plethora of studies have been reported for producing hierarchically structured SiC-ceramic materials using various wood materials as natural templates. The carbothermal reduction method is a very well known reaction of silica with carbon, in order to prepare SiC. In the literature, biomorphic SiC has been produced by the infilteration of the carbon preform (obtained by heat treatment of wood at 600 °C in inert atmosphere) with silicon containing precursors and subsequent pyrolysis in an inert atmosphere. The most commonly used silicon containing precursors are silicon melt, silicon, silicon monoxide vapors, organosilicon compounds and silica sols [128-130].

Greil *et al.* investigated different types of the wood template (ebony, beech, oak, maple, pine, balsa) for the preparation of biomorphic SiC. The templates were infiltrated with liquid silicon to obtain β-SiC formed by a solid-liquid reaction [128]. Ota et.al. tried to vacuum-infiltered the carbon template with tetraethylorthosilicate (TEOS) which further converted into the silica sol by hydrolysis with ammonia solution. Later on, number of studies have been reported in which the template has directly infiltered with as prepared silica sol which on high temperature treatement converts into SiC [131].

The polymer-derived ceramic route is also used in the preparation of porous materials. In case of PDCs, the template (synthetic or natural) is infiltrated with a ceramic suspension(derived from PDCs) or with the preceramic polymeric precursor to be cast, subsequent drying or optional processing (crosslinking and pyrolysis).

Another most commonly used industrial manufactured natural product is paper. Paper-based template have shown advantages compared to natural products like wood with respect to its reproducible properties. The advantage of being an industrial manufactured product, the properties of the paper preforms like composition, porosity and density remain constant for different batches [132]. This method also involves the formation and than infiltration of paper preform with silicon liquid, methyltrichlorosilane or polymeric precursor which subsequently convert into SiC by controlled heat treatment [133].

Another technology for producing porous non-oxide ceramic monoliths is the sacrificial filler technique which involves extrusion or pressing of preceramic polymeric powder together with a sacrificial filler (e.g., poly(methyl methacrylate) (PMMA)) and sintering additives. The removal of the sacrificial filler at high temperature helps to provide the porosity to the sample whereas sintering additives are added to impart a higher mechanical strength [124, 134-136].

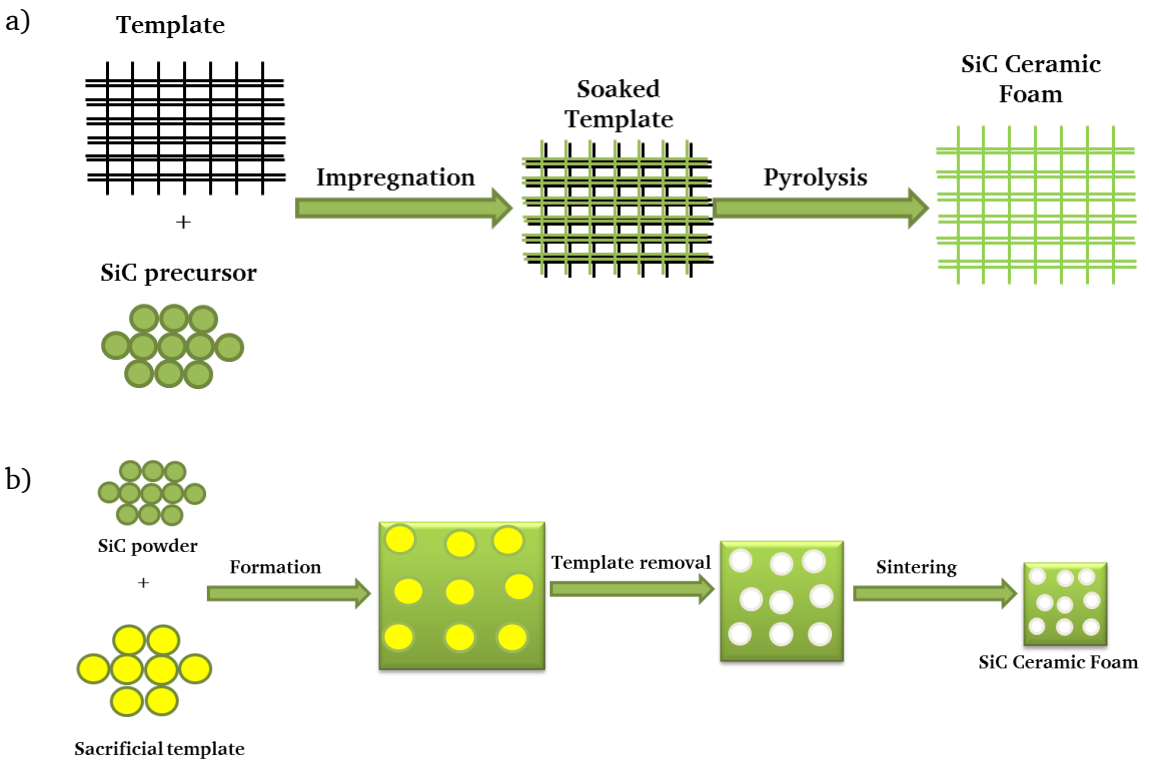

Figure 1-6. Schematic of processing methods for porous silicon carbide: replica (a), and sacrificial template (b) [124].

Direct foaming includes the generation of bubbles inside ceramic or preceramics polymer precursor suspension with the help of blowing agents to create stabilized foam. The stabilized foam of ceramic is further dried and subsequently sintered to obtain macroporous SiC ceramics. The blowing agents can be volatile liquids, gas evolving solids, or gases that can be evolved *in situ* by chemical reactions or can be added to the liquid mixture by mechanical stirring or bubbling (gas injection)[124].

The last method is the bonding technique which is the low-temperature fabrication of porous SiC ceramics. It includes the *in situ* reaction of bonding materials with ceramic and formation of prorous material. Alkali, cordierite ($2MgO{\cdot}2Al_2O_3{\cdot}5SiO_2$), mullite ($3Al_2O_3{\cdot}2SiO_2$), silica ($SiO_2$), silicon (Si), silicon nitride (Si_3N_4), and silicon oxycarbide (SiOC) were investigated as bonding materials for porous SiC ceramics [124]. Porous SiC ceramics were fabricated from Al_2O_3 and graphite in air by the *in situ* reaction bonding technique. This process is based on the oxidation of SiC and the formed SiO_2 reacts with Al_2O_3 to fabricate porous mullite ($3Al_2O_3{\cdot}2SiO_2$)-bonded SiC at 1400-1550 °C in air. Meanwhile, the graphite (templates) are decomposed or burned out, leaving pores inside the materials [137].

1.5. Application of SiC-based ceramics in the energy sector

Energy is considered as a prime agent in the generation of wealth and a significant factor in economic development. The worldwide demand of energy is increasing continuously and high emphasis is placed on the effort for the reorganization of the current energy supply structure. The energy resources have been split into three categories: fossil fuels, renewable, and nuclear resources. Most of the primary energy source is covered by fossil fuels. In the foreseeable future we are going to face problem of depletion of fossil fuel in addition with the global warming issue [138].

Nuclear energy covers the part of the present energy demands without climate effect but it also face the problem of depletion of nuclear fuel [139]. Following the event at Fukushima in 2011, several work has also going to improve the efficiency of the Nuclear power plant [140].

In the long run for green energy, Hydrogen, a zero emission fuel seems to be a promising source for environmental friendly energy supply. There are number of institutions, and association are working on the topic of NanoEnergy (application of nanotechnologies in the energy sector). Hydrogen and Fuel cell initiatives Hessen (H2BZ) is one of the leading network in the field of NanoEnergy [139].

However to solve energy and climate problems, it is not only necessary to economically utilize renewable alternatives to fossil fuels but focused on optimizing the complete chain of the energy sector starting from development and conversion, transport and storage up to the consumer utilization. Figure 1-7 shows the value added chain of the energy sector [139].

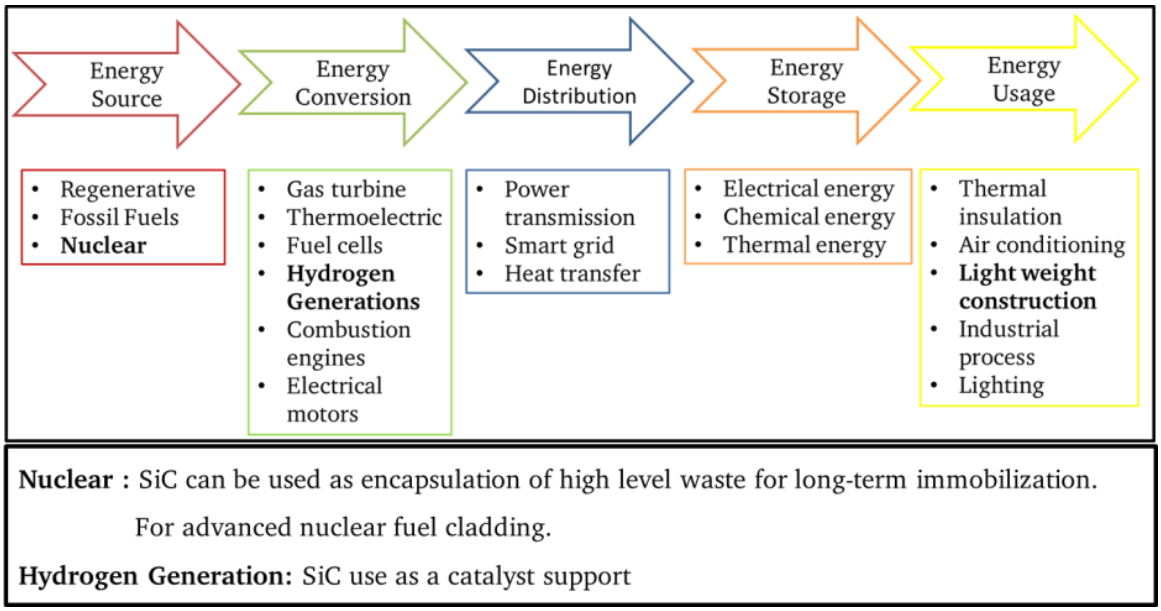

Figure 1-7. The value added chain in the energy sector [139].

1.5.1. SiC in nuclear power plants

In order to improve the efficiency of the Nuclear power plant, SiC was shown in the last decades to be a promising candidate (zirconium alloy substitute for cladding purposes, carrier material in fission reactors, and first wall protection in fusion reactors).

Following the event at Fukushima in 2011, enhancing the accident tolerance of light water reactors (LWRs) became a topic to be addressed more seriously. There are several groups which conducting research and development on enhanced accident-tolerant fuels (ATF) and cladding for light water reactors (LWRs). Under extreme condition, greatest damage and release of radiation might be caused by explosion of H_2 gas which is the result of the hot steam coming into contact with overheated nuclear fuel rods covered by a cladding of zirconium alloy, or "zircaloy" [140].

Several leading candidates for advanced nuclear fuel cladding incorporate SiC. It has the potential to offer significant improvements in the performance over zirconium-alloy cladding. It has demonstrated exceptionally low oxidation rates up to 1700 °C and has been shown to withstand temperatures exceeding 2500 °C. Currently available data on monolithic SiC samples indicates oxidation rates that are 2-3 orders of magnitude lower than that of zirconium-based alloys. Oxidation kinetics of SiC, coupled with lower heat of oxidation, translates to lower maximum temperatures under postulated accident conditions and significant reduction in hydrogen generation [140].

A cross-sectional view of the proposed SiC cladding, for nuclear fuel rods, is shown in Figure 1-8. The fuel pellets are in the center (shown as a gray crosshatch). Then, after a thin layer of inert helium gas, the three layers of cladding are shown in black (solid SiC), green (composite material made up of SiC fibers infused with SiC), and blue (another solid layer of SiC). However, due to the high covalent character of the Si-C bond, it is difficult to be sintered to high relative densities without using sintering additives, which might consequently have detrimental effects on the structural properties of the SiC-based ceramics [141].

The potential new application of SiC ceramics in nuclear fission industry is presented and is based on that SiC are currently produced in different microstructure form with almost single phase α-SiC with significant low amount of additives such as Al_2O_3, TiC, TiB_2 etc (but their low content will not have a significant effect on neutron economy), high melting temperature, high thermal conductivity, high stability in the presence of reactor coolant, and the absence of swelling under the heavy ion bombardment [142].

SiC-based ceramic composites have also been studied for fusion applications for more than a decade. The potential for these materials have been widely discussed and is now understood to be (1) the ability to operate in temperature regimes much higher than for metallic alloys, (2) an inherent low level of long-lived radioisotopes that reduces the radiological burden of the structure, and (3) perceived tolerance against neutron irradiation up to high temperatures [143].

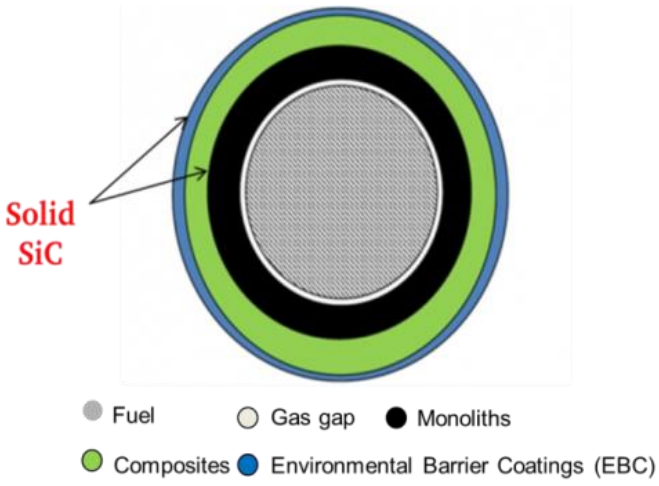

Figure 1-8. Cross-section view of the proposed silicon carbide cladding for nuclear fuel rods [141].

Silicon carbide was shown in the last decades to be a promising candidate for applications in nuclear energy (fission reactors and fusion reactors). However, due to the high covalent character of the Si-C bond, it is difficult to be sintered to high relative densities without using sintering additives, which might consequently have detrimental effects on the structural properties of the SiC-based ceramics. Thus, there is an obvious and urgent need to find new processing techniques which allow for producing dense silicon carbide parts without using additives.

1.5.2. SiC as catalyst support

Heterogeneous catalysts are composed of support material and catalytic active component(s). The catalyst often present as a minor phase homogeneously dispersed in a support. The support provides a porous framework (micro, meso, and macroporous) which help in improving the properties of catalyst. Large macroporous material has an advantage in order to provide easy inlets of the reactant and outlet of the product and avoid diffusional limitation without generating any pressure drops in the catalytical reactor. Micro or meso porous materials help in the dispersion of the active site (catalyst) in the support. The dispersion of the catalyst is very important as it increases the number of accesible active site which in turn reduce the incorporation of the amount of the expensive active phase [10].

Mainly impreganation and coprecipitaion technique have been used to prepare supported catalyst: [144]. As the name of the method itself explain its process that catalyst in liquid form impreganated into the solid catalyst e.g. SiC support with a moderate surface area of 28 m^2/g (BET) was synthesized by a sol-gel route. The supported nickel catalysts were prepared by impregnation of $Ni(NO_3)_2$ aqueous solution which finally lead to the fomation of Ni/SiC catalysts [145]. Whereas in coprecipitation both the phase has been precipitated at the same time. For instance, the solution of nickel nitrate hexahydrate and aluminum nitrate nonahydrate of appropriate concentration was precipitated by the sodium carbonate solution. The precipitate was filtered and dried. The dried sample was then calcined in order to get Ni/Al_2O_3 catalyst [146].

The majority of commercial catalysts are supported on alumina, silica or carbon. All these support materials suffer drawbacks. Due to the poor heat conductivity and chemical reactivity of alumina and silica, it can induce a decrease in surface area and loss of active phase during operation. The weak oxidation resistance of carbon hinders its use for high-temperature oxidative reactions as support. It is consequently of interest to discover and develop a new support materials that can efficiently replace the above cited drawbacks [10].

SiC is well known for its extreme hardness, high thermal conductivity, high resistance towards oxidation, high thermal stability, high resistance to aggressive media (acidic or basic), high chemical inertness, and its lightness [10]. Several reviews recently summarized the physico-chemical properties of SiC for use as catalyst support. SiC has been proved as a very good catalytically support for several known reactions e.g., for the hydrogenation

of carbon monoxide, for the methanation of CO, or the selective H_2S oxidation etc [7, 147]. The main limitation resides is the difficulty in shaping since the industrial SiC typically available as powder and thus not directly suitable for use as catalyst support [7].

Another important topic that should be neccesarily discussed here relates to hydrogen (zero emission fuel). It seeks tremendous attention in the field of fuel cell technology research. It can be produced from a variety of feedstocks. These include fossil resources and renewable resources. Chemical, biological, electrolytic, photolytic, and thermo-chemical process technologies can also be used for the production of hydrogen [148]. However there are number of issues which restrict its direct use i.e., it does not occur naturally and it is not easy to store or transport it. The concept of using ammonia and hydrocarbon as a hydrogen source for fuel cell has gained attention. As from them hydrogen can be extracted by the thermal catalytic decomposition and it also has some significant advantage in terms of storage and transport [149].

Ruthenium (Ru) is the most active metal for ammonia decomposition, and its activity varies with respect to support used (Table 1-2). Though the most active catalyst is Ru most of the catalysis process runs by iron as a catalyst because it is economically cheaper. Nickel is also in the race of catalyst especially in microstructured reactors, due to low cost compared to Ru and high activity as compared to iron. Ganley et al. gave an order of activity (as turnover frequency) Ru>Ni>Rh>Co>Ir>Fe. Another possible choice as catalyst for the decomposition of ammonia are carbide and nitride of transition metals [150].

Table 1-2. Decomposition of NH_3 over supported 5 wt.%-Ru catalysts with different supports at 550 ^oC [151]

Catalysts	NH_3 conversion (%)
Ru/CNTs	100
Ru/MgO	91.8
Ru/ZrO_2	77
Ru/Al_2O_3	73.7

Carbides and nitrides of early transition metals have been the focus, as they display Pt-like behavior in several catalytic reactions. Vanadium carbide has been shown to be an active catalyst for dehydrogenation of hydrocarbons [152, 153], decomposition of ammonia [27, 154], and hydrogenolysis [155], etc. Pure vanadium carbide is proven to be active for the decomposition of ammonia but the activity found to be very low as compared to

commercial available catalyst. The possible reason might be the particle size (≥ 35 nm), surface area (≥ 31.4 m^2/g) [27] or agglomeration upon catalysis process which in turn decreases the active site and decreases the activity for ammonia conversion. Since vanadium carbide has not been extensively studied, its catalytic activity might still has potential for improvement.

2. Experimental Procedure

2. Experimental Procedure

2.1. Commercial available materials

A commercially available allyl-hydrido polycarbosilane (SMP-10, Starfire systems) was used as a suitable polymer for the synthesis and processing of SiC-based nanocomposites. SMP-10 is a clear, amber-colored, viscous liquid which requires no solvents for processing.

Table 2-1. Properties and structure of SMP-10 as provided by the supplier.

Density	0.998 g/cm^3
Appearance	clear, amber liquid
Viscosity	40 to 100 cps at 25 °C
Compatible Solvents	Hexanes, Tetrahydrofurane, Toluene, Insoluble in water
Flash Point	89 °C
Odour	None
DOT/IATA Regulation	Non-Hazardous
Storage	Vacuum container or inert environment; Refrigerator
Structure	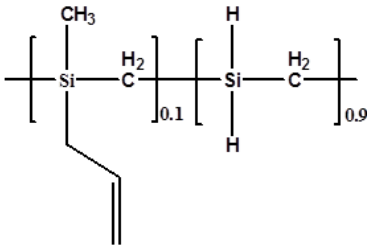

In this study, single-source-precursors (SSPs) have been synthesized by the modification of SMP-10 with boron and vanadium containing compound. In order to modify the SMP-10 with boron; borane dimethylsulfide complex (BMS, Sigma-Aldrich), allyl-functionalized carboranes (AFC) has been used. AFC has been prepared in the laboratory using *o*-carborane (Kat Chem ltd). Vanadyl acetylacetonate (VAAc, Sigma-Aldrich) and liquid vanadium oxytriisopropoxide (VISO, Sigma-Aldrich) were used to synthesized vanadium-containing SSPs. Toluene (Sigma-Aldrich) was used as a solvent in all preparation, modification, and processing. Regular filter paper (Carl Roth Germany) and pine wood have been used for the processing of porous monoliths using template assisted method.

2.2. Synthesis of single-source-precursors

2.2.1. Synthesis of boron-containing SSPs using borane dimethylsulfide

A typical reaction has been carried out using Schlenk technique. A number of experiments were performed using different BMS:SMP-10 weight ratios (see Table 2-2.). In a two neck round bottom-flask SMP-10 was dissolved in toluene. The flask was cooled to -50 °C and backfilled with argon. Subsequently, a BMS solution in toluene was added dropwise. Some gas evolution was observed. The reaction mixture was stirred under the same condition for 2h, allowed to reach room temperature and then stirred overnight. The obtained highly cross-linked single-source-precursor was finally dried in vacuum (10^{-2} mbar) at 60 °C for 5h. In order to understand the effect of temperature on the crosslinking of the modified polymer and also to compare it with the pure SMP-10, the samples were thermally treated at 250 °C for 3h.

Table 2-2. Different BMS:SMP-10 weight ratio used for the preparation of the SiC-based monoliths.

BMS:SMP-10 (weight ratio)	Amount of BMS (weight%)	Amount of SMP-10 (weight%)	Sample assigned
1:99	1	99	SiBC-1
5:95	**5**	**95**	**SiBC-5**
30:70	30	70	SiBC-30

2.2.2. Synthesis of boron-containing SSPs using allyl-functionalized carboranes

2.2.2.1. Synthesis of allyl-functionalized *o*-carborane and *m*-carborane

In order to synthesize the allyl-functionalized *o*-carborane (S1), *o*-carborane (1, 2-$C_2B_{10}H_{10}$) has been used as a starting material. In a completely dried flask, *o*-carborane (1.0095 gm, 7.00 mmol) was dissolved in a mixture of solvent toluene (14 ml) and diethyl ether (7 ml) with stirring. Then the solution was cooled at 0 ^oC using ice bath and n-BuLi (9.7 ml, 14.7 mmol) was added dropwise with constant stirring. The obtained white cloudy solution was stirred for 1h at room temperature and subsequently cooled again down to 0 ^oC and allyl-bromide (1.2 ml, 13.9 mmol) was added dropwise under constant stirring. The mixture was stirred for 2h at room temperature and refluxed overnight. Then it was cooled at room temperature and separated from the unreacted salts using water and diethyl ether with separating funnel. Then the organic layer was dried with $MgSO_4$ and finally yellow oil was obtained after solvent removal under vacuum [156].

The synthesis of the allyl-functionalized *m*-carborane (S2) has also been successfully prepared by using above mentioned method. The synthesis starts using *m*-carborane (1, 7-$C_2B_{10}H_{10}$) as a starting material instead of *o*-carborane. It has been obtained by the rearrangement of *o*-carborane upon heat treatment (500 ^oC/2h).

2.2.2.2. Synthesis of the SSPs for SiBC ceramic

The reaction for the synthesis of the SSPs was carried out in argon atmosphere using the Schlenk technique. Thus, a solution of SMP-10 in toluene (4.5 gm in 1.5 ml) was introduced in a two neck round bottom-flask equipped with a magnetic stirrer. Subsequently, a solution of desired amount of AFC in toluene (0.25 gm in 1.5 ml) was added dropwise under stirring and the reaction mixture was stirred at ambient temperature for 1h. The obtained solution was heated at 150 ^oC for 4h and subsequently the solvent was removed under vacuum at 90 ^oC. In order to understand the effect of temperature on the crosslinking of the modified polymer and also to compare it with the pure SMP-10, the samples were thermally treated at 250 ^oC for 3h.

2.2.3. Synthesis of vanadium-containing SSPs using vanadyl acetylacetonate

In a typical experiment, vanadium modified polycarbosilane (V-SMP-10) has been synthesized by adding SMP-10 to a solution of vanadyl acetylacetonate (VAA) in toluene (weight ratio SMP-10:VAA 70:30), followed by stirring for 24h and subsequent removal of the solvent in vacuum. The obtained sample was dried at 120 ^{o}C for 2h in argon atmosphere.

2.2.4. Synthesis of vanadium-containing SSPs using vanadium oxytriisopropoxide

In order to fabricate vanadium-containing SSPs using template assisted method, the single-source-precursor should be in liquid state. So the liquid vanadium oxytriisopropoxide (VISO) is used as a starting material. The reaction for the synthesis of the single-source-precursor was carried out in argon atmosphere using the Schlenck technique. Thus, a solution of 5 g VISO in 20 ml toluene was introduced in a two neck round bottom-flask equipped with a magnetic stirrer. Subsequently, 5 g of SMP-10 was added dropwise under stirring and the reaction mixture was stirred at ambient temperature for 24h. The obtained solution was used to infiltrate the templates (i.e., paper and wood templates, details shown in section 2.3.2).

2.3. Processing of the single-source-precursors

2.3.1. Processing of dense monolithic SiC ceramics

The powder obtained from the thermal curing process of SMP-10 (250 °C, 3h) was uniaxially warm-pressed in a steel dye (diameter 10 mm) at temperatures between 180-300 °C under different applied pressures (Table 3-2). The optimized green-body fabrication process involved a pre-compaction step at room temperature (ca. 127 MPa), followed by pressure release and pressureless cross-linking at 300 °C. Thus, while uniaxial pressing, further cross-linking of the polymer (by means of dehydrocoupling reactions) occurred and led to infusible SMP-10-based monoliths.

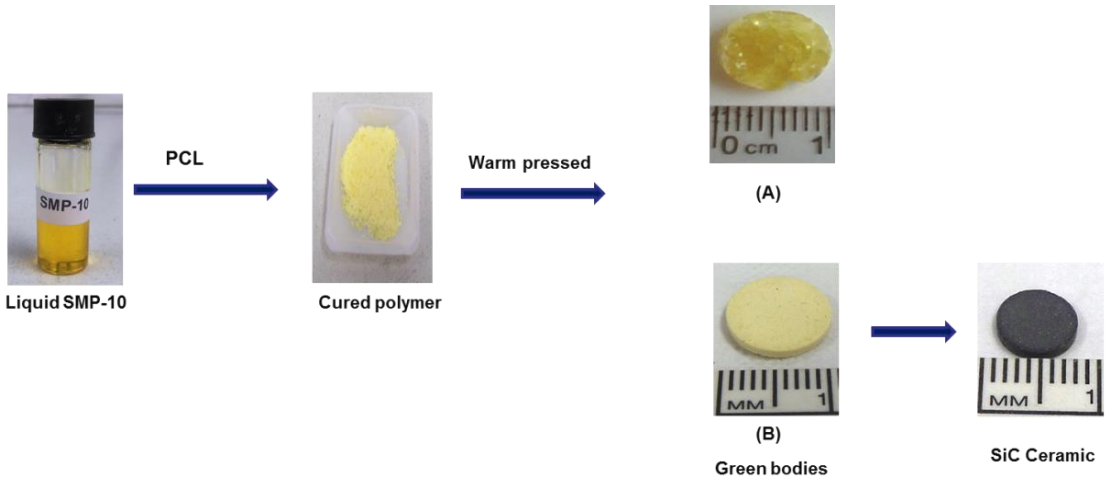

Figure 2-1. Scheme of the processing of SMP-10-based ceramic monoliths.

In order to reduce the residual porosity of the obtained SiC ceramic parts, the polymer-infiltration and pyrolysis (PIP) technique was applied. Thus, the ceramic monoliths prepared upon pyrolysis of the green-bodies at 1100 °C and subsequently annealing at 1700 °C were immersed in SMP-10 in argon atmosphere for >24 hours (PIPSiC). The infiltrated monoliths were removed from the liquid polymer, placed in quartz crucibles and pyrolyzed at 1050 °C under argon. The same process was repeated for several cycles.

In case of the boron modified sample, the obtained dried solid single-source precursor (without thermal crosslinking) was uniaxially pressed in a steel dye (diameter 10 mm) at ca. 300 °C using a pre-compaction pressure of 127.4 MPa applied at room temperature/at 45 °C.

Table 2-3. Optimized parameter for the processing bulk monolith (RT = room temperature).

Sample Name.	Temperature [°C]	Pressure [MPa]	Temperature at force applied [°C]	Holding Time [min.]
SiC	300	127.4	RT	60
SiBC	300	127.4	45	60

2.3.2. Processing of porous monolithic SiC ceramics

In the present study, wood and paper are used as templates for the processing of vanadium-containing SSPs. In case of paper, processing starts with the as received paper whereas in case of wood, it was first heat treated at 1000 °C for 2h in order to get C-preform which is further used for the processing. Typically, the infiltration procedure consisted of a soaking step (4 minutes soaking of the template in the single-source-precursor solution) followed by a drying step (2 minute drying at ambient temperature and pressure). The soaking-drying cycle was repeated up to 4 times (see Table 2-4). After each cycle the obtained infiltrated templates were dried at ambient temperature and pressure for 3h as well as for 6 days.

Table 2-4. Processing parameters used with paper templates.

SMP-10:VISO:Toluene	Infiltration cycle	Drying (at ambient condition)
1:1:4	1 time	3 hours
		6 days
	4 times	3 hours
		6 days

Furthermore, vanadium-containing SSPs were also been fabricated by using the sacrificial filler technique. Poly(methyl methacrylate) (PMMA) micro-beads (diameter 8 μm) were used as sacrificial filler. A solution of 1 g of VISO in 20 ml toluene was reacted with SMP-10 in a similar way as previously described. After stirring the reaction solution, 9.50 gm of PMMA micro-beads were added and the suspension was stirred for additional 2 days. The solvent was removed in vacuum (10^{-2} mbar) and the obtained powder was uniaxially warm-pressed in a steel dye at 165 °C (diameter 10 mm, pressure 127 MPa). The optimized green-body fabrication process involved a pre-compaction step at room temperature (ca. 127 MPa), followed by pressure release and pressureless cross-linking at 165 °C.

2.4. Ceramization and high temperature annealing

The obtained boron-containing SSPs and the optimized green bodies (with and without boron modification) were converted into ceramic materials by pyrolysis at 1050-1100 °C under argon environment. Additionally, the ceramics (powders and monoliths) were annealed in argon atmosphere at 1300 °C, 1500 °C, 1700 °C, and 1900 °C for 3h using a high-temperature graphite furnace.

The obtained vanadium modified single-source precursor (dried at 120 °C), cross-linked upon annealing at 600 °C in argon and ceramized in argon at 1100 °C (2h dwell) using schlenck technique. The high-temperature annealing experiments were performed with the ceramic material at temperatures of 1300, 1500 and 1700 °C (2h dwell).

The obtained template assisted green bodies were converted into V_8C_7/SiC amorphous nanocomposites via pyrolysis at 800 °C under argon atmosphere. The obtained SiC/V_8C_7-based samples were further annealed subsequently at 1300 °C, and 1700 °C for 3h in a high-temperature graphite furnace (Ar atmosphere).

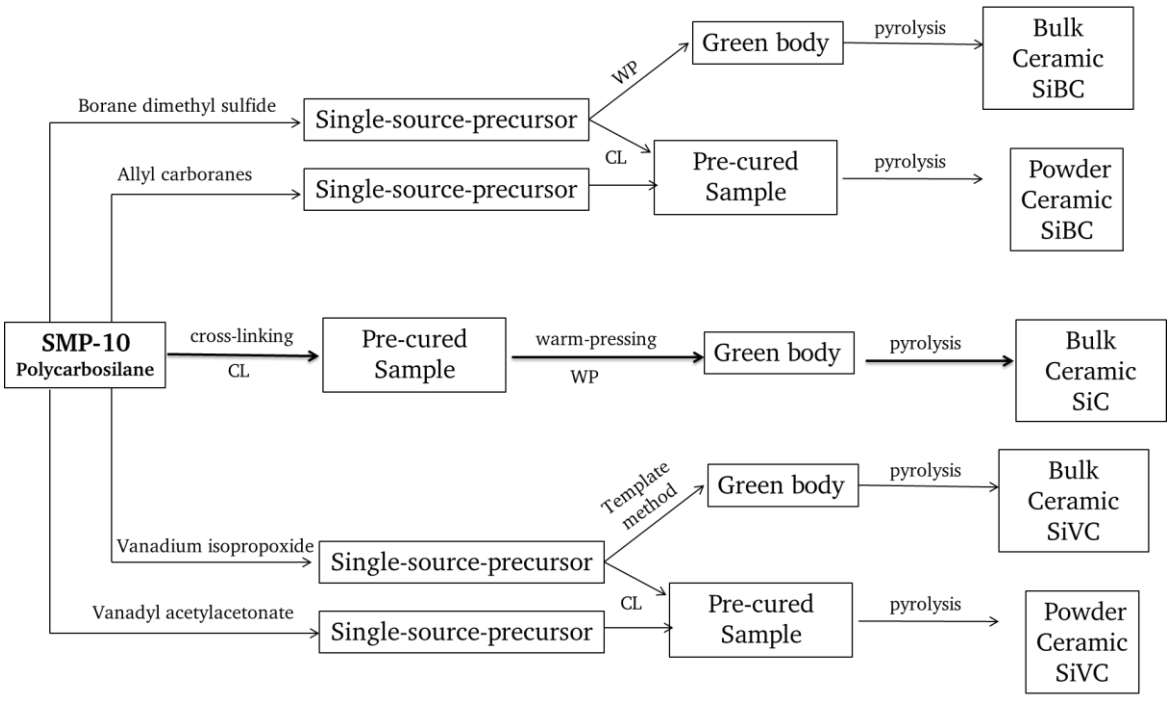

Figure 2-2. Procedure utilized for the synthesis of ceramic powder and bulk ceramic.

2.5. Materials characterization

Attenuated-total-reflectance FT-IR spectroscopy (ATR-FTIR) was performed using Bruker instrument (ATR-FTIR, Bruker Vertex 70, USA).

The thermogravimetric (TGA) experiments were performed using Netszch equipment (TGA, 449C Jupiter, Netzsch, Gerätebau GmbH, Selb, Germany) coupled with evolved gas analysis, EGA (*in situ* mass spectrometry, QMS, 403C Aëolos, Netzsch, Germany). The heat treatment was carried out under an argon atmosphere at a flux of 50 ml/min, with a heating rate of 5 °C/min up to 1400 °C.

Elemental analysis is used to determine the composition of different elements present in the system. The carbon content of the samples was determined with a carbon analyzer, CS 800 (Eltra GmbH, Neuss) and the oxygen content of ceramics were investigated by means elemental analysis (Neuss and N/O analyzer, Leco TC-436, Leco Corporation, Michigan) whereas silicon and boron content were determined at Mikroanalytisches Labor Pascher (Remagen, Germany).

X-ray diffraction (XRD) studies are an important characterization technique to understand the crystalline/ amorphous nature of ceramic materials. Crystalline phases of the produced ceramic materials were investigated by powder X-ray diffractometer (STOE & Cie GmBH Germany) with MoKα radiation at a scanning speed of $1^{o}min^{-1}$ in the 2θ range of $5\text{-}45^{o}$.

The bulk density and porosity of the obtained SiC ceramics was measured by the Archimedes method, using water as the medium. The dry weight (Md), the weight of the sample saturated with water (Mw), and the weight of the saturated sample submerged in water (Ms) were measured, and the bulk density of the SiC ceramics was calculated using the equation Md/ (Mw-Ms).

The specific surface area measurement and nanostructure evolution has been evaluation using N2 physisorption and TEM measurement. The specific surface area (SBET) values were calculated by the Brunauer-Emmett-Teller (BET) method from the linear portions of the adsorption isotherms. Transmission electron microscopy (TEM) measurements were performed using a Model JEM2100F (JEOL, Tokyo, Japan) operating at 200 kV. The samples were pulverized and dropped on a carbon-coated copper grid, followed by a light carbon coating to minimize charging under the incident electron beam. Scanning electron

microscopy (SEM) studies were performed on a Philips XL30 FEG, Netherlands with an acceleration voltage of 10–15 kV.

The micro-Raman spectra were recorded with a Horiba HR800 micro-Raman spectrometer (Horiba Jobin Yvon, Bensheim, Germany) equipped with a blue laser (irradiation wavelength 488 nm). The excitation line has its own interference filter (to filter out the plasma emission) and a Raman notch filter (for laser light rejection).

X-ray photoelectron spectroscopy (XPS) measurements were done using a PHI VersaProbe 5000 spectrometer equipped with a monochromatic Al Kα source (hυ= 1486.6 eV). The binding energies are referred to the Fermi level of Ag foil. Photoelectrons were collected with the pass energy, E_{pass} = 23.5 eV at θ = 45° with respect to the surface normal.

The catalytic tests were conducted at Micrometrics GmbH & Co. KG (Aachen, Germany). A typical catalytic measurements was performed as described in the following: 1) Blank measurement: this measurement has been performed without the presence of SiVC(O) composites 2) Sample measurement: 0.2970 g of the SiVC(O) sample was loaded in a quartz tube fixed bed reactor. The sample resides in a 10 mm internal diameter region and the exhaust of the tube is 2 mm. Furnace heated region - 5.08 cm W x 6.35 cm H.

In both measurements a mixture of gas of NH_3/He (10/90) was passed through the reactor. Prior to the test, the catalyst was treated in H_2 at 400 °C for 14 h (the set-point was approached with a temperature ramp of 2 K min^{-1} in H_2). After the pretreatment, the catalytic measurement was performed in the temperature range from RT to 1000 °C.

Catalytic tests were conducted for the sample obtained by the modification of SMP-10 with vanadium oxytriisopropoxide were done at QUANTACHROME GmbH & Co. KG at Odelzhausen, Germany. Details of catalytic measurements: 100 mg of the sample (catalyst + support) were loaded in a quartz tube fixed bed reactor. Mixture of gas of NH_3/He (1.46/32 ml/min) was passed through the blank and catalyst bed. The experiment was carried out on an Autosorb iQ2 equipped with an additional gas mixing unit and an on-line mass spectrometry for measuring NH_3, N_2 and H_2 concentrations. The catalyst was pretreated in H_2 at 673 K for 14h (the set point was approached with a temperature ramp of 2 K min^{-1} in H_2). After the pretreatment, the catalytic measurement started and measured in between 500-1000K.

3. Results and Discussion

3. Results and Discussion

1. This chapter is sub-divided into three main sections: Section 1 includes the characterization of the allyl-hydrido polycarbosilane (SMP-10) and obtained crosslinked precursors, polymer-to-ceramic transformation, and phase evolution at high temperatures. The feasibility of the polymer-processing route for preparing dense, crack-free, and near stoichiometric silicon carbide monoliths has also assessed. It also includes discussion regarding the change in porosity of the monolithic sample with respect to temperature. Lastly, in order to get near dense monolith, the effect of polymer-infiltration and pyrolysis (PIP) is also discussed.
2. Section 2 is sub-divided into two parts; part 1 covers the synthesis and characterization of boron-modified single-source-precursors (SSPs) using borane dimethyl sulfide (BMS). The effect of boron on the crosslinking, ceramic yield, and high temperature phase separation is also addressed. Moreover, optimization of the parameter for the processing of the selected sample (as per crosslinking degree and amount of boron) in order to get green body from SSPs and the effect of processed temperature on the porosity are also considered. The second part covers the synthesis and characterization of allyl-functionalized carboranes. It also discuss the synthesis and characterization of boron-modified single-source-precursors (SSPs) using allyl-functionalized carboranes (AFC). The effect of molecular architecture and chemism of SSPs on the polymer-to-ceramic of the samples has also discussed.
3. Section 3 is also sub-divided into two parts. It covers the synthesis and characterization of the feasibility study of the SSPs route for the preparation of V_8C_7/SiC ceramic nanocomposites. Vanadium modified SSPs has been synthesized by using two different vanadium precursors (vanadyl acetylacetonate-part 1 and vanadium oxytriisopropoxide-part 2). Detailed studies has been done related to the thermal conversion of the obtained single-source-precursor with respect to phase composition and microstructure. The preliminary investigation of the catalytic activity for the selected V_8C_7/SiC samples has also discussed. Further, the feasibility study for the fabrication of porous SiC-based ceramic nanocomposites via polymer-processing route using templates assisted method (paper, wood, and sacrificial) has also been discussed in part 2.

3.1. Pressureless fabrication of dense monolithic SiC ceramics

This section of the thesis presents the pressureless fabrication of dense and crack-free near stoichiometric SiC monoliths via cross-linking and pyrolysis of an allyl-hydrido polycarbosilane (SMP-10), followed by polymer-infiltration and pyrolysis cycles. The present study emphasizes the potential of the polymer processing technique for the fabrication of crack-free, near stoichiometric and dense SiC monoliths, which might be used for different structural applications at high temperatures and in harsh environments. Their high potential in applications for next generation nuclear energy will be emphasized. Thus, the overall process for the fabrication of dense silicon carbide-based ceramic parts involved four major steps:

(i) curing/pre cross-linking of the liquid preceramic polymer at moderate temperatures to obtain a SMP-10-based powder;

(ii) shaping using warm-pressing techniques;

(iii) ceramization process of the shaped green-bodies, which are converted into SiC-based monoliths by heat treatment at temperatures ranging from 1050 to 1700 °C and

(iv) liquid polymer infiltration and pyrolysis (PIP).

The prepared green bodies and the ceramic monoliths were investigated with respect to their phase and chemical composition as well as concerning their evolution at high temperatures.

3.1.1. Characterization of pre cross-linked/cured precursors

A commercially available allyl-hydrido polycarbosilane was used as suitable polymer for the preparation of SiC monoliths (SMP-10, Starfire Systems). SMP-10 is a clear, amber-colored, viscous liquid which requires no solvents for processing. The molecular structure of SMP-10 (Figure 3-1) indicates that two main mechanisms can contribute to its thermal cross-linking process, i.e., hydrosilylation and dehydrocoupling reactions.

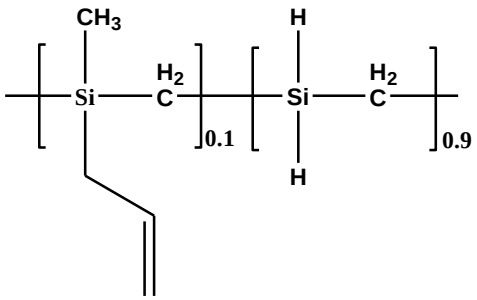

Figure 3-1. Structure of allyl-hydrido polycarbosilane (SMP-10) used for this study [76, 157].

The liquid SMP-10 was thermally cured at different conditions in order to obtained SMP-10-based powders. The obtained powders were investigated by means of ATR-FTIR spectroscopy (Figure 3-2). The band at around 1034 cm^{-1} (CH_2 bending in Si-CH_2-Si) and at 2900 cm^{-1} (C-H stretching in Si-CH-) present in all samples indicates the existence of a Si-CH_2-Si chain, the backbone of polymer. The strong band at ca. 2115 cm^{-1} and 928 cm^{-1} was assigned to Si-H groups, whereas the bands at 1625 and 3076 cm^{-1} were assigned to the allyl-groups (low intensity, due to the low amount, i.e., 5 mol%). The absorption at 747 and 833 cm^{-1} is attributed to Si-CH_3 rocking and Si-C stretching.

As obvious from the FTIR spectra, there is a large excess of Si-H groups (if related to the amount of allyl-groups) is present. As the polycarbosilane is thermally treated at high temperatures, the disappearance of the allyl-bands indicates that hydrosilylation occurred under these conditions. There is not any considerable change has been observed with respect to Si-H band till 300 °C.

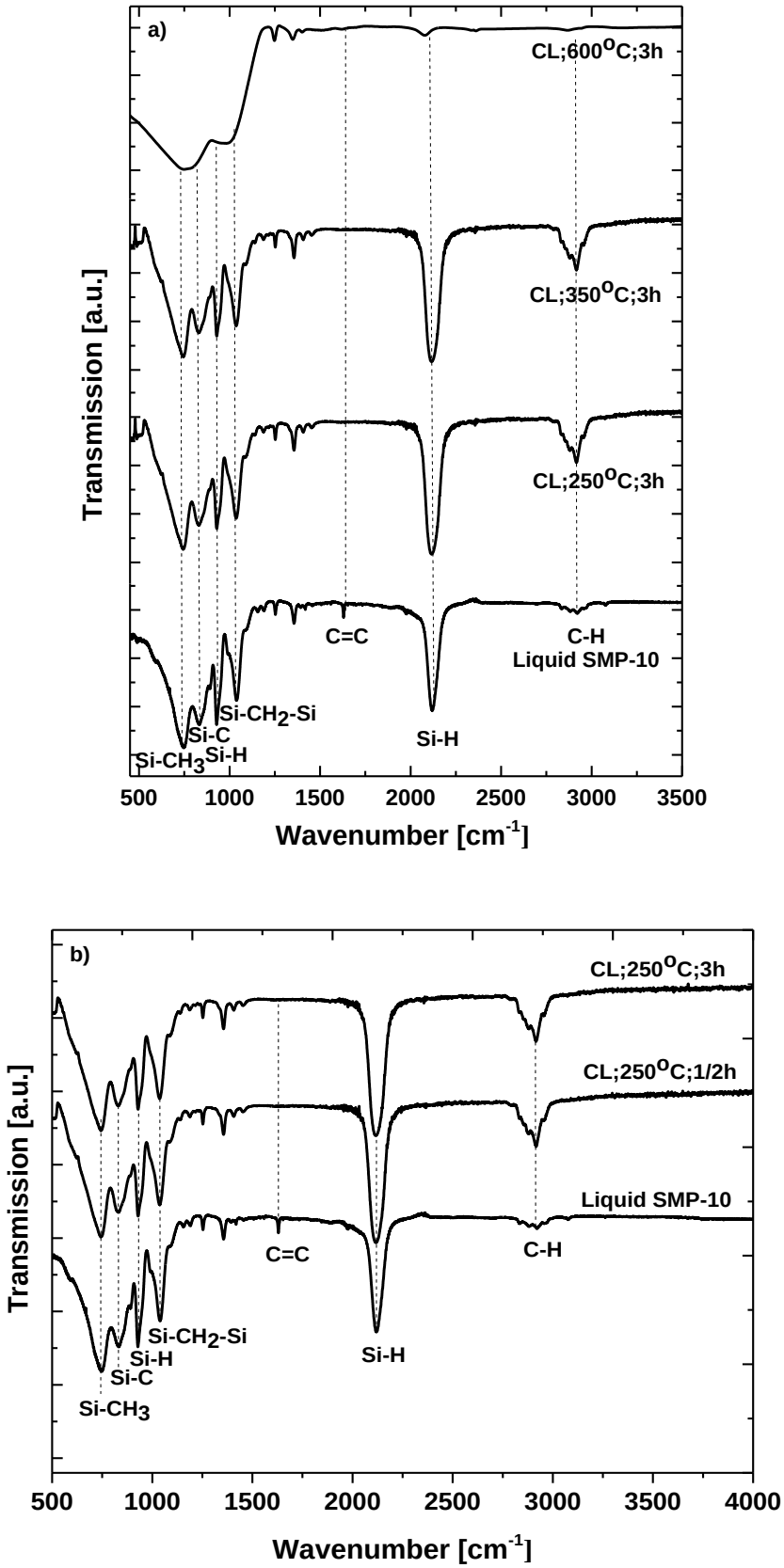

Figure 3-2. ATR-FTIR spectra of liquid SMP-10 as well as cross-linked samples at different temperatures (a) for different holding time (b).

Accordingly, after the complete hydrosilylation process, subsequent cross-linking is expected to rely only on dehydrocoupling reactions [158]. The Si-H band intensity is sharply reduced/almost diminished at 600 °C, which confirms the completion of the crosslinking of the polymer. At higher temperatures the process of the ceramization starts which leads to the formation of amorphous SiC ceramic.

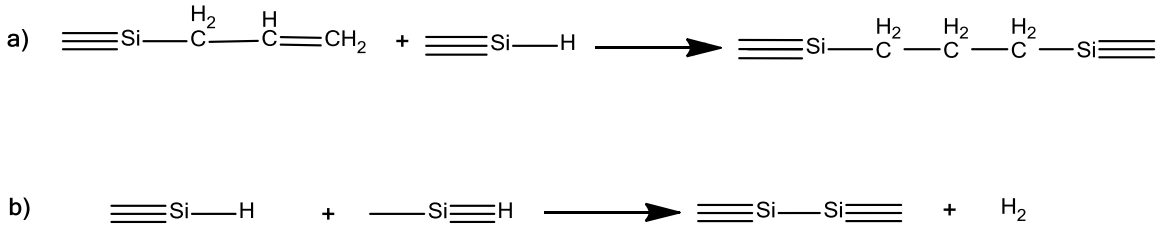

Figure 3-3. Hydrosilylation (a) and dehydrocoupling (b) reactions occuring upon thermal cross-linking of SMP-10.

Upon pre cross-linking of SMP-10 under various conditions, mass loss was recorded (as shown in Table 3-1), indicating that dehydrocoupling reactions occur (in addition to hydrosilylation) at these temperature. The effect of temperature and holding hours on the weight loss was also investigated. The results show that the increase of holding time increases the weight loss of the sample. In order to study in detail the polymer-to-ceramic transformation, thermogravimetric (TG) experiments coupled with evolved gas analysis (EGA) has been done.

Table 3-1. Mass losses of SMP-10 upon thermal treatment at different temperature for different dwelling times.

Curing temperature [°C]	Dwelling time [h]	Mass loss [wt%]
250	0.5	3-4
250	1.0	4-5
250	3.0	7-8
300	3.0	6-7

3.1.2. Polymer-to-ceramic transformation

The polymer-to-ceramic conversion of SMP-10 was studied by means of TG/EGA. As the TG curve shows (Figure 3-4), the decomposition of SMP-10 occurs mainly in two major steps. Major mass loss has been observed in the temperature range of 300-650 °C, due to dehydrocoupling reactions, as discussed above. At temperatures beyond 800-850 °C, no significant mass change is recorded, thus it is concluded that the polymer-to-ceramic transformation is completed at temperatures up to 800-850 °C. The ceramic yield amounts ca. 77 wt%.

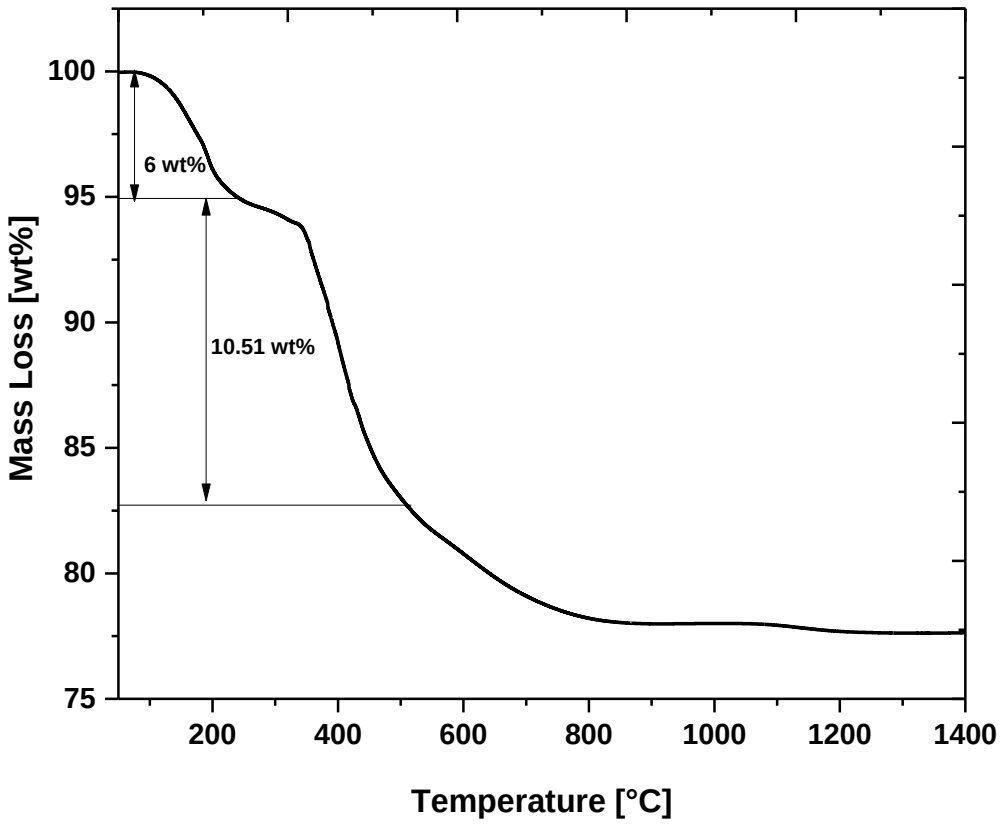

Figure 3-4. TG curve of the polymer-to-ceramic transformation of SMP-10.

In situ EGA study indicates that in the first main decomposition step (T < 250 °C) hydrogen (m/z = 2) and small polymer fragments evolve. These processes occur in the same time as the hydrosilylation process (zero mass change process) that means that under this temperature dehydrogenation and decomposition of polymeric fragment starts. In the second major decomposition step (400-850 °C), which represents the conversion of the preceramic polymer into an inorganic materials, H_2 (m/z = 2), SiH_4 (m/z = 32), and CH_3SiH_3 (m/z = 46) has been analyzed.

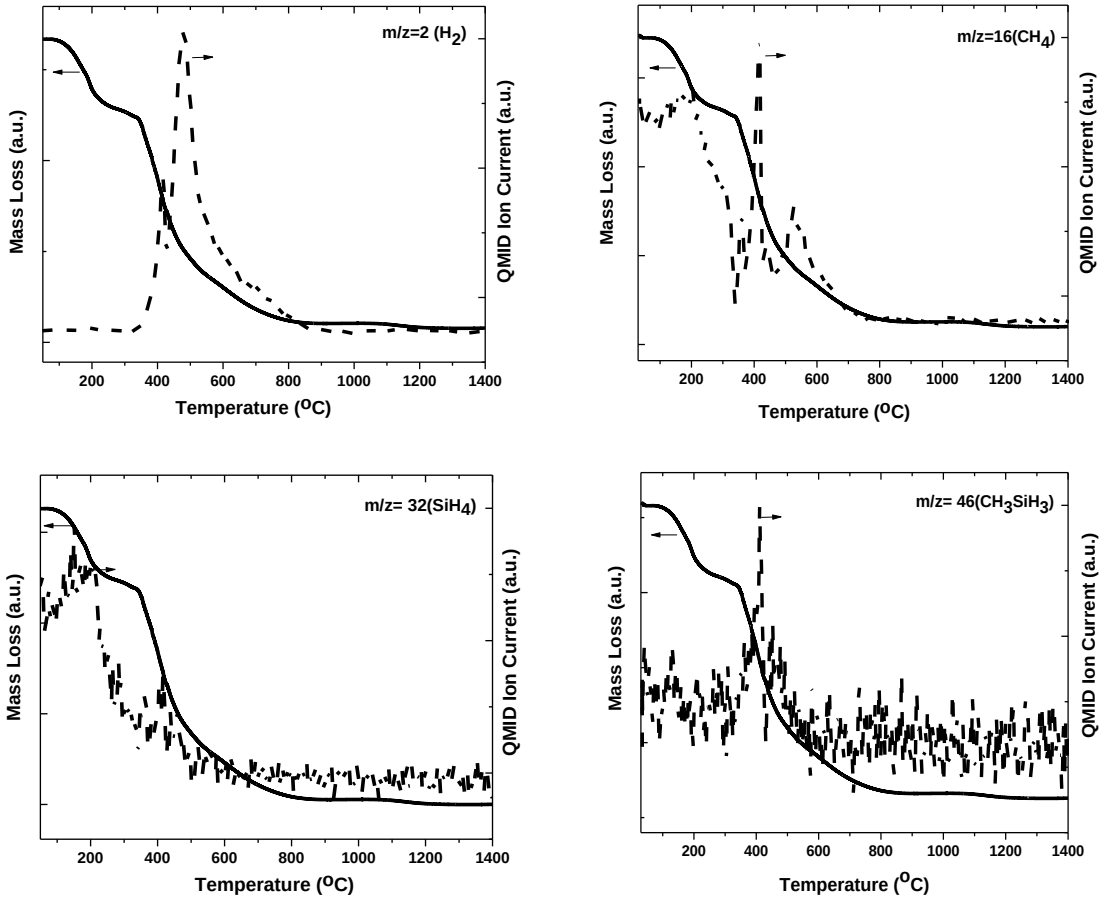

Figure 3-5. Quasi multiple ion detection (QMID) current curves during the polymer-to-ceramic transformation of SMP-10.

3.1.3. Phase separation at high temperature and elemental analysis

Figure 3-6 shows the XRD pattern of the samples annealed at different temperature under argon. The ceramic obtained by heat treatment at 1300 °C for 3h was X-ray amorphous. The XRD data of the ceramic materials annealed at higher temperatures indicate the crystallization of β-SiC. Additionally, small amounts of α-SiC were identified. Interestingly, despite the high temperature, the samples were not fully crystalline. Differences in thermal stability against crystallization between the prepared monolithic materials and SiC-based powders synthesized upon pyrolysis and annealing of SMP-10 were significant and mostly rely on their different specific surface areas, as it was observed also for other PDCs [159].

The elemental analysis of the ceramics obtained *via* pyrolysis of the liquid SMP-10 handled completely under argon shows a carbon content of 34-35 wt% and 3-4 wt% of oxygen present in the ceramic. This is thought to be related to a specific amount of

oxygen present in the SMP-10 polymer. The presence of minor amounts of the oxygen has been reported in the literature to range from 3 to 7 wt% and might be related to polymer synthesis and handling issues [62, 160, 161].

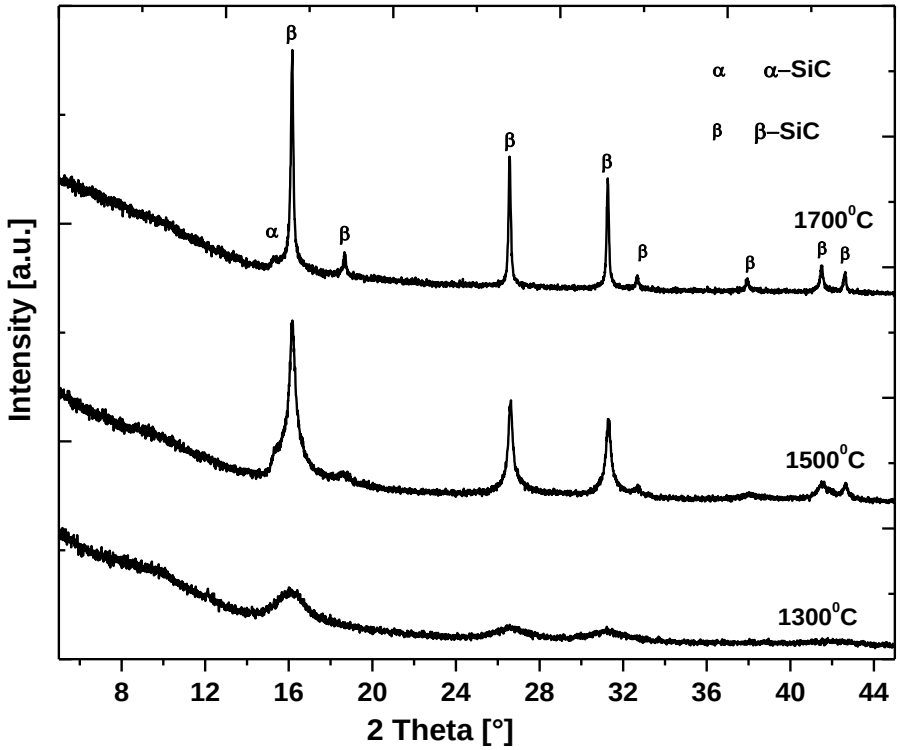

Figure 3-6. XRD patterns of polymer-derived silicon carbide obtained via annealing at high temperatures.

3.1.4. Processing of SiC-based monoliths

In order to obtained crack free green bodies, several experiments were done using different parameters. At low temperatures (180-250 °C), no compaction of the powders was observed. This is due to the fact that obviously the hydrosilylation process is already completed during curing/pre cross-linking of the liquid SMP-10 polymer and dehydrocoupling processes need higher temperatures. Thus, the compaction of the powder occurred at temperatures as high as 300 °C. However, crack formation within the green bodies occurred and was related to the high uniaxial pressures applied. Further optimization of the process (see Table 3-2) eventually led to the fabrication of crack-free SMP-10-based green bodies.

Table 3-2. Green-body fabrication from the cured SMP-10 powder (* - in these experiments the force was applied prior to the thermal loading; i.e., cold pressing + pressure release + pressureless cross-linking).

No.	Crosslinking temperature [°C]	Temperature [°C]	Pressure [MPa]	Holding Time [min.]	Remark
1	250	180	80-160	30	*No compaction*
2	250	250	80-160	90	*No compaction*
3	250	300	51-63.7	30	*Compaction; however, crack formation*
4*	**250**	**300**	**51-254.8**	**60**	***Crack-free green body***
5*	300	300	51-254.8	60	*No compaction*

The elemental analysis of the ceramic monoliths prepared within this study (i.e., obtained via warm-pressing of cured SMP-10 followed by pyrolysis at 1050-1300 °C) shows the incorporation of 5-6 wt % of oxygen within the ceramic network (Table 3-3). The slightly higher amount of oxygen (if compared to that of the sample prepared upon pyrolysis from liquid SMP-10, which was not warm-pressed) can be explained as a consequence of the warm-pressing step, during which the materials comes in contact with air for a short period of time. The incorporation of oxygen within the ceramic in turn produces

amorphous silica in the ceramic upon annealing at high temperatures [162]. The results of the elemental analysis of ceramic also show that the content of carbon as well as oxygen decreases with increasing the annealing temperature (Table 3-3). This consequently leads at higher temperatures (i.e., 1700 °C) to near stoichiometric silicon carbide composition, due to the carbothermal conversion of silica to silicon carbide.

$$SiO_2 + 3C \longrightarrow SiC + 2CO$$

Due to the fact that the ceramic monoliths prepared exhibit slight excess of carbon, the question was addressed whether a deliberate incorporation of small amount of oxygen will lead to the removal of the excess carbon upon annealing/pyrolysis at temperatures of 1300-1500 °C. Additionally, the intention was to assess to which extent processing of SMP-10 in ambient environment will affect its chemical composition (e.g., its oxygen content). Thus, the polycarbosilane was processed (cross-linked and warm pressed) under ambient atmosphere; whereas the polymer-to-ceramic conversion occurred in Ar atmosphere. The chemical compositions of the ceramics obtained upon heat treatment at 1050, and 1500 °C are shown in Table 3-3. Interestingly, air processing only slightly increases the oxygen content in the ceramic annealed at 1050 and 1300 °C if compared to the oxygen content of SiC processed in inert gas atmosphere. Moreover, the chemical composition of the SiC ceramics annealed at 1500 °C was found to be the same, independent of whether the polymer was processed in air or inert gas atmosphere (see Table 3-3).

Table 3-3. Elemental composition of SMP-10-derived SiC monoliths (*- these samples heat treated under air whereas other samples have pyrolysed under argon).

Sample	Temp. [°C]	Elemental content [wt%]			Empirical formula	Calculated content [wt%]		
		Si	C	O		SiC	C	SiO_2
11SiC	1050	62.45	31.88	5.67	$SiC_{1.19}O_{0.16}$	82.08	7.21	10.69
13SiC	1300	64.12	29.65	6.23	$SiC_{1.08}O_{0.17}$	83.80	4.52	11.66
15SiC	1500	64.95	32.22	2.83	$SiC_{1.16}O_{0.07}$	91.22	3.82	4.95
17SiC	1700	69.65	30.24	0.73	$SiC_{1.02}O_{0.01}$	98.50	0.74	0.74
11SiC-a*	1050	61.26	31.43	7.31	$SiC_{1.19}O_{0.20}$	79.17	7.64	13.18
15SiC-a*	1500	65.06	32.09	2.85	$SiC_{1.15}O_{0.07}$	89.94	5.56	4.88

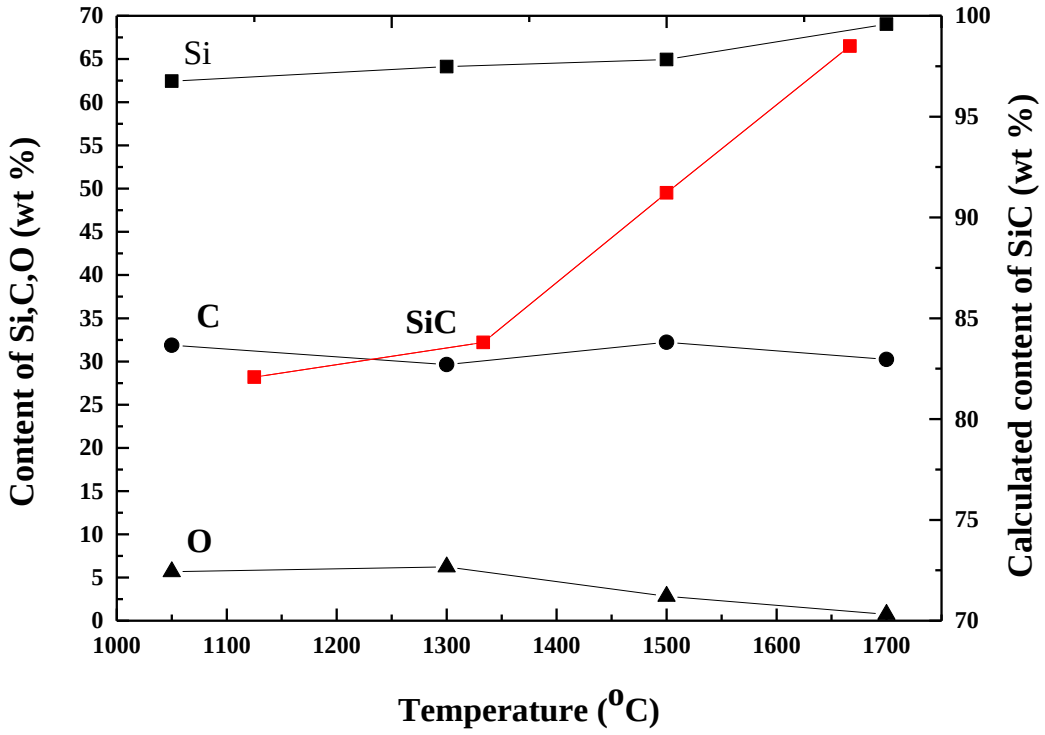

Figure 3-7. Variation of the elemental contents and silicon carbide with respect to temperature.

Mass loss, volume shrinkage, density and porosity of SiC-based ceramic monoliths at higher temperature are indicated in Table 3-4. The results show that the mass loss and the porosity of the ceramic monoliths increase with the temperature.

Table 3-4. Mass loss, volume shrinkage, density, and porosity of SiC-based ceramic monoliths annealed at different temperatures (the sample at 1050 °C was set as reference sample).

Sample	Temp. [°C]	Annealing Time [h]	Mass loss [wt%]	Volume shrikage [vol%]	Bulk Density [g/cm^3]	Porosity [vol%]
11SiC	1050	2	-	-	2.67	12.37
13SiC	1300	3	0.64	11.07	2.63	13.59
15SiC	1500	3	4.52	13.17	2.69	15.57
17SiC	1700	3	12.29	18.99	2.67	22.42

From the results obtained here we can conclude that the SiC ceramic monoliths obtained upon pyrolysis at 1050 °C contains some excess carbon (ca. 7 wt%) and oxygen; however, annealing at high temperatures leads to near stoichimetric SiC compositions (as for the monolith prepared upon annealing at 1700 °C). At the same time, the release of oxygen and of excess carbon (in form of CO) increases the porosity of the monoliths. The bulk

density of the obtained SiC ceramics was 2.63-2.69 g/cm^3, thus indicating that probably closed porosity is present within the samples, as it will be discussed later.

In Figure 3-8, SEM micrographs of silicon carbide monolithic samples heat treated at 1050 °C and at 1700 °C are presented and clearly show the effect of the annealing temperature on the porosity. Thus, the porosity of the SiC monolith significantly increases upon annealing at 1700 °C, as it was also determined by means of water immersion technique (~12 vol% for the sample prepared at 1050 °C vs. ~22 vol% upon annealing at 1700 °C). In addition, the pores in the sample prepared at 1050 °C were smaller than those found in the sample annealed at 1700 °C (smaller and larger than 10 μm, respectively).

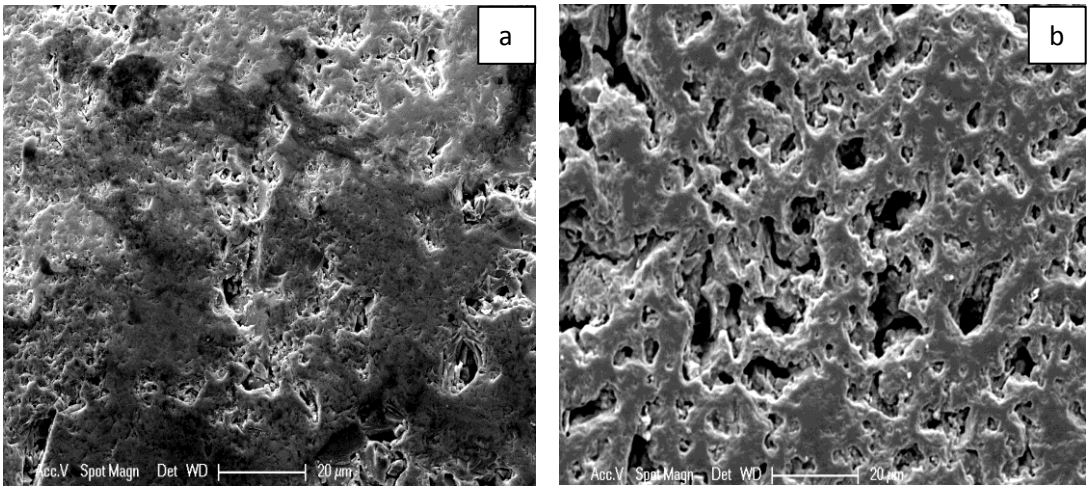

Figure 3-8. SEM images of cross section of silicon carbide monolith at 1050 °C (a) and at 1700 °C (b).

For further densification of the silicon carbide ceramic, the technique of liquid polymer-infiltration and pyrolysis (PIP) has been used [163]. As liquid precursor for the infiltration step, the same polymer used for the fabrication of the silicon carbide ceramic monoliths (i.e., SMP-10) has been taken, as it fulfills the requirements needed for liquid infiltration and pyrolysis, e.g., low and modifiable viscosity, high ceramic yield, phase and chemical purity upon pyrolysis, ease of use, relatively low volume shrinkage, etc. [164] . As shown in Table 3-5, PIP clearly helps in decreasing the porosity of the monolith. Thus, after only 6 PIP cycles the residual porosity of the SiC monoliths was reduced to less than 1 vol% [76].

Table 3-5. The porosity of SiC monoliths after PIP processing (pyrolysis was performed at 1050 °C) and subsequent annealing at 1700 °C.

No of infiltration cycles	Sample	Porosity at 1050 °C [vol%]	Porosity at 1700 °C [vol%]
1	PIPSiC-1	16.62	18.28
2	PIPSiC-2	ND	ND
3	PIPSiC-3	10.65	13.24
4	PIPSiC-4	3.25	7.87
6	PIPSiC-5	0.49	ND

As the SEM micrographs of 4-times PIP-ed sample clearly shows (Figure 3-9), the pores were filled by ceramic and thus a dense and crack-free surface was obtained. However, annealing of the PIP-ed samples at 1700 °C induced a slight increase of their open porosity. This relates to the fact that the infiltrated SiC(O) material exhibits some mass loss (upon CO release) while annealed at 1700 °C.

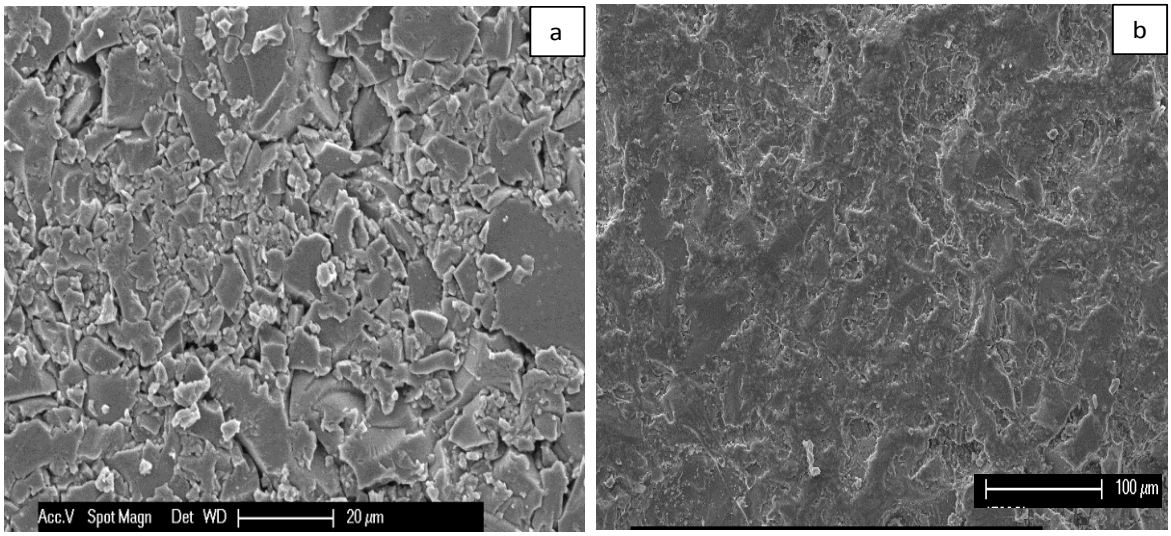

Figure 3-9. SEM images of silicon carbide (a) and infiltered silicon carbide monolith (4 PIP cycles) (b) after annealing at 1050 °C.

Indeed, the PIP-ed samples prepared at 1050 °C showed, similarly to the prepared SiC monoliths, some low amount of oxygen and excess carbon (Table 3-6). Thus, a three times PIP-ed SiC monoliths have ca. 3.8 wt% oxygen and 5.5 wt% excess carbon. However, upon annealing of the sample at 1700 °C the oxygen and the excess carbon were effectively removed and however, contributed to a slight increase of the residual porosity of the samples.

Table 3-6. Elemental composition of PIP-derived SiC monoliths.

Sample	Temperature (°C)	Elemental content [wt%]			Empirical formula	Calculated content [wt]%		
		Si	C	O		SiC	C	SiO_2
PIPSiC-3	1050 °C	64.13	31.36	4.51	$SiC_{1.14}O_{0.12}$	86.25	5.49	8.24
PIPSiC-3	1700 °C	67.94	31.79	0.27	$SiC_{1.09}O_{0.008}$	96.68	2.73	0.58

3.1.5. Summary

The present study indicates that crack-free and dense silicon carbide monoliths can be prepared by pressureless cross-linking and pyrolysis of a polycarbosilane (SMP-10) followed by PIP treatment. The obtained monoliths were shown to be crack-free even upon annealing at high temperatures, despite of a large volume shrinkage occurring upon pyrolysis. The elemental analysis data revealed that at low annealing temperatures some excess carbon is present within the ceramic monoliths; additionally, oxygen has been found to be present (several wt%). Both the carbon and the oxygen contents decrease upon increasing the annealing temperature; thus, at temperatures beyond 1500 °C near-stoichiometric SiC can be obtained. The bulk density of the obtained SiC ceramics (2.63-2.69 gm/cm^3) was rather low as compared to other silicon carbide-based ceramics, due to the presence of some excess carbon and porosity in the monoliths. Thus, the obtained ceramic monoliths have been shown to exhibit residual porosities of 15-25 vol%, which however can further be reduced to less than 1 vol% by using the PIP method to obtain crack-free and dense SiC-based monoliths.

3.2. Boron modified SiC-based ceramics

3.2.1. Boron-containing SSPs using borane dimethylsulfide

3.2.1.1. Characterization of boron-containing SSPs

Single-source-precursors have attracted attention for boron-containing SiC due to the improved homogeneity of the resulting ceramics. The allyl- and hydrido-substituents at silicon in the allyl-hydrido polycarbosilane (SMP-10) help to adjust its chemistry and network architecture. The incorporation of boron within the network of SMP-10 was achieved upon hydroboration reactions of the allyl-groups [62, 81, 165]. Thus, borane complexes (such as borane dimethyl sulfide complex, BMS) was used for hydroboration purposes.

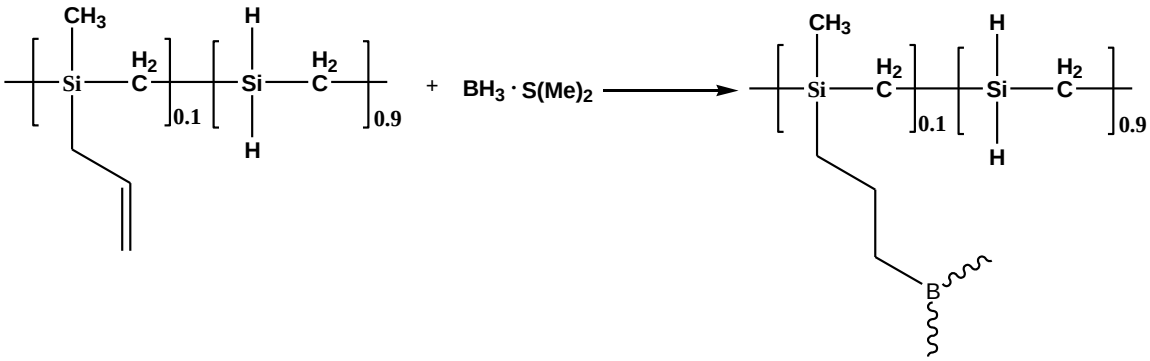

Figure 3-10. Hydroboration reaction of SMP-10 by using BMS.

Hydroboration and dehydrocoupling reactions are the two main mechanisms contributing to the thermal cross-linking process of the boron-containing SSPs. A number of experiments has been performed with different BMS to SMP-10 ratios, e.g., 1 wt%, 5 wt%, and 30 wt% of BMS (SiBC-1, SiBC-5, and SiBC-30), in order to investigate the effect of boron on the precursor-to-ceramic transformation as well as on the densification behavior of the resulting ceramic. The approximate boron content in the resulting ceramic samples is shown in Table 3-7, indicating that the amount of boron which has been incorporated within SiC upon pyrolysis of the boron-containing SSPs samples containing 5 and 30 wt% boron does not differ significantly (0.98 and 1.27 wt%, respectively). This clearly indicates that the borane only reacts with the allyl-groups. As this reaction is complete, the excess borane will be removed from the mixture during the processing steps involving high temperatures.

Table 3-7. SiBC ceramic samples prepared in the present study upon using different BMS : SMP-10 weight ratios (the molar ration BH_3 : allyl- was estimated by assuming the molar mass of SMP-10 being 450 Da and that SMP-10 contains 5 mol% allyl-groups [166]).

Sample	BMS : SMP-10 [weight ratio]	BH_3 : allyl-groups [molar ratio]	Empirical formula (as prepared at 1100 °C)	B content in ceramic [wt%]
SiBC-1	1 : 99	1 : 1	$Si_1B_{0.007}C_{1.31}O_{0.13}$	0.18
SiBC-5	5 : 95	6.5 : 1	$Si_1B_{0.04}C_{1.32}O_{0.15}$	0.98
SiBC-30	30 : 70	56.3 : 1	$Si_1B_{0.05}C_{1.28}O_{0.16}$	1.27

Experiments on pressure-assisted sintering of silicon carbide containing boron addition indicate that there is a lower limit of efficiency (0.3-0.4 wt%) below which there is essentially no effect thereof on densification [97]. It has been reported that the incorporation of <1 wt% boron into SiC ceramics significantly improved sintering [165, 167]. Thus, the composition derived from SMP-10 modified with 5 wt% BMS (i.e., SiBC-5) was used for the preparation of the monoliths.

The prepared polymeric samples were investigated by means of ATR-FTIR spectroscopy. The ATR-FTIR spectrum of the boron-free cross-linked SMP-10 (250 °C, 3h) shows an absorption band at 1034 cm^{-1} which was attributed to the Si-CH_2-Si stretching; furthermore, two bands at 1360, 2900 cm^{-1} were assigned to C-H bending and stretching, respectively, in Si-CH_2. The band at ca. 1253 cm^{-1} shows the existence of Si-CH_3 stretching. The strong bands at ca. 2119 cm^{-1} (Si-H stretching) and 933 cm^{-1} (Si-H bending) were assigned to Si-H groups, whereas the bands at 1631 (C=C stretch in -CH=CH_2) and 3076 cm^{-1} (C-H stretch in -CH=CH_2) were assigned to the allyl- groups (low intensity, due to the low amount, i.e., 5 mol%). The absorption at 747 and 833 cm^{-1} was attributed to Si-C stretching and Si-CH_3 rocking [62, 165].

The SiBC-1 sample contains a small amount of allyl-groups, probably due to the incomplete hydroboration reaction and thus there is still possible to further incorporate more boron within the structure of SMP-10; whereas for the other boron-modified SSPs (i.e., SiBC-5 and SiBC-30), the disappearance of the bands corresponding to the allyl-groups indicates that their reaction with $BH_3{\cdot}SMe_2$ occurred under the reaction conditions to completion. Furthermore, the cross-linked boron-modified SMP-10 samples (250 °C / 3h) showed the disappearance of the band corresponding to Si-H; as the amount of the allyl-substituents is markedly lower than that of Si-H bonds, this fact indicates that

dehydrocoupling reactions (*cf*. ≡Si-H + H-Si≡ = ≡Si-Si≡ + H_2) occured under these conditions. However, the activation of dehydrocoupling reaction leads to a cross-linking degree of the preceramic polymer which is too high (i.e., the cross-linked polymer possesses no softening point) and thus does not allow for its further processing. The dehydrocoupling reactions of the Si-H units in the boron-modified precursor were shown to be activated already at temperatures as low as 100 °C.

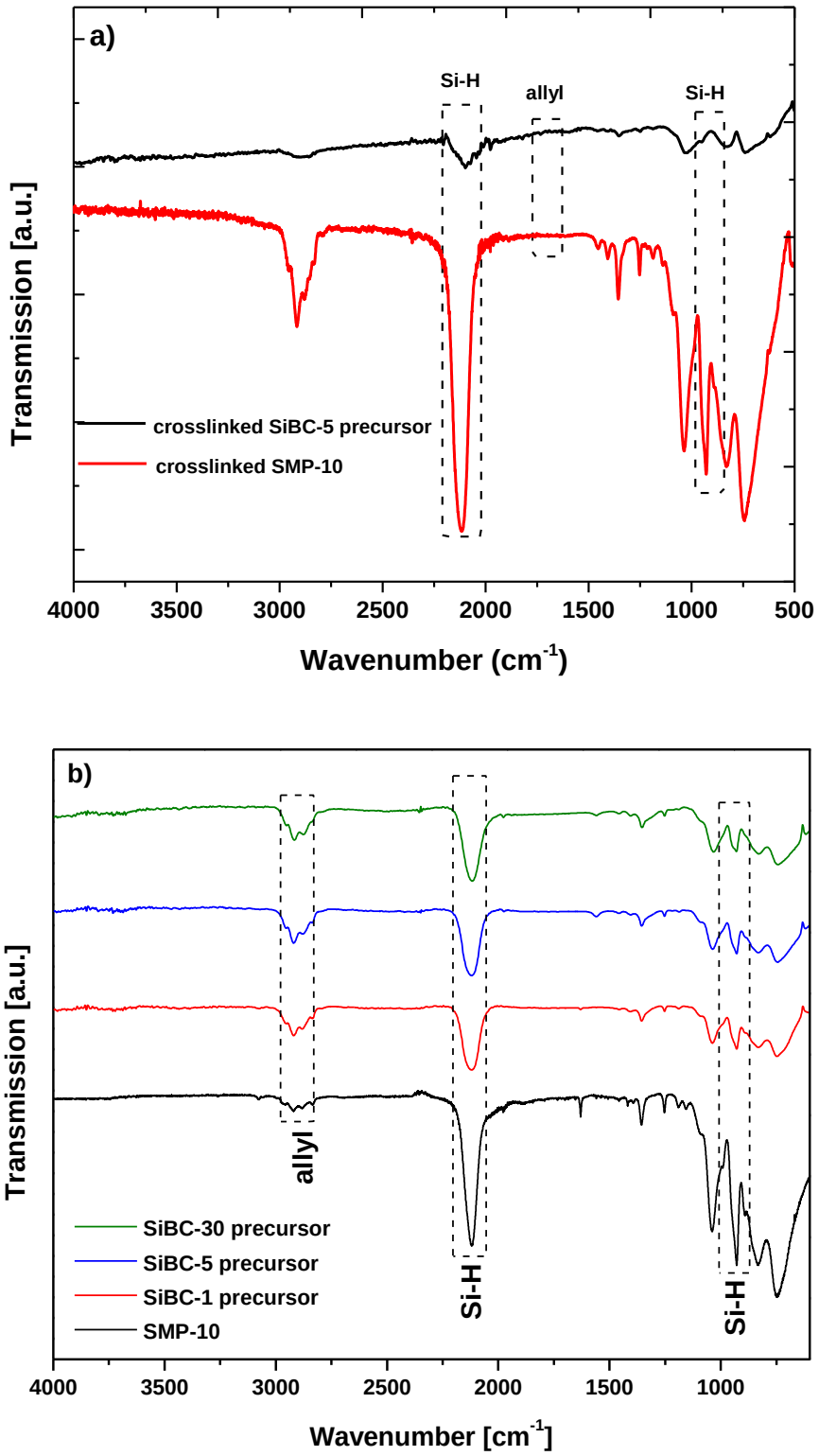

Figure 3-11. FTIR spectra of cross-linked SMP-10 and cross-linked SiBC-5 precursor (a); SMP-10 and boron-modified precursors (b).

3.2.1.2. Polymer-to-ceramic transformation

Considering the facts mentioned above related to the incorporation of boron into SMP-10 and its strong effect on the cross-linking behavior (and thus on the processability) of the modified SMP-10, the most suitable composition for the subsequent processing to obtain dense SiC monoliths corresponds to the SiBC-5 precursor, which was processed via warm-pressing and pyrolysis into ceramic SiBC monoliths. The incorporation of boron increases the cross-linking degree of SMP-10 and thus the SiBC-5 is a solid; nevertheless, as only hydroboration and hydrosilylation reactions took place, the precursor was still able to be processed as a thermoset, thus allowing for the preparation of SiBC-5-based green bodies upon warm pressing. This is a significant advantage as compared to the processing of the boron-free SMP-10 precursor, which requires a pre-crosslinking step (thermal treatment at 250 °C for 3h) prior to its processing via warm pressing and pyrolysis.

The polymer-to-ceramic conversion of SMP-10 and SiBC-5 was studied by means of TGA. As the TGA curves show (Figure 3-12), the decomposition of both samples occurs mainly in two major steps. Major mass loss has been observed in the temperature range of 300-650 °C, due to dehydrocoupling reactions as discussed in our previous work [26]. At temperatures beyond 800-850 °C, no significant mass change is recorded, thus it is concluded that the polymer-to-ceramic transformation is completed at temperatures up to 800-850 °C. The ceramic yield of the ceramic increases significantly upon boron-modification from ca. 77 wt% (as for SMP-10) to ca. 90 wt% (as for SiBC-5).

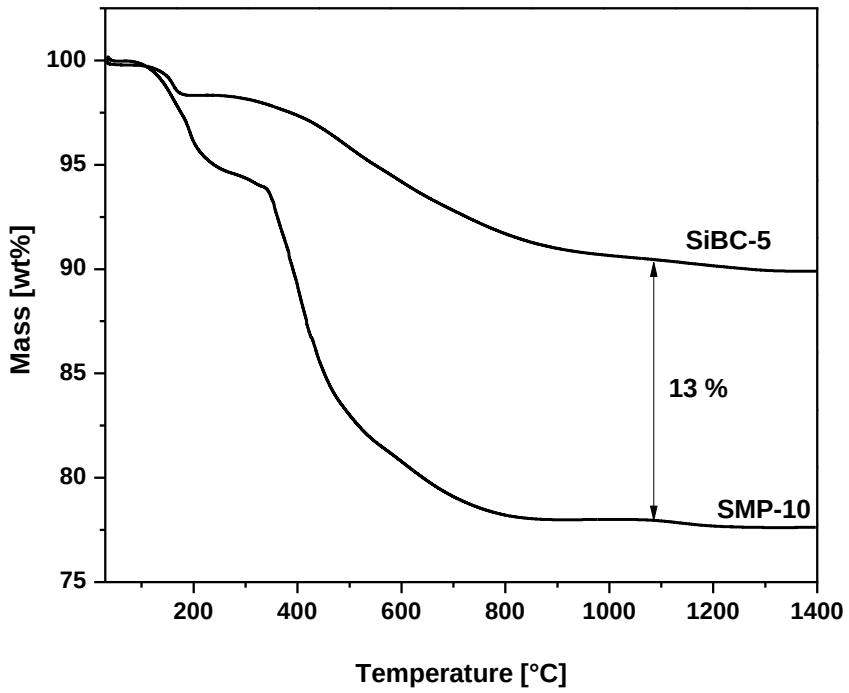

Figure 3-12. TG curve of the polymer-to-ceramic transformation of SMP-10 and SiBC-5.

3.2.1.3. Characterization of ceramic obtained at high temperatures

In order to investigate the fate of boron and its incorporation into the SiC ceramic, the SiBC-5 sample prepared upon pyrolysis at 1100 °C was characterized by FTIR as well as X-ray photoelectron spectroscopy (XPS). In the FTIR spectrum of SiBC-5 (Figure 3-13 a), a broad and intense band related to Si-C was observed at 790 cm^{-1}. The band at ~ 478 cm^{-1} has been assigned to rocking motion of oxygen atoms bridging silicon atoms (Si-O-Si) whereas at band at ~1079 cm^{-1} resulting from antisymmetric motion of silicon atom in Si-O-Si [168]; both indicating the presence of oxygen contamination within the SiBC-5 sample. Furthermore, broad bands at 1351.4 and 1552.0 cm^{-1} were assigned to sp^2 hybridized amorphous carbon, as reported in literature [169]. Interestingly, the presence of two additional bands at 1448.5 and 1662.0 cm^{-1} indicate the presence of boron within the segregated carbon phase, i.e., corresponding to BCB and CBC stretching vibrations, respectively [170]. Thus, the FTIR data indicate that SiBC-5 consists of silicon carbide, sp^2 amorphous carbon as well as boron-doped/boron-containing amorphous carbon. The existence of boron within the carbon phase was additionally substantiated by XRD, XPS and Raman data (see discussion below).

The sample SiBC-5 prepared at 1100 °C was also studied via XPS. As the XPS envelopes in Figure 3-13 b) show, the surface of SiBC-5 mainly consists of Si, C, and O. No B1s signal

was observed, probably because of the low amount of boron and the very low sensitivity of the B1s peak.

The O1s peak with a binding energy of 532.8 eV is fairly large and was mainly attributed to oxygen bonded to silicon [27]. This was further confirmed by the peak in Si2p at binding energy of 103 eV [171]. Whereas the Si2p peak at 100.9 eV was assigned to Si-C bonds, evidence the presence of the silicon carbide in the sample.

The deconvoluted C1s envelope consists of five peaks. The peaks centered at binding energies of 284.46 and 285.17 eV were assigned to sp^2 and sp^3 hybridized carbon, respectively [172]. Interestingly, there is a rather large amount of sp^3 carbon in the SiBC-5 samples; within this context, the XPS data are considered being complementary to the FTIR and Raman data, which mainly deliver information about the sp^2 hybridized segregated carbon phase. The C1s peak related to C-Si is centered at a binding energy of 283.06 eV. Moreover, a C1s peak at 286.2 eV was attributed to C-O bonding and relies on the presence of oxygen contamination (either in the sample or in the XPS chamber). One more signal centered at 283.8 eV was attributed to boron-containing carbon, as also reported in other studies [173], and relies on C-C-B bondings. Thus, the XPS results confirm the FTIR data and indicate that the boron is located within the segregated carbon phase.

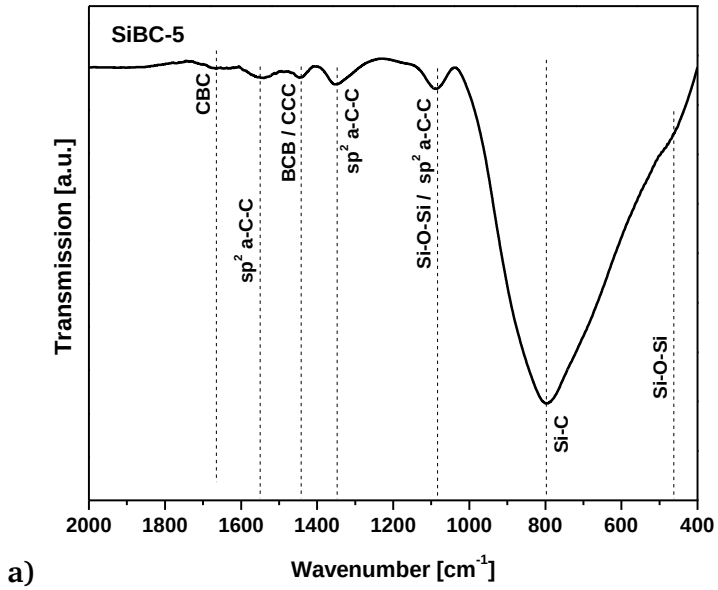

a)

b)

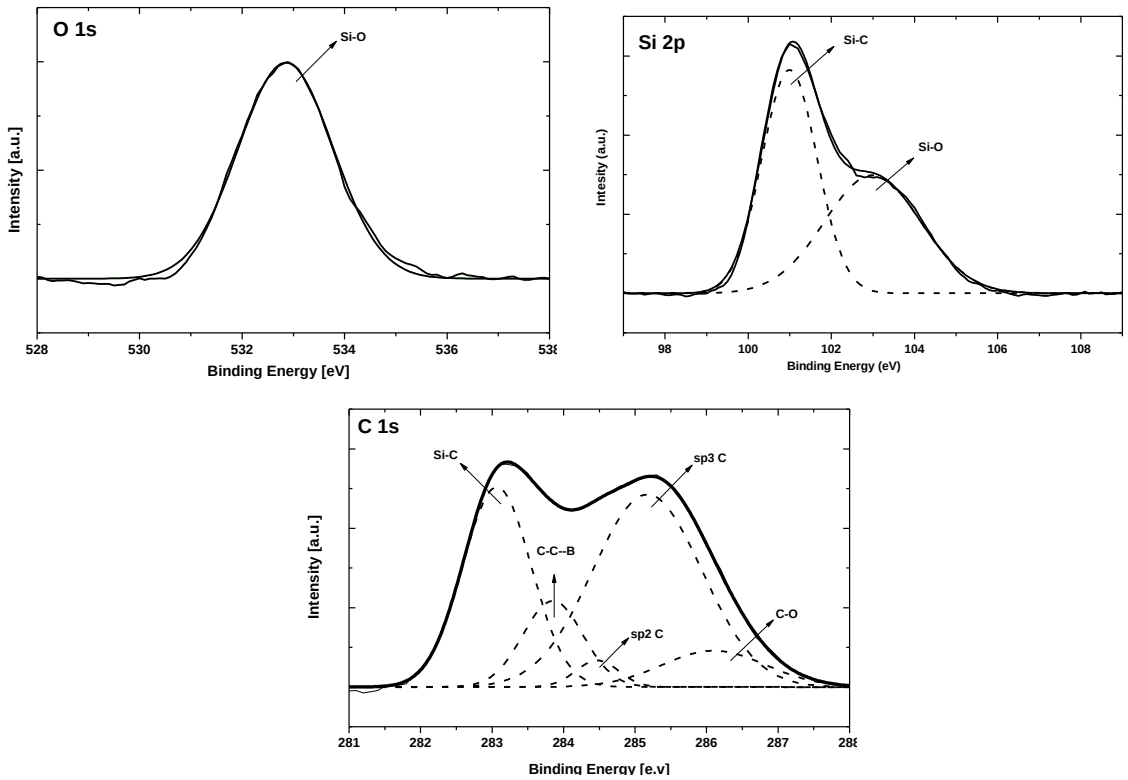

Figure 3-13. Base-line corrected FTIR spectrum (a) and deconvoluted XPS envelopes of C1s, Si2p and O1s (b) for the SiBC-5 sample, as prepared at 1100 °C.

The as-prepared Si(B)C samples were sintered at 1300, 1500, 1700, and 1900 °C (Ar, 3h). The crystalline phase composition of the produced materials was determined by

powder X-ray diffraction. Figure 3-14 shows the XRD patterns of the samples sintered at different temperatures under argon.

The boron-free SiC samples prepared upon heat treatment at temperatures up to 1300 °C were found to be X-ray amorphous and above this temperature crystallization starts in all samples. The main phase was β-SiC, characterized by main reflexes at 2θ values of 16.2, 18.7, 26.6, 31.3, and 32.7 °, which correspond to the (111), (200), (220), (311), and (222) reflections, respectively. The low-intensity reflection at ca. 15.3° (α-SiC) corresponds to stacking faults in β-SiC [174, 175]. The boron-containing samples showed upon annealing at high temperatures also the crystallization of β-SiC. The lattice parameter of β-SiC seems to be only marginally affected by the incorporation of boron into the preceramic polymer. Thus, the lattice parameter of β-SiC was 4.365 Å for the boron-free SiC sample annealed at 1900 °C; whereas for SiBC-5 it was slightly lower 4.362 Å. According to the literature, it is considered that the presence of substitutional boron in the β-SiC lattice leads to an increase of the lattice constant [176]; whereas the reduction of the β-SiC lattice parameter has been associated with the formation of a SiC-C solid solution [177], indicating that no boron was incorporated into the SiC phase. This agrees well with the reported solubility of B in SiC grains, which is very low (i.e., < 0.4 wt.% at 2200 °C [178]). Instead, probably some carbon was incorporated within the crystal lattice of β-SiC. The increase of the amount of stacking faults in the boron-containing sample as compared to that of the boron-free SiC sample further supports the assumption of solute carbon present within the SiC phase.

Upon annealing of the SiC and SiBC samples at high temperatures, an additional reflection related to graphitic carbon (i.e., the (002) reflection [179]) was detected (Figure 3-14 a). The interlayer spacing d_{002} was 3.415 Å in the the boron-free SiC sample, indicating the presence of a highly disordered segregated carbon phase (compare to d_{002} of 3.456 Å in carbon blacks) [180]. Whereas it significantly decreases upon incorporation of boron. Thus, in the SiBC-5 sample (containing 0.98 wt% boron) the d_{002} for the segregated carbon phase amounts 3.393 Å. Upon increasing the boron content from 0.98 wt% (as in SiBC-5) to 1.25 wt% (as for SiBC-30), a slight decrease of the d_{002} value from 3.393 to 3.390 Å has been observed. Thus, we consider the decrease of the interlayer spacing in the segregated carbon phase as being a consequence of the boron incorporation into carbon, as previously mentioned in various studies [179, 181-188].

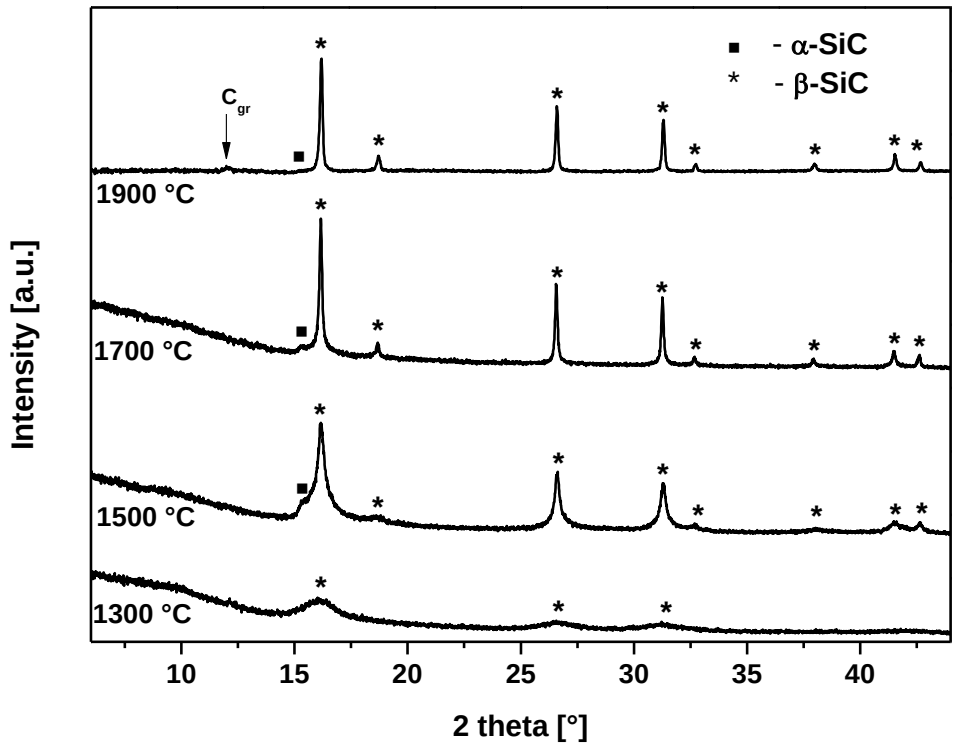

a)

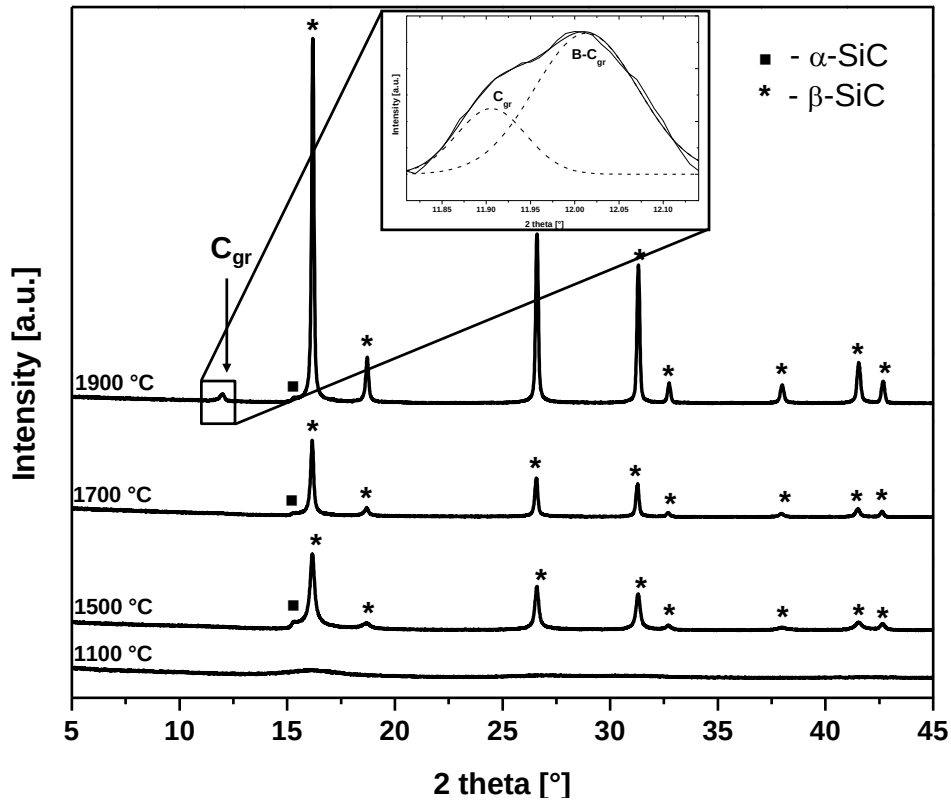

b)

Figure 3-14. XRD patterns of SiC (a) and SiBC-5 (b) annealed at different temperatures.

In order to understand the effect of boron incorporation into the carbon phase of the SiC ceramics, the prepared materials were analyzed with respect to their chemical composition. The results of the elemental analysis of the boron-free SiC ceramic samples prepared at different temperatures show that the content of carbon (30 wt %) as well as oxygen decreases with increasing temperature. This consequently leads at higher temperatures (i.e., 1700 °C) to near stoichiometric silicon carbide composition, due to the carbothermal conversion of the silica impurity to silicon carbide (cf. SiO_2 + 3 C = β-SiC + 2 CO) [26]. Thus, the SiC sample prepared at 1700 °C consisted of 98.5 wt% β-SiC; whereas the contents of segregated carbon and silica (a consequence of the presence of oxygen within the material) were below 1 wt% each. In comparison, the SiC sample prepared at 1100 °C exhibit ca. 7.2 wt% segregated carbon and more than 10 wt% silica. Interestingly, boron incorporation into polycarbosilane leads to an increase of the amount of the segregated carbon. Thus, SiBC-5 and SiBC-30 prepared at 1100 °C have carbon contents of 11.8 and 9.3 wt%, respectively. As the preparation temperature increases, the effect of boron on the content of segregated carbon becomes more accentuated. Thus, the SiBC-5 and SiBC-30 samples annealed at 1700 °C exhibit segregated carbon contents of 7.4 and 5.1 wt%, respectively, significantly larger than that found in the SiC sample annealed under the same conditions (i.e., < 1wt%).

If considering that boron is present exclusively in the segregated carbon phase, the estimated composition of the boron-containing carbon in SiBC-5 and SiBC-30 prepared at 1100 °C is BC_{11} and $BC_{7.3}$, respectively. Whereas the boron content slightly decreases upon annealing at 1700 °C, with the carbon phase having the estimated compositions $BC_{9.1}$ and $BC_{4.6}$ for SiBC-5 and SiBC-30 /Table 3-8).

The boron content in the segregated carbon phase of the prepared SiBC samples is rather large as compared to the maximum solubility of boron in graphite (i.e., ca. 2 wt% at 2900 °C) [189] and it seems to be for SiBC-30 even higher than the solubility of boron in amorphous carbons (ca. 10 wt%) [181]. Comparable and even larger boron contents in carbon were achieved only by using gas-phase techniques such as CVD. For example, Kouvetakis et al. [190] synthesized at 800 °C BC_3 (i.e., B content of 25 at%) by CVD techniques using benzene and BCl_3 as precursors [173]. Thus, one can conclude that the carbon phase generated *in situ* upon pyrolysis of polyborocarbosilane in the present study has the ability to accomodate significant amounts of boron and this might be a consequence of its high disorder. Interestingly, whereas other boron-rich carbons (such as BC_3) have a high tendency of crystallization and thus convert into B_4C ($B_{12}C_3$) at high

temperatures [173] (please note that the compositional stability range of B_4C has the lower boundary at ca. 8 at% and the upper boundary at ca. 19.5 at% [191-193]), the segregated boron-containing carbon phase in our materials does not convert into boron carbide, despite the very high annealing temperatures. The reason for this rather unique behavior might be related to the very low activity of the segregated carbon in polymer-derived ceramics [194], but this is still unclear and necessits further investigation.

Table 3-8. Elemental composition of SiC and SiBC samples as prepared at 1100 °C

Sample	**Temp. [°C]**	**Elemental content [wt%]**				**Empirical formula**
		Si	**C**	**O**	**B**	
SiC	1100	62.45	31.88	5.67	-	$Si_1C_{1.19}O_{0.16}$
SiBC-5	1100	59.79	33.98	5.27	0.98	$Si_1B_{0.04}C_{1.32}O_{0.15}$
SiBC-30	1100	60.21	32.90	5.62	1.27	$Si_1B_{0.05}C_{1.28}O_{0.16}$
SiC	1700	69.65	30.24	0.73	-	$Si_1C_{1.02}O_{0.01}$
SiBC-5	1700	63.93	34.46	0.65	0.80	$Si_1B_{0.03}C_{1.26}O_{0.017}$
SiBC-30	1700	65.56	33.2	0.14	1.10	$Si_1B_{0.04}C_{1.18}O_{0.003}$

Calculated content [wt%]				**Estimated composition of the boron-containing carbon phase / Boron content [at% of B]**
SiC	C	SiO_2	B	
82.08	7.21	10.69	-	-
79.29	10.14	9.63	0.92	BC_{10} / [9.09]
79.22	9.28	10.32	1.16	$BC_{7.3}$ / [12.05]
98.50	0.74	0.74	-	-
90.73	7.36	1.16	0.74	$BC_{9.1}$ / [9.90]
93.61	5.10	0.26	1.01	$BC_{4.6}$ / [17.86]

The boron-containing carbon phase in the prepared silicon carbide samples was also investigated by means of Raman spectroscopy (see Figure 3-15). Two main bands centered at 795 and 970 cm^{-1} (see Figure 3-15b, as for SiBC-5) were assigned to the transversal optic (TO) and longitudinal optic (LO) modes of β-SiC, respectively [195]. Whereas the other bands (i.e., at 1337, 1594, 2663 and 2926 cm^{-1}) are related to the segregated carbon phase in the samples, as discussed in detail below (see also Table 3-9). In addition, the spectrum shows a shoulder peak at 1627 cm^{-1} (D´), which is thought to directly correlate with the local structural distortion in graphite induced by the boron incorporation [196, 197].

There have been numerous spectral indicators being proposed in order to characterize and describe the nature, hybridization, crystallinity/degree of ordering in carbonaceous materials [198-201]. The structure of poly-/nanocrystalline graphites or disordered carbons are usually characterized by the average in-plane length (L_a, also called lateral cluster size), the average stacking height (so called L_c) and the average interplanar distance (i.e., in the 002 direction, as discussed above in this study). Additionally, the presence of tortuosity in disordered carbons (i.e., curvature of the graphene planes, described by L_{eq}) as well as the type and density of various defects (described by L_D, which gives the average distance between two defects) has been taken into account when describing their structure.

Raman spectroscopy is able to estimate the L_a values for carbonaceous materials from the first-order modes [198, 199, 201]. For values smaller than 2 nm, the equation proposed by Ferarri and Robertson was shown to be valid, i.e., $L_a^2 \times 0.0055$ Å^{-2} = I(D)/I(G) (as for a irradiation laser wavelength of 514 nm) [198]. Additionally, an average continuous graphene length (L_{eq}) parameter has been defined, which consider both L_a and the so-called tortuosity ratio (R_{tor}, being defined as the ratio between the number of phonons generated at the K point with second-order Raman process, and the number of phonons generated at the C point in the Brillouin zone with first-order Raman process, i.e., the ratio between the 2D band and the G band) and might be considered as an estimate of the equivalent phonon mean free path in disordered carbons [200]. L_{eq} can be determined for a laser wavelength of 514.5 nm cf. L_{eq} [nm] = 8.8 (A_{2D}/A_D), with A_{2D} and A_D being the integrated intensities of the 2D and D modes [200].

The parameter L_D can be determined cf. $I_D/I_G = C(\lambda)/L_D^2$, with C (514.5 nm) = 107 nm^2 (this relationship is valid only for $L_D > 6$ nm) and indicate the density of defects in carbonaceous materials [202, 203].

a)

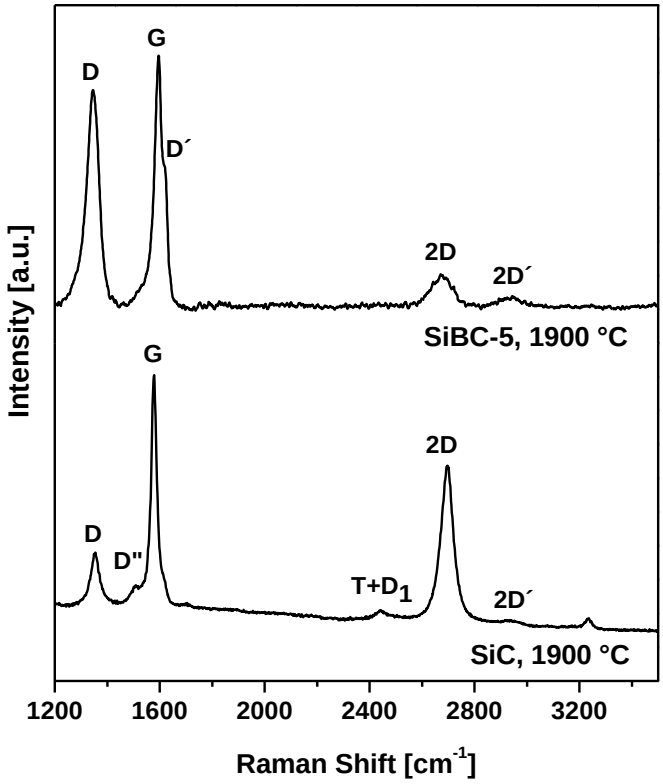

b)

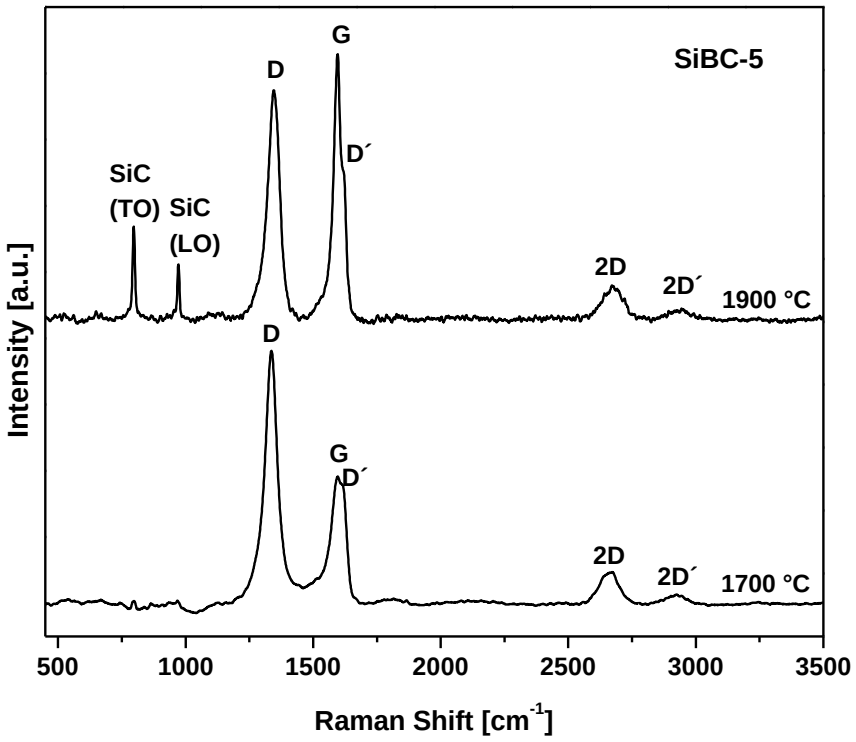

Figure 3-15. Raman spectra of (a) SiC and SiBC-5 annealed at 1900 °C, showing clear differences concerning the relative intensity of the D band; and (b) of SiBC-5 samples annealed at 1700 and 1900 °C, showing the LO and TO modes of crystalline SiC at 1900 °C.

Table 3-9. Raman data of the segregated carbon phase in SiC, SiBC-5 and SiBC-30 annealed at 1900 °C.

Raman Mode	SiC (1900 °C)		SiBC-5 (1900 °C)		SiBC-30 (1900 °C)	
	Raman shift ω [cm^{-1}]	FWHM Δω [cm^{-1}]	Raman shift ω [cm^{-1}]	FWHM Δω [cm^{-1}]	Raman shift ω [cm^{-1}]	FWHM Δω [cm^{-1}]
D (A_{1g})	1353.24	43.47	1347.11	52.10	1356.08	69.50
D"	1506.89	38.41	-	-	-	-
G (E_{2g})	1579.66	60.44	1582.81	84.22	1586.13	33.88
D´	-	-	1622.60	18.17	1617.99	17.17
T+D_1	2443.60	48.43	-	-	-	-
2D	2695.29	61.36	2674.39	91.64	2699.88	91.54
2D´	3233.74	26.01	2936.23	83.06	2940.16	93.75

The first order Raman spectrum of the boron-free SiC sample shows the presence of a band of E_{2g} symmetry, which relates to bond stretching of sp^2 carbon pairs contained in rings or chains [198]. This band is called G band and appears at around 1579 cm^{-1}. Disordered or nanostructured carbon-based materials (which might contain also some amount of sp^3 hybridization) exhibit additional bands in their first order Raman spectrum, such as a band of A_{1g} symmetry which relates to breathing modes of sp^2 carbon atoms within rings (so-called D band; its position depends on the laser wavelength; ca. 1345-1354 cm^{-1} at 514.5 nm), a band related to C-C sp^3 vibrations (ca. 1150-1200 cm^{-1}; can be observed upon UV laser excitation), a D" band (ca. 1500 cm^{-1}, related to amorphous carbon), as well as a D' band (ca. 1620 cm^{-1}) [198, 204, 205]. Also two-phonon modes such as 2D or 2D' are present (Figure 3-15 a).

The boron-free SiC sample annealed at 1900 °C shows the presence of relatively ordered carbon, as shown in Figure 3-15 a and indicated in Table 3-10 from the graphitization parameters I_D/I_G, L_a, L_D and L_{eq} [200]. Thus, the large value of L_D (21.6 nm) indicates a rather low defect density in the carbon phase, whereas the value of L_{eq} (38.7 nm, significantly higher than L_a with ~ 7 nm) supports the assumption of a rather ordered, tortuous carbon phase being present in the boron-free sample (Table 4). For the sake of comparison, the L_{eq} of a highly crystalline carbon sample obtained at 2500 °C in an acetylene flame (so-called graphitic carbon black) was determined to be 11.0 nm [200].

Please note within this context that L_{eq}/L_a ratios of 3-5 indicate high graphitization of the carbon phase, i.e., high-aspect-ratio, tortuous graphitic crystals [200] (in the case of the mentioned highly crystalline graphitic carbon black L_{eq}/L_a = 2.75; whereas for our SiC sample the L_{eq}/L_a value was as high as 5.5).

Boron incorporation induces a significant amount of disorder in the carbon phase [206]. Thus, for the SiBC-5 sample annealed at 1900 °C the intensity of the D band increases markedly as compared to that of the boron-free sample annealed under the same conditions (Figure 3-15 a). Moreover, the incorporation of boron into the carbon phase also induces a shift of the G band to higher frequency (probably related to the generation of holes due to the presence of substitutional boron in the carbon phase) and the appearance of a new band in the spectrum, i.e., the D' band (E_{2g} symmetry, ca. 1624-1643 cm^{-1}), which relates with disorder in the graphitic lattice related to surface defects [207]. Thus, both effects, i.e., the increase in the intensity of the D band and the appearance of the D' band, indicate an enhancement of the number of defects upon incorporation of boron into the carbon lattice. This indeed is also supported by the L_D value, which also strongly decreases from 21.6 nm in the boron-free SiC sample to 11.2 nm in SiBC-5 (Table 3-10). Additionally, the L_a and L_{eq} values (1.87 and 2.11 nm, respectively) and the L_{eq}/L_a ratio being close to unity clearly suggest the presence of a poorly graphitized carbon phase within the boron-containing samples.

Table 3-10. Graphitization indices for SiC, SiBC-5, and SiBC-30 prepared at 1900 °C.

Sample	I_D/I_G	A_D/A_G	L_a [nm]	L_{eq} [nm]	L_D [nm]
SiBC-30	0.659	1.533	2.87019	3.371153	12.7405226
SiBC-5	0.856	2.35	1.87234	2.112933	11.1640491
SiC	0.229	0.62879	6.99757	38.71038	21.6159411

As a main conclusion of the diffraction and spectroscopic study related to the effect of boron incorporation on the phase composition of silicon carbide, the fact that the *in situ* segregated carbon phase which precipitates during the pyrolysis of the polycarbosilane is able to incorporate significant amounts of boron upon inducing a strong disordering thereof is worth mentioning. Boron obviously prefers to substitute the carbon phase and does not incorporate within the SiC phase. Despite the achieved compositions of the segregated BC_x phase are in the compositional stability range of crystalline B_4C, no

crystallization of boron carbide is observed up to very high temperatures. This is a rather unique behavior which however still has to be clarified.

The effect of boron and carbon addition on the sintering behavior of silicon carbide has been investigated since longer time. For instance, it was found that a boron concentration of at least 0.3 wt % and a carbon additon of ca. 2 wt % were necessary to promote the densification of silicon carbide. The boron concentration is related to the solubility of the boron in the silicon carbide, as mentioned above [178]. Boron segregates along the grain boundaries and decreases the grain boundary energy; whereas carbon is useful for the removal of silica from the surface of the silicon carbide grains. Moreover, carbon addition results in the increase of the number of the silicon vacancies, thus promoting the silicon diffusion in SiC.

3.2.1.4. Processing of SiBC-based monoliths

The approximate content of boron in the prepared samples is shown in Table 3-7. The reason for taking SiBC-5 precursor for processing into monoliths is that in order to obtain densification, the optimum amount of boron should be equivalent to 0.3 wt% - 3 wt% is probably related to the solubility of boron in silicon carbide [208]. Moreover upon further increase of boron the oxidation resistance of the product is degraded [209]. Also the processing of SSPs obtained with 1 wt% and 30 wt% of boron was not possible to processed because of too low and too high degree of crosslinking repectively.

Experiments on pressure sintering of silicon carbide with the boron containing addition indicate that there is a lower limit of efficiency (0.3-0.4%) below which there is essentially no effect [97]. It has been reported that the incorporation of <1 wt % boron into SiC ceramics significantly improved sintering [165, 167]. These results support us to move further as we only able to processed SiBC-5 monoliths.

Mass loss, volume shrinkage, density and porosity of monolithic SiC and SiBC-5 samples are shown in Table 3-11. It is obvious that the incorporation of boron induces a significant improvement of the densification behavior of silicon carbide. Thus, SiC monoliths prepared at 1700 °C exhibit an open porosity of >22 vol%; whereas the SiBC-5 monoltihs prepared under the same conditions had a residual open porosity as low as ca. 4 vol%.

Interestingly, the skeletal density of the obtained SiBC ceramics was in the range from 2.5 to 2.65 g/cm^3, thus indicating that some closed porosity is present within the samples.

Longer annealing time at the sintering temperature probably will help to further suppress the closed porosity in the monolithic SiBC samples.

Table 3-11. Mass loss, volume shrinkage, density, and porosity of SiC and SiBC monolithic ceramics as prepared via cross-linking at 300 °C, followed by pyroylsis at 1100 °C and subsequent annealing at different temperatures.

Sample	Temp. (°C)	Holding Time [h]	Mass loss [%]	Volume shrikage [%]	Skeletal Density [g/cm^3]	Open Porosity [vol %]
SiC	1100	2	-	-	2.67	12.37
	1700	3	12.29	18.99	2.67	***22.42***
SiBC-5	1100	2	-	-	2.47	**4.59**
	1300	3	<1	6.52	2.56	**3.30**
	1700	3	12.59	11.78	2.65	**4.27**
	1900	3	11.7	17.13	2.48	***3.68***

Figure 3-16 shows the SEM micrographs of monolithic silicon carbide and SiBC samples as prepared at 1700 °C. The SEM micrographs support the data related to the residual porosity of the monoliths, indicating that the incorporation of boron reduces significantly the open porosity of the monoliths.

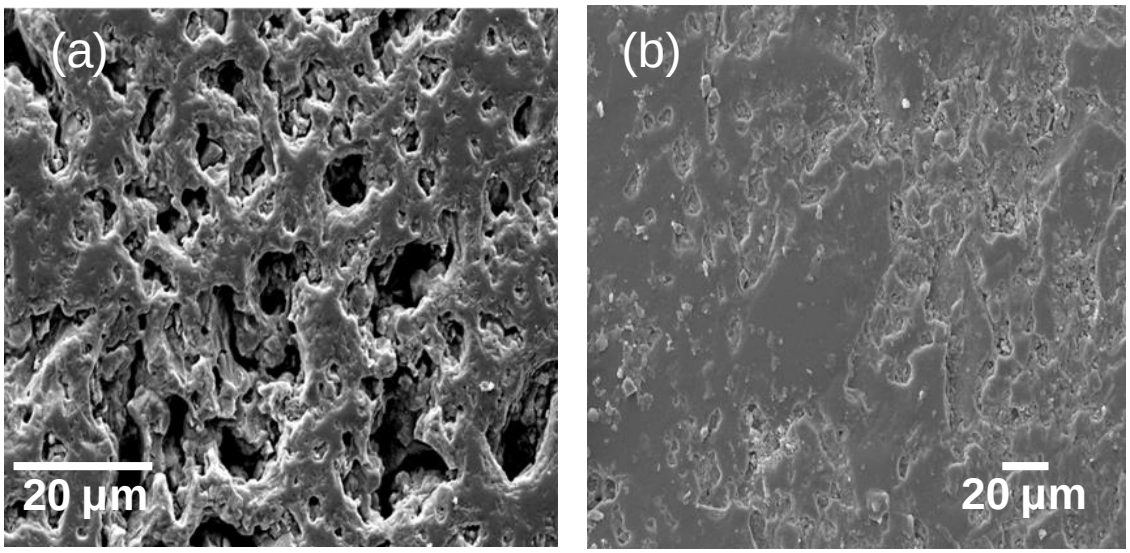

Figure 3-16. SEM micrographs of the surface of SiC (left) and SiBC (right), as prepared upon annealing at 1700 °C. Note that the measured open porosity in the SiC sample was 22.4 vol%; whereas the SiBC sample showed a value as low as ca. 4.3 vol%.

3.2.1.5. Summary

The present study shows that boron preferentially enters the carbon phase in polymer-derived SiBC materials and does not get incorporated into the silicon carbide lattice (at least not in significant amounts). Interestingly, the incorporation of boron into the structure of polycarbosilane induces an increase of the amount of segregated carbon in the resulting ceramics. Moreover, the resulting segregated carbon in the SiBC samples is shown to be markedly less graphitized than that present in boron-free SiC. Additionally, despite the rather large amount of boron present in the segregated carbon (i.e., 9 to 19 at%), no crystallization thereof to furnish boron carbide was found. Finally, results concerning the pressureless preparation of low-porosity SiBC monolithic samples confirms the beneficial effect of boron on the sintering behavior of silicon carbide.

3.2.2. Boron-containing SSPs using allyl-functionalized carboranes

In this part of work Boron-containing single-source-precursors were synthesized upon reactions of SMP-10 with allyl-functionalized carboranes (AFC). A detailed structural characterization of the allyl-functionalized carboranes (AFCs), SSPs obtained by the modification of allyl-hydrido polycarbosilane (SMP-10) with AFCs, and derived SiBC ceramics has been done by means of various spectroscopic techniques.

It also covers the effect of the architecture of the boron precursor onto the crosslinking degree of the SSPs, polymer-to-ceramic transformation, and phase composition of the final ceramics. In order to understand the effect of the molecular architecture, borane dimethylsulfide (BMS; detailed discussion in Section 3.2.1) and AFCs derived sample has been taken into consideration.

3.2.2.1. Characterization of allyl-functionalized carboranes and obtained SSPs

The AFCs which were selected for this studies are 1, 2-diallyl-*o*-carborane (S1) and 1, 7-diallyl-*m*-carborane (S2). The reason for selecting this compound is the presence of unsaturated C=C bond which has a strong affinity toward Si-H bond, present in the SMP-10 for hydrosilylation reaction. The synthesis of the allyl-substituted carborane derivatives was achieved upon nucleophilic substitution at the $C_{cluster}$ atoms (C_c). The protons bonded to the C_c atoms were removed by addition of n-BuLi and subsequent reaction with RCl (R=allyl-).

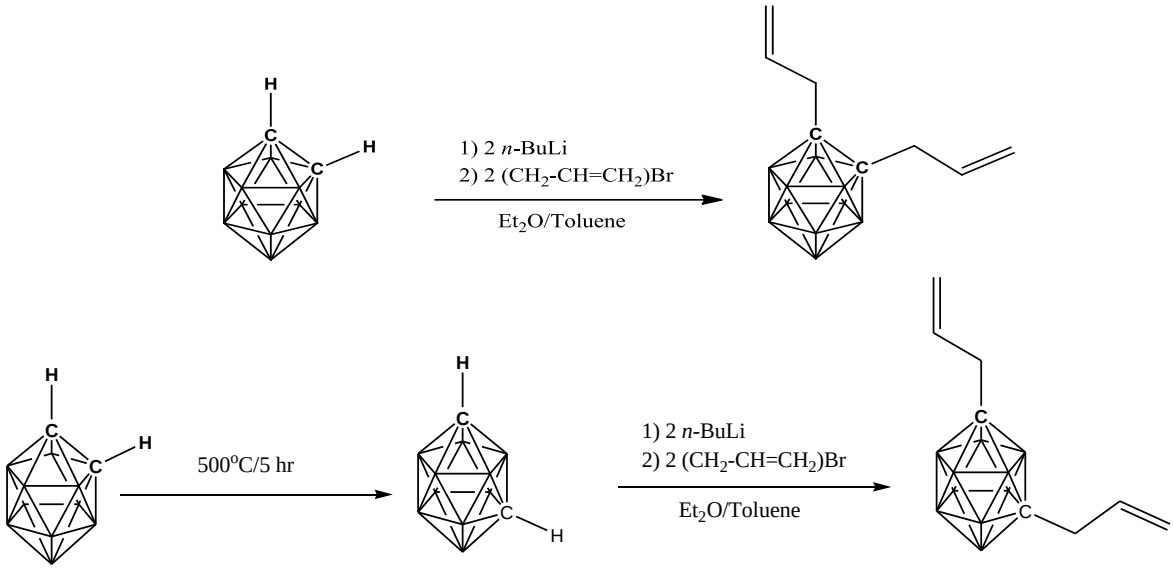

Figure 3-17. Synthesis of the diallyl-functionalized *o*-carborane (S1) and *m*-carborane (S2).

The synthesized functionalized carboranes were characterized by ^{1}H and ^{11}B NMR spectroscopy (Figure 3-18) [156, 210, 211]. The confirmation of the presence of the allyl-group has been done by ^{1}H (^{11}B) NMR, which shows three resonances at 2.9, 5.2, and 5.8 ppm being attributed to C_c-C*H*$_2$, CH=C*H*$_2$, and C*H*=CH$_2$, respectively. In the case of S2, the ^{11}B NMR spectrum exhibits three resonances at 7.47, 11.45 and 14.15 ppm which were assigned to CBC, BBB, and CBB, thus confirming the formation of the diallyl-functionalized-*m*-carborane. In addition to the diallyl-functionalized carborane, small amounts of unreacted *m*-carborane (-4.32 ppm) and monoallyl-substituted *m*-carborane (-15.8 ppm) were identified in the spectrum.

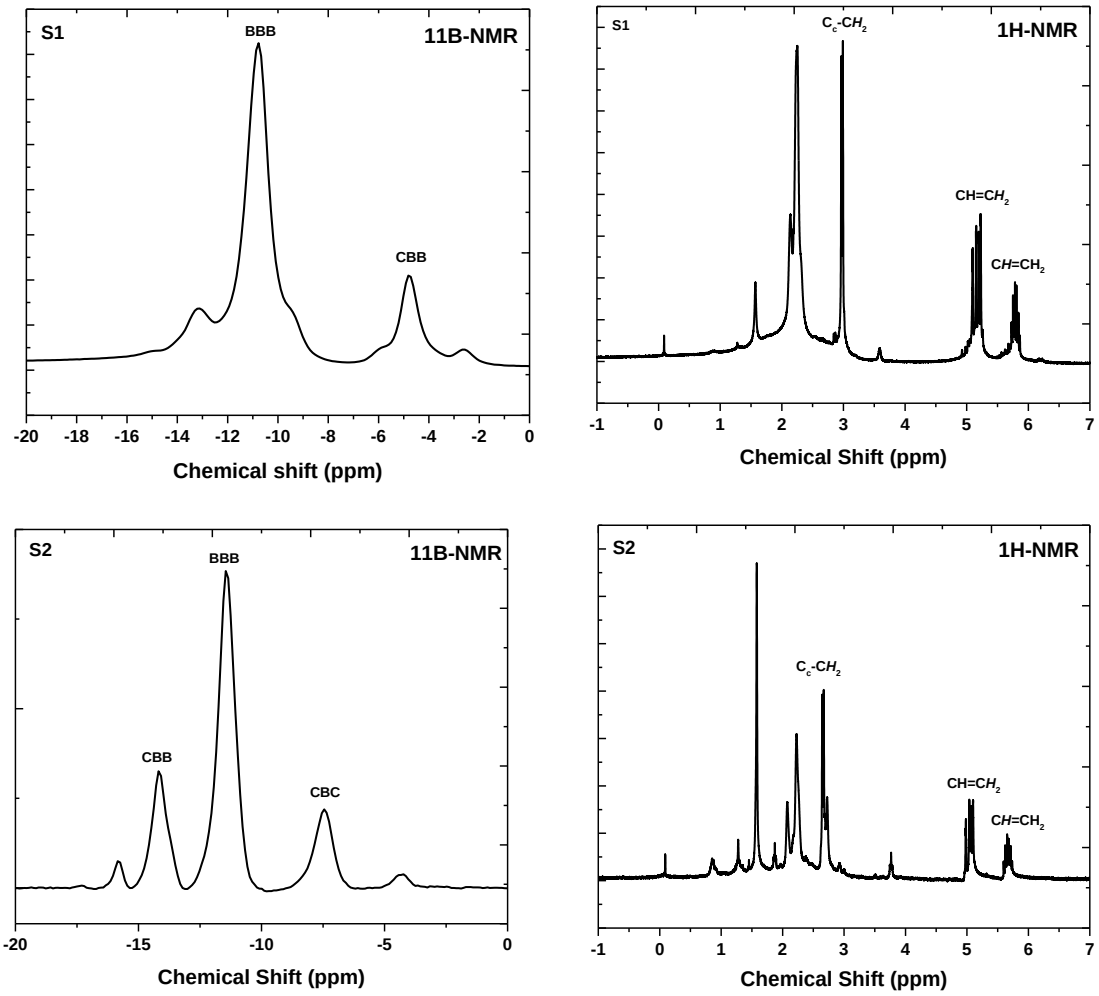

Figure 3-18. ^{1}B (left) and ^{1}H (right) NMR of the diallyl-functionalized *o*-carborane (S1) and *m*-carborane (S2).

The ATR-FTIR spectra (Figure 3-19) of the functionalized carborane samples show a typical ν(B-H) strong band at ~ 2588 cm^{-1}, a ν(C_c-H) band observed at ~ 3063 cm^{-1} and a

band at around 1643 cm^{-1} which was assigned to ν(C=C) indicating the successful synthesis of the allyl-substituted carboranes.

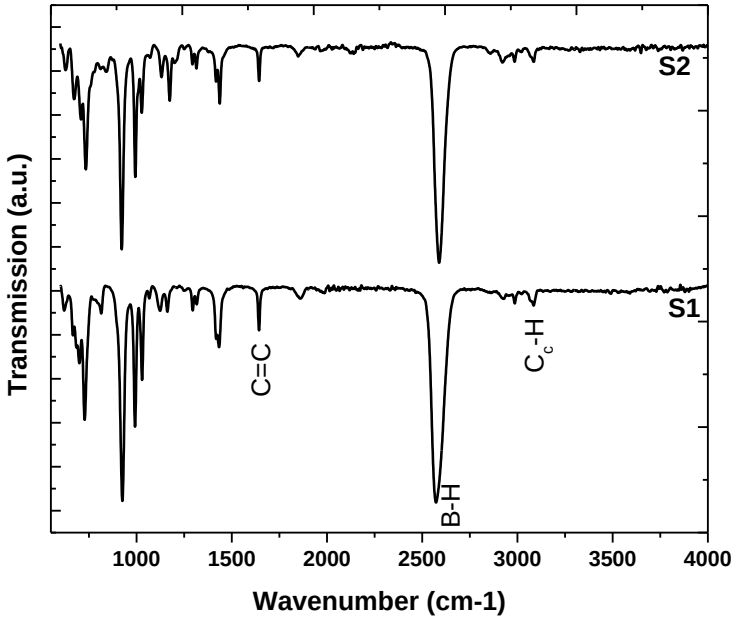

Figure 3-19. ATR-FTIR spectra of the synthesized *o*-carborane (S1) and *m*-carborane (S2).

The homogeneous mixture of SMP-10 and functionalized carboranes in toluene was dried in vacuum and the obtained precursors (*o*-AFC-SiBC pre/*m*-AFC-SiBC pre) were structurally characterized by ATR-FTIR spectroscopy. For the sake of comparison, the neat, SMP-10 without modified was also processed in the same way as the carborane-containing precursors and characterized by ATR-FTIR spectroscopy. As the Si-H groups in SMP-10 have been shown to be highly reactive, the reaction was performed without the use of a catalyst.

All prepared AFC-SiBC pre samples were shown to exhibit the characteristic bands related to SMP-10 and to the AFCs. Thus, the band at ca. ~2121cm^{-1} in the FTIR spectra was assigned to Si-H groups, whereas the bands at 1631 and 3070 cm^{-1} were assigned to the allyl-groups; moreover, ν(B-H) at ~2588 cm^{-1} and ν(C_c-H)(~ 3063 cm^{-1}) were observed and assigned to the carborane substituents in the precursors. There is no observable changes has been found in the ATR-FTIR spectra of the samples.

The AFC-SiBC pre samples are further thermally treated at 150 °C and the obtained samples (*o*-AFC-SiBC /*m*-AFC-SiBC) were further studied. The first observation made during the synthesis of the single-source-precursors refers to their physical state in the as-synthesized form. Thus, the chemical modification of the liquid SMP-10 with the allyl-

functionalized carboranes yielded gel-like, insoluble single-source-precursors (Table 3-12).

The ATR-FTIR spectrum shows, a relative decrease in the intensity of the Si-H band (unlike in SMP-10). The vibrational band corresponding to the allyl-group can be detected in all prepared carborane-containing precursors, but, unlike in SMP-10, a decrease in its relative intensity was observed (as with respect to Si-CH_3, ~1253 cm^{-1}). This indicates that the hydrosilylation occurred but was not completed (as it probably needs elevated temperatures to be completed). This is in agreement with the literature, which indicates that hydrosilylation reactions start at temperatures of ca. 120 °C and may need temperatures as high as 200 °C in order to complete.

Table 3-12. Physical state of the synthesized SSPs (as prepared - initial; and after heat treatment - final).

Sample Name	Functionalized carborane	SMP-10: functionalized carborane weight ratio	Physical state	
			Initial	Final
SMP	-	100:00	Liquid	Liquid
***o*-AFC-SiBC**	diallyl-functionalized *o*-carborane (S1)	95:5	Liquid	oil
***m*-AFC-SiBC**	diallyl-functionalized *m*-carborane (S2)	95:5	Liquid	gel

In all prepared carborane-containing single-source-precursors also a change in the intensity of the B-H band was observed, indicating that it might be involved within cross-linking reactions such as hydroboration reactions with allyl-groups or dehydrogenation processes as also discussed below. The first example of catalytic hydroboration of terminal alkyne with o-carborane was found in 1988 at 70 °C [212].

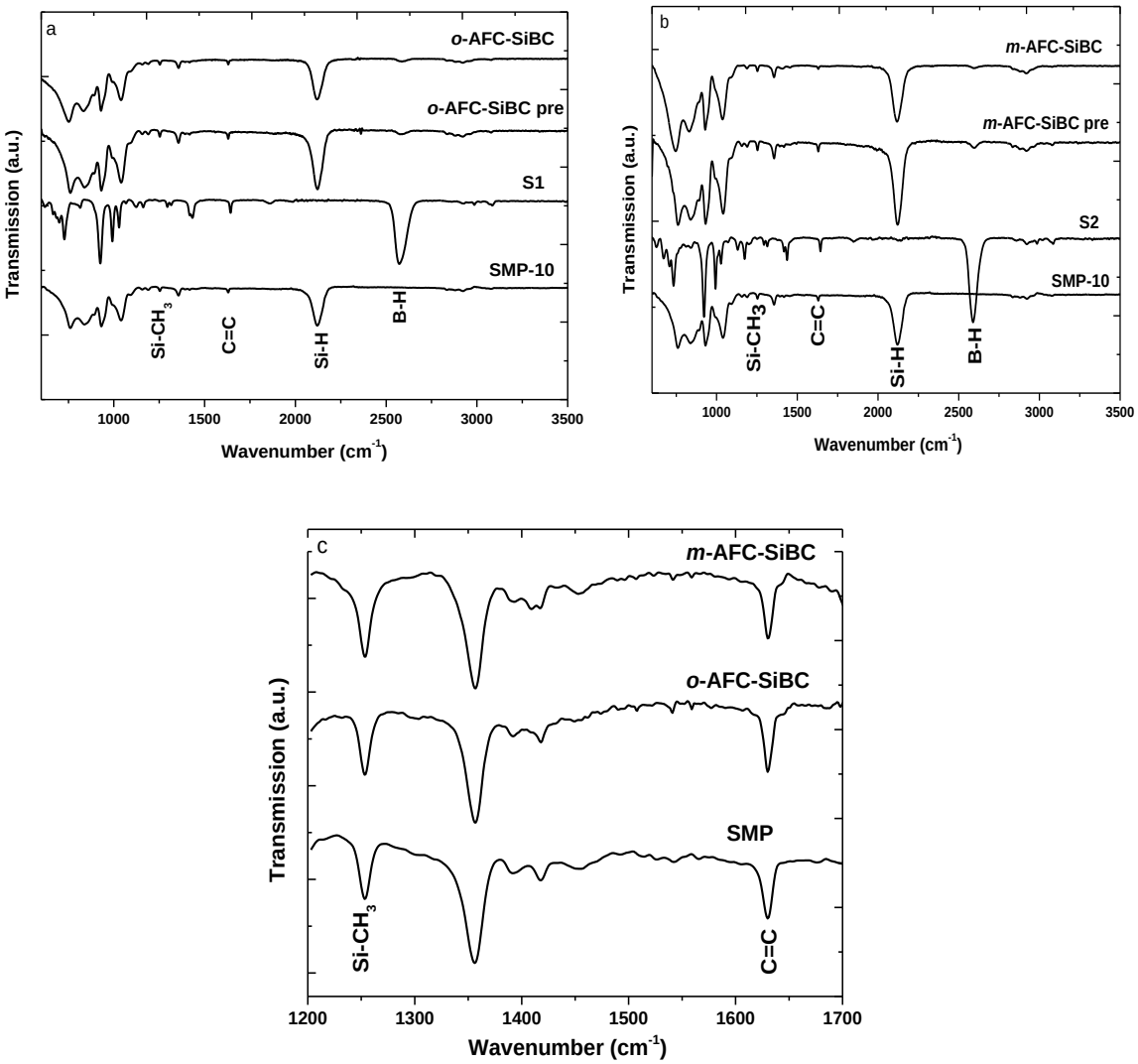

Figure 3-20. ATR-FTIR spectra of all the obtained samples (pre: homogeneous mixture of functionalized carborane and SMP-10 stirred at ambient temperature for 1 h) (AFC-SiBC : The obtained precursor was heated at 150 ^{o}C for 4 hr and subsequently the solvent was removed under vacuum at 90 ^{o}C. *o* and *m* denotes for the ortho and meta respectively).

The obtained AFC-SiBC samples are further subjected to crosslinked at higher temperature (250 ^{o}C; 3h) and the results show the disappearance of allyl-band and decrease in the relative intensities of the Si-H and B-H band. One of the most important features of carborane is its ability to enter into substitution reactions at both the cage carbon and boron atoms without degradation of the cage. The stability of the carborane cage is demonstrated under many reaction conditions used to prepare a wide range of C- and B-substituted carborane derivatives [213]. So the molecular cluster of the carboranes will not been affected by the hydrosilylation reaction and hydroboration reaction.

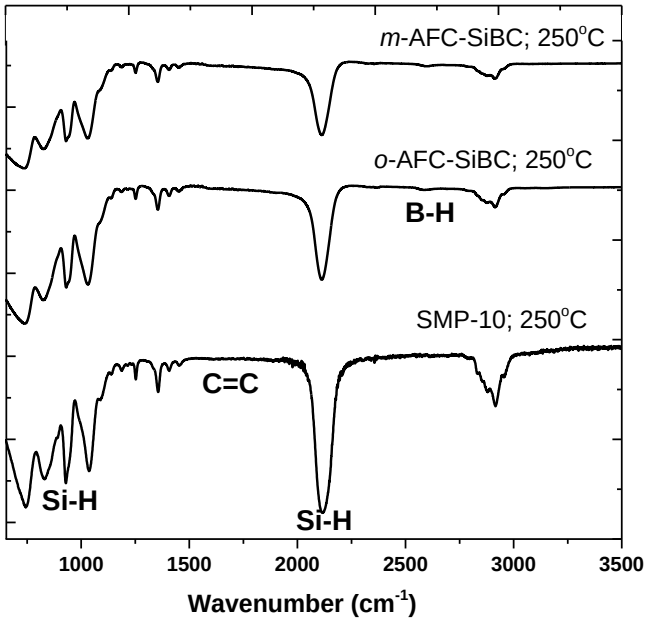

Figure 3-21. ATR-FTIR spectra of cross-linked samples at 250 °C.

3.2.2.2. Polymer-to-ceramic transformation

The polymer-to-ceramic conversion of SMP-10, *o*-AFC-SiBC and *m*-AFC-SiBC was studied by means of thermogravimetric analysis (TGA; Figure 3-23). The ceramic yield amounts ca. 77 wt% for SMP-10; whereas the ceramic yield of the *o*-AFC-SiBC it is observed to be ca. 76 wt%. The major difference in the mass loss of SMP-10 and *o*-AFC-SiBC occurred in the low-temperature regime (250-300 °C). This might be attributed to dehydrocoupling reactions between Si-H and B-H groups (as mentioned previously) and does not occur in SMP-10. The sample *m*-AFC-SiBC shows the highest ceramic yield (ca. 79 wt%) upon heating at temperatures beyond 1000 °C, as it probably shows a better cross-linking degree than *o*-AFC-SiBC. Thus, in *o*-AFC-SiBC the steric hindrance of the allyl-groups (*ortho*) obviously leads to a lower cross-linking of the polymeric backbone of the single-source-precursor and consequently to a lower ceramic yield.

Table 3-13. Mass loss obtained upon heating SMP-10, *o*-AFC-SiBC, and *m*-AFC-SiBC in argon during thermogravimetric analysis.

Temperature range (°C)	Mass loss (wt %)		
	SMP-10	***o*-AFC-SiBC**	***m*-AFC-SiBC**
20-236	5.2	5.5	2.7
236-500	11.81	11.03	10.50
500-880	4.79	6.57	6.20
Ceramic Yield	77 wt%	76 wt%	79 wt%

In situ infrared spectroscopy was done in order to elucidate the evolution of the gaseous species during the thermolysis under Ar atmosphere. In both the cases CH_4, CH_2=CH-, SiH_4, silanes ($CH_3SiH_2CH_2CH_2$- and $CH_3SiH_2CH_2$-) are the main gaseous species detected by *in situ* IR whereas the formation of H_2 (m/z=2) due to the dehydrocoupling reactions has been proved by the *in situ* mass spectra.

(i) The evolution of CH_4 has been confirmed by the two bands at ~3016 cm^{-1} and ~1305 cm^{-1}. The condensation of Si-CH_2-Si and/or terminal Si-CH_3 bonds results in the formation of CH_4 [214]. (ii) Absorption band at ~949 cm^{-1} confirms the release of C_2H_4. The formation of C_2H_4 is related to the rearrangement reactions, leading to the combination of -CH_2-linkages of carbosilane bonds (Si-CH_2-Si).

(iii) The formation of SiH_4 (~905, ~940, ~2183 cm^{-1}), and $CH_3SiH_2CH_2CH_2$- (~871, ~899, ~1051, ~2147, ~2917, 3081 cm^{-1}) are basically due to the decomposition of the polymeric network during the thermolysis.

While comparing the temperature range of the decomposition of polymer in case of *o*-AFC-SiBC and *m*-AFC-SiBC; it has been found that the decomposition of the polymer starts at considerable low temperature (200-300 °C) in case of *o*-AFC-SiBC. In case of *o*-AFC-SiBC, due to steric hindrance the polymer undergoes the process of decomposition (with wide range of temperature) in combination with the crosslinking process which in turns affects the ceramic yield of the final ceramic.

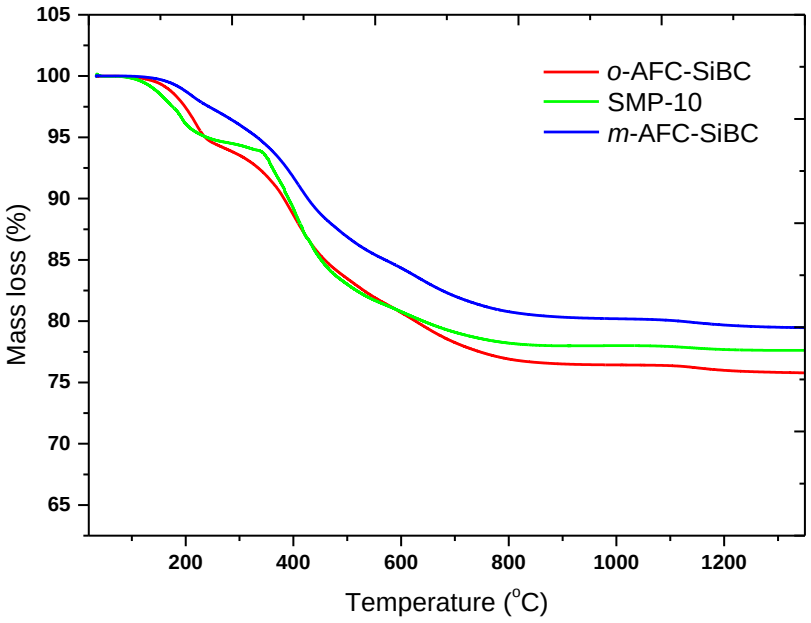

Figure 3-22. TG curve of the polymer-to-ceramic transformation of SMP-10, diallyl-functionalized *o*-carborane (*o*-AFC-SiBC) and *m*-carborane (*m*-AFC-SiBC).

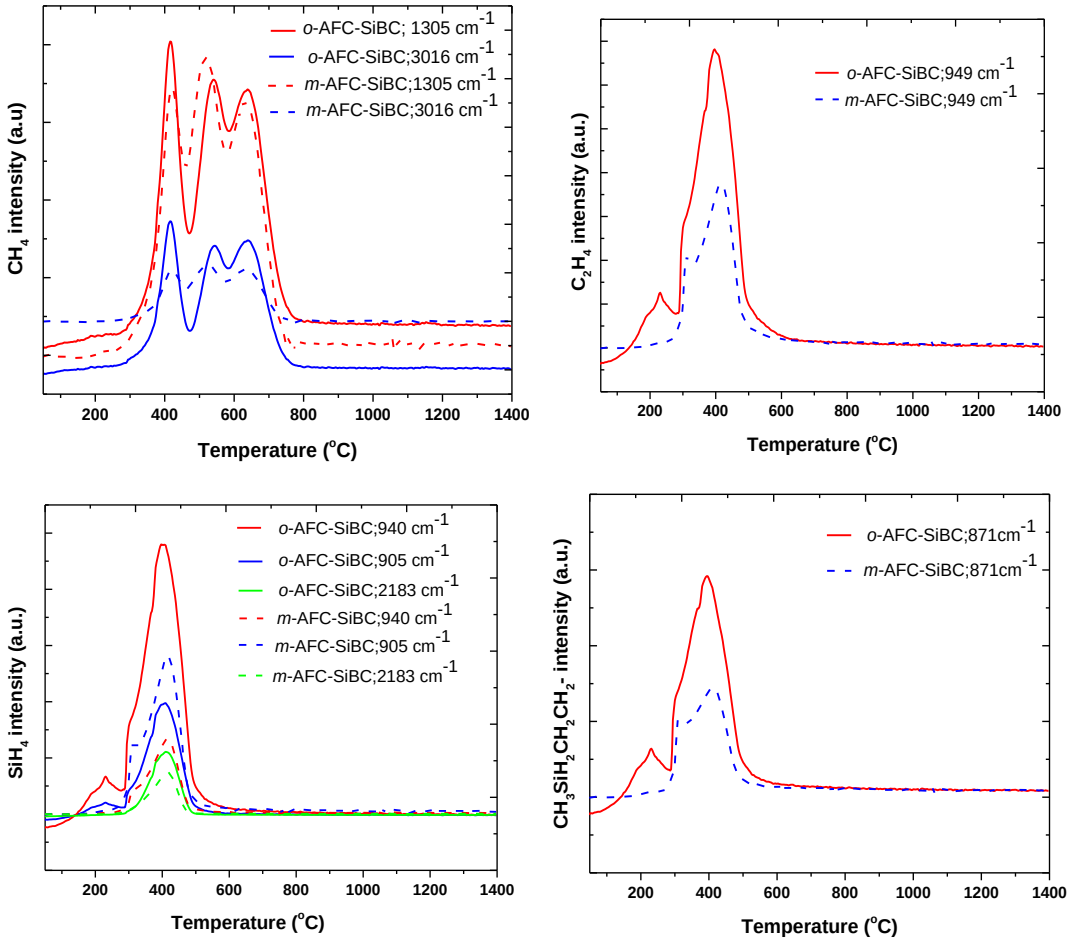

Figure 3-23. Insitu-FTIR date recorded during ceramization of *o*-AFC-SiBC and *m*-AFC-SiBC .

The as-prepared *o*-AFC-SiBC; and *m*-AFC-SiBC; samples were sintered at 1700 °C, and 1900 °C (Ar, 3h). Crystalline phases of the produced materials were investigated by powder X-ray diffraction. Figure 3-24 shows the XRD patterns of the samples sintered at different temperatures under argon. The samples prepared upon heat treatment at temperatures up to 1400 °C were found to be X-ray amorphous and above this temperature crystallization starts in all samples. The XRD data of the crystalline ceramic material show the crystallization of β-silicon carbide; nonstoichiometric boron rich boron carbide ($B_{10}C$; some reflection are matching) and at higher temperature crystallization of carbon is also observable. Additionaly a shoulder appears in more intense peak is assigned to stacking fault like α-SiC in β-SiC. Unfortunately there are some reflection which cannot able to index to any of the expected phase in the ceramic.

The unidentified reflection might be of $B_{10}C_2$ clusters. Due to electron deficiency, a "standing alone" $B_{10}C_2$ neutral cluster is unstable [215] but it might be possible that it stabilized by the matrix in the present work. Another possibily is the transformation of the boron cluster into stable boron rich boron carbide. It is hard to comment on the relection confirmly. In order to get detailed information regarding the unidentified phase TEM-EELS can be useful.

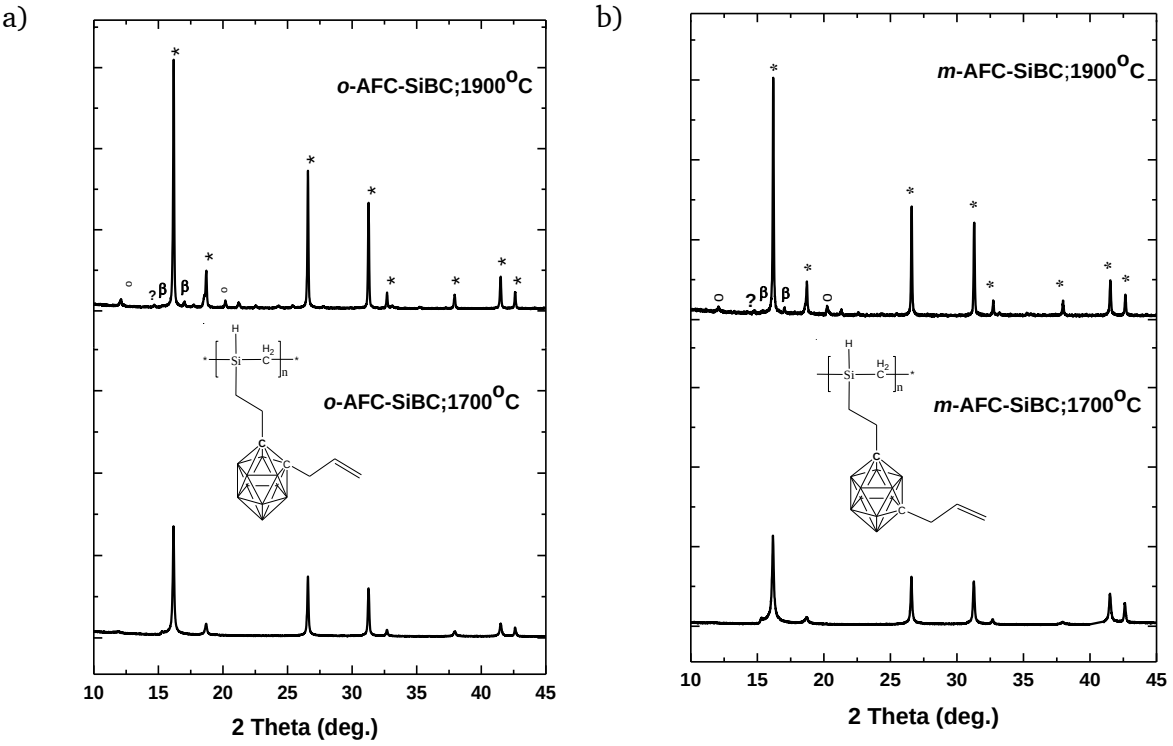

Figure 3-24. XRD patterns of *o*-AFC-SiBC (a) and *m*-AFC-SiBC (b) at different temperatures (°: carbon; β: $B_{10}C$; *: SiC).

The lattice parameter of β-SiC was 4.365 Å for the boron-free and AFCs derived SiC sample annealed at 1900 °C. Upon annealing of the samples at high temperatures, an additional reflection related to graphitic carbon (i.e., the (002) reflection [179]) was detected. The interlayer spacing d_{002} was 3.415 Å in the boron-free SiC sample, whereas in case of AFCs derived samples 3.362 Å has been observed which shows more boron incorporation into the carbon or might be the incorporation of boron clusters as it is, in the graphitic carbon. The presence of *o*-carborane within single walled nanotubes (SWNT) bundles and individual SWNTs was already reported in the literature, confirmed by complimentary EELS studies, and HRTEM imaging and simulation by D. A. Morgan in 2002 [216].

The samples obtained after pyrolysis at different temperatures (1400, 1700 and 1900 °C) were also investigated by means of Raman spectroscopy (see Figure 3-25). Two main bands centered at ~795 and ~970 cm^{-1} were assigned to the transversal optic (TO) and longitudinal optic (LO) modes of β-SiC, respectively [195]. Whereas the other bands (i.e., at 1345-1360, 1585-1596, 2668-2710 and 2916-2962 cm^{-1}) are related to the segregated carbon phase in the samples [196, 197].

The first order Raman spectrum of the samples shows the presence of a band of E_{2g} symmetry, which relates to bond stretching of sp^2 carbon pairs contained in rings or chains [198]. This band is called G band and appears at around 1585-1596 cm^{-1}. Disordered or nanostructured carbon-based materials (which might contain also some amount of sp^3 hybridization) exhibit additional bands in their first order Raman spectrum, such as a band of A_{1g} symmetry which relates to breathing modes of sp^2 carbon atoms within rings (so-called D band; its position depends on the laser wavelength; ca. 1345-1360 cm^{-1} at 514.5 nm), D" band (ca. 1500 cm^{-1}, related to amorphous carbon) [198, 204, 205]. Furthermore, overtone bands at 2668-2710 and 2916-2962 cm^{-1} (2D and D + G modes, respectively) were also found in spectra.

The segregated carbon present in the annealed samples till 1400 °C was found to be highly disordered. In all spectra till the 1700 °C, the intensity of the D-band is significantly larger than that of the G-band, indicating the disordered feature of the segregated carbon. The relative intensity of the D-band with respect to G-band starts to decrease with increasing temperature, illustrating that the structural organization of the carbon phase increases. This conclusion is supported by the decrease in the full width at half maximum (fwhm) of the bands.

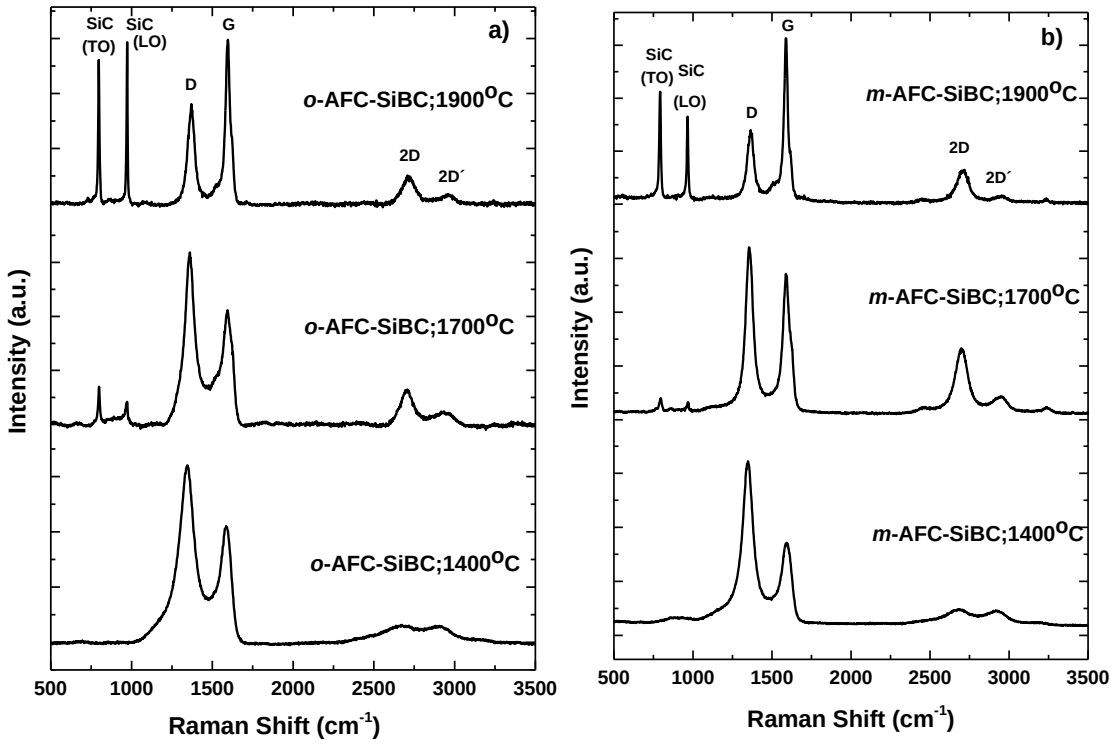

Figure 3-25. Raman spectra of *o*-AFC-SiBC and *m*-AFC-SiBC annealed at different temperature (1400, 1700, and 1900 °C).

Table 3-14. Raman data of the segregated carbon phase in *o*-AFC-SiBC and *m*-AFC-SiBC annealed at different temperature (1400, 1700, and 1900 °C).

Sample	Temp (°C)	I_D/I_G	A_D/A_G	Raman shift ω_D [cm^{-1}]	FWHM $\Delta\omega$ [cm^{-1}]	Raman shift ω_G [cm^{-1}]	FWHM $\Delta\omega$ [cm^{-1}]	La	L_D (nm)	Leq
***o*-AFC-SiBC**	1400	1.51	1.76	1345.10	112.05	1589.06	90.02	2.49	8.40	3.77
***m*-AFC-SiBC**	1400	2.02	2.65	1345.45	93.97	1594.74	69.26	1.65	7.26	1.55
***o*-AFC-SiBC**	1700	1.73	2.25	1357.71	98.71	1598.77	67.32	1.94	7.86	2.22
***m*-AFC-SiBC**	1700	1.16	1.05	1356.64	54.52	1592.99	61.09	4.18	9.56	6.58
***o*-AFC-SiBC**	1900	0.74	1.02	1369.17	50.03	1597.02	32.31	4.30	12.01	4.42
***m*-AFC-SiBC**	1900	0.59	0.99	1364.72	55.98	1588.89	26.98	4.40	10.34	6.00

In the AFC-SiBC sample annealed at 1900 °C, the intensity of the D band increases markedly as compared to that of the boron-free sample annealed under the same conditions. Morover, it also induces a shift of the G band to higher frequency (1580 cm^{-1} for boron free sample) and the appearance of a new band in the spectrum, i.e., the D' band (E_{2g} symmetry, ca. 1590 cm^{-1}), which relates with disorder in the graphitic lattice related to surface defects [207]. Thus, both effects, i.e., the increase in the intensity of the D band and the appearance of the D' band, indicate an enhancement of the number of defects upon in the carbon lattice. This indeed is also supported by the L_D value, which also strongly decreases from 21.6 nm in the boron-free SiC sample to 12.01 nm in *o*-AFC-SiBC and 10.34 nm in *m*-AFC-SiBC. Additionally, the L_{eq}/L_a ratio being close to unity clearly suggest the presence of a poorly graphitized carbon phase within the carborane-containing samples. Again the defects in the carbon lattice is consider to rely on the presence of boron clusters. There is still no direct evidence of this comment and needs to further characterized carefully (TEM-EELS).

The probable mechanism for the crosslinking and ceramization of the functionalized carboranes with SMP-10 has been broadly summarized into three steps.

Step 1: As from the ATR-FTIR results of the precursors, it has been observed that the relative intensity of Si-H, B-H and C=C has decreased. The reaction of the AFCs with the SMP-10 has been started at above 100 °C via hydroboration reactions involving C=C and B-H bonds and hydrosilylation reactions start at temperatures of ca. 120 °C and may need temperatures as high as 200 °C in order to complete.

As both the reactions are without weight loss mechanism (so no evidence from TG), it would be difficult to separate the hydroboration and hydrosilylation reaction (in term of starting reaction) as the temperature range given here is expected as per the literature.

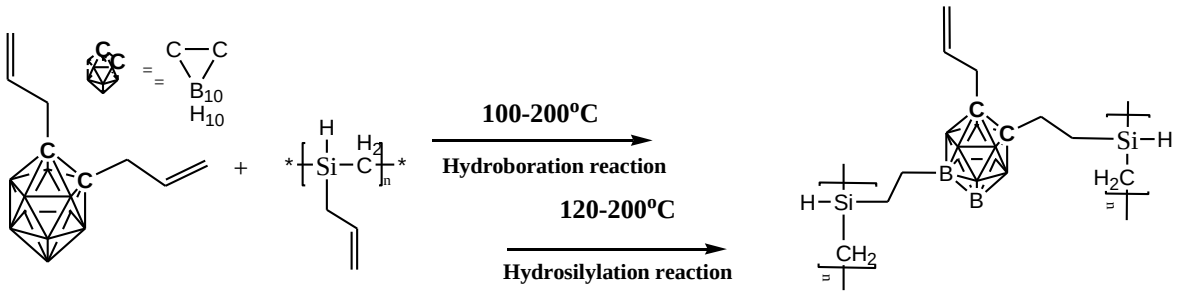

Step 2: As the obtained SSPs was thermally treated above 200 °C in order to further cross-linked, weight loss has been observed due to the evolution of H_2 (detected in TG/MS) and it was expecting because of dehydrogenation reactions which were also confirmed by ATR-FTIR.

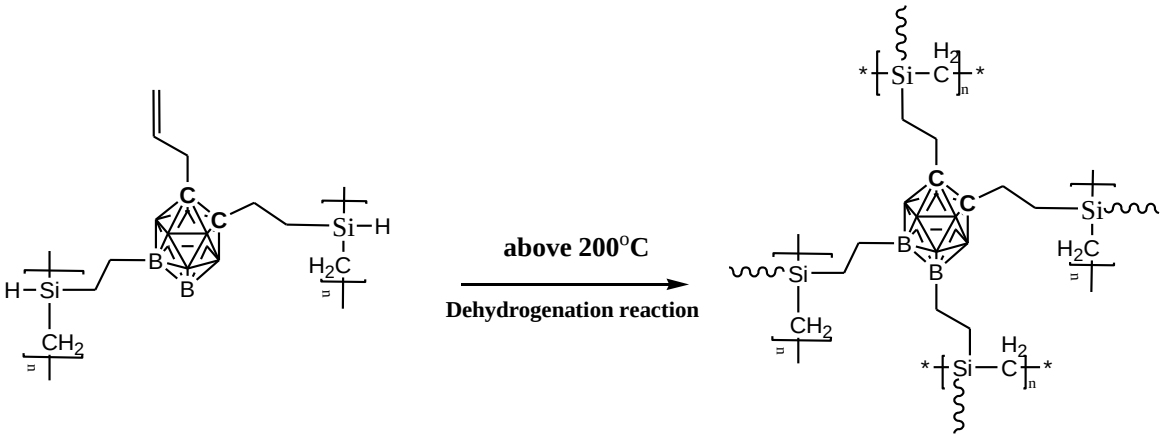

Step 3: At temperatures beyond 800-850 °C, no significant mass change is recorded, thus it is concluded that the polymer-to-ceramic transformation is completed. XRD results confirms the presence of an amorphous material. As like polymer-derived-ceramic (already reported in the literature) that it proceed with the formation of single-phase amorphous $Si_xC_yB_z$ which on high temperature treatment convert into three phase amorphous SiC, C, and $B_{10}C$ nanocomposites. Above 1500 °C, crystallization of these amorphous phases takes place, which has been proved by the XRD results.

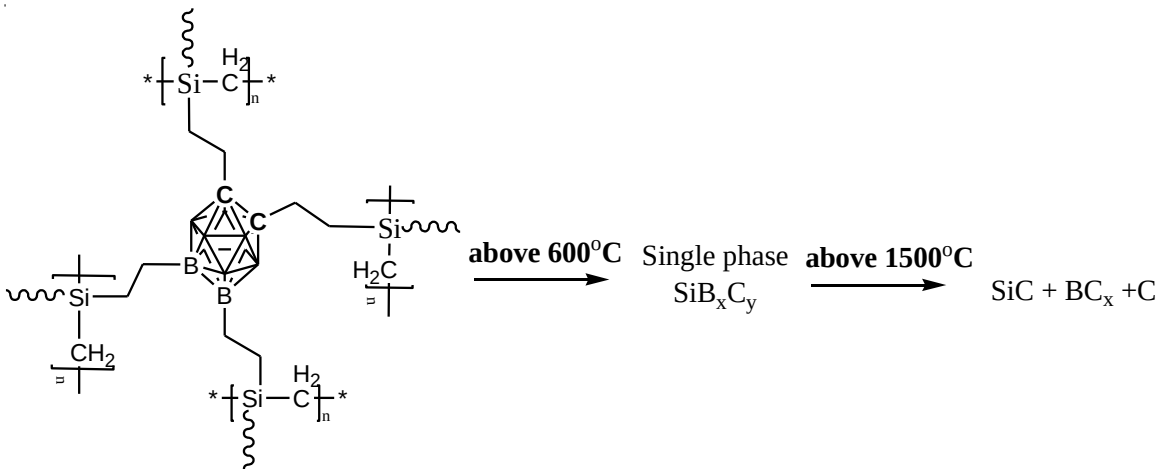

3.2.2.3. Effect of boron on the SSPs synthesis and phase composition of the final ceramic

In order to understand the effect of boron precursor on SSPs synthesis and phase composition of the final ceramic, the amount of boron in the ceramic should be comparable. Table 3-15 shows the amount of the boron in the ceramic obtained by the modification of the BMS (BMS-SiBC-30 and BMS-SiBC-5 prepared by 30 and 5 wt % of BMS respectively) and AFCs (*o*-AFC-SiBC and *m*-AFC-SiBC). It clearly shows that the weight of the boron in the ceramic is quite comparable. The effect of boron clusters onto the boron content can be clearly visible, the use of 5 wt% of *o*-AFC-SiBC can reach to the incorporation of the 1.63 wt% of the boron in the final ceramic whereas in case of BMS, it is only 1.63 wt% even after using 30 wt% of BMS. The reason is quite clear, in case of the BMS (elemental boron) whereas in AFCs (cluster of boron) reacts with the allyl-groups and attached directly to the polymer.

Table 3-15. The amount of boron in the ceramic.

S.No.	Sample	BP:SMP	wt% of B in ceramic	Ceramic yield(wt%)
1.	BMS-SiBC -30	30:70	1.27	-
2.	BMS-SiBC -5	5:95	0.96	90
3.	*o*-AFC-SiBC	5:95	1.63	76
4.	*m*-AFC-SiBC	5:95	0.74	79

The precursor plays a crucial role in the synthesis condition and the crosslinking of respective SSPs which in turns affects the ceramic yield of the final ceramic. In case of the BMS-modified precursor, the reaction with BMS occurred under the reaction conditions whereas in case of AFC derived samples not any observable changes were found (ATR-FTIR). The main reaction participating in the reaction of BMS with SMP-10 is hydroboration at ambient temperature whereas in case of AFCs, thermally conducted hydrosilylation and hydroboration reaction.

a)

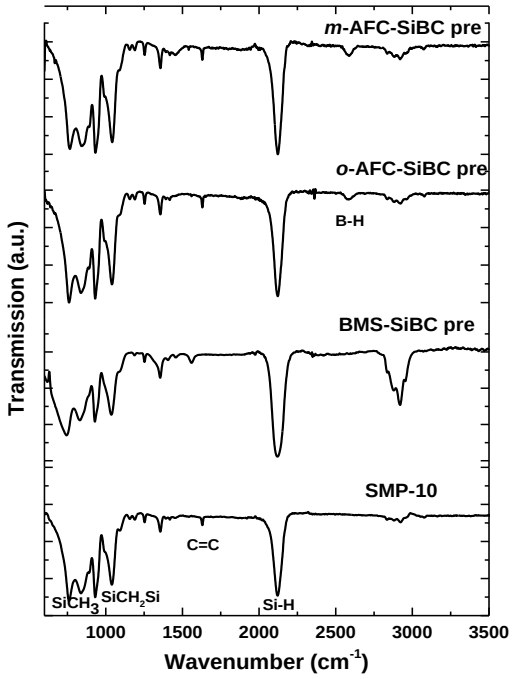

b)

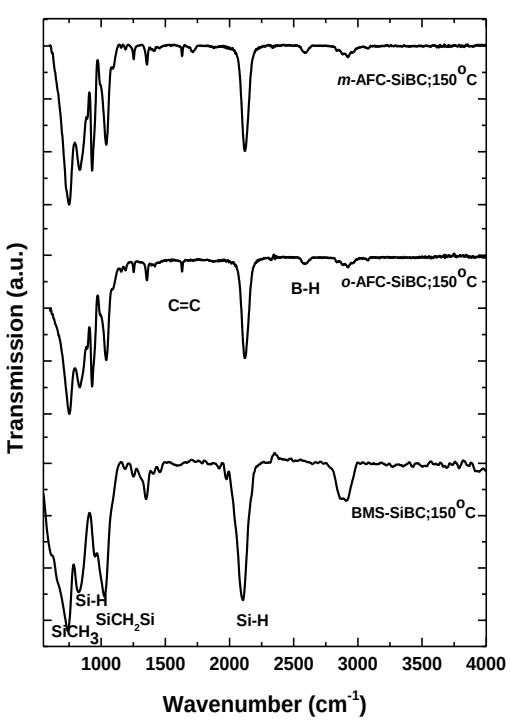

c)

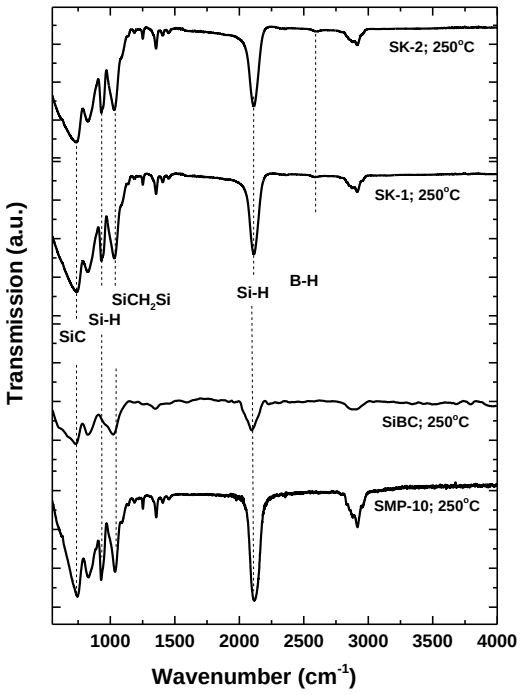

Figure 3-26. Comparison of the ATR-FTIR spectra of all precursor and cross-linked samples obtained after modification with BMS and carboranes.

ATR-FTIR results clearly confirms the high crosslinking degree of the sample obtained by the BMS modification than AFC. The ceramic yield of the highly crosslinked samples obtained by BMS are also very high as compared to AFC modified samples (Table 3-15).

While looking to the XRD results of the samples it has been shown that the ceramic obtained by the carboranes derived SSP enhances the boron carbide phase formation. The SiBC material prepared from the AFC-modified polycarbosilane (AFC-SiBC) shows different phase composition, indicating the presence of a boron-rich boron carbide phase, which was not detected in BMS-SiBC. The reason might be related to the diffusion of boron within SiC/C matrix (no clear evidence and need further characterization TEM-EELS).

The lattice parameter of β-SiC seems to be only marginally affected by the incorporation of boron by BMS into the preceramic polymer whereas it is not at all affected by AFCs. Thus, the lattice parameter of β-SiC was 4.365 Å for the boron-free and AFCs derived SiC sample annealed at 1900 °C; whereas for BMS-SiBC-5 it was slightly lower 4.362 Å. Upon annealing of the samples at high temperatures, an additional reflection related to graphitic carbon (i.e., the (002) reflection [179]) was detected. The interlayer spacing d_{002} was 3.415 Å in the the boron-free SiC sample, boron content from 0.98 wt% (as in BMS-SiBC-5) to 1.25 wt% (as for BMS-SiBC-30), a slight decrease of the d_{002} value from 3.393 to 3.390 Å has been observed. Thus, we consider the decrease of the interlayer spacing in the segregated carbon phase as being a consequence of the boron incorporation into carbon, as previously mentioned in various studies. But interestingly in case of AFCs derived samples 3.362 Å has been observed. While studying the Raman spectra, the comparable observation has been found between AFC-SiBC and BMS-SiBC samples which shows more boron incorporation into the carbon or might be the incorporation of boron clusters (in case of AFC-SiBC) as it in the carbon. The only difference while comparing the Raman spectra of SiBC and *o*-AFC-SiBC sample is the intensity of the D-band which is comparatively less and also the D´-band which is less pronounced.

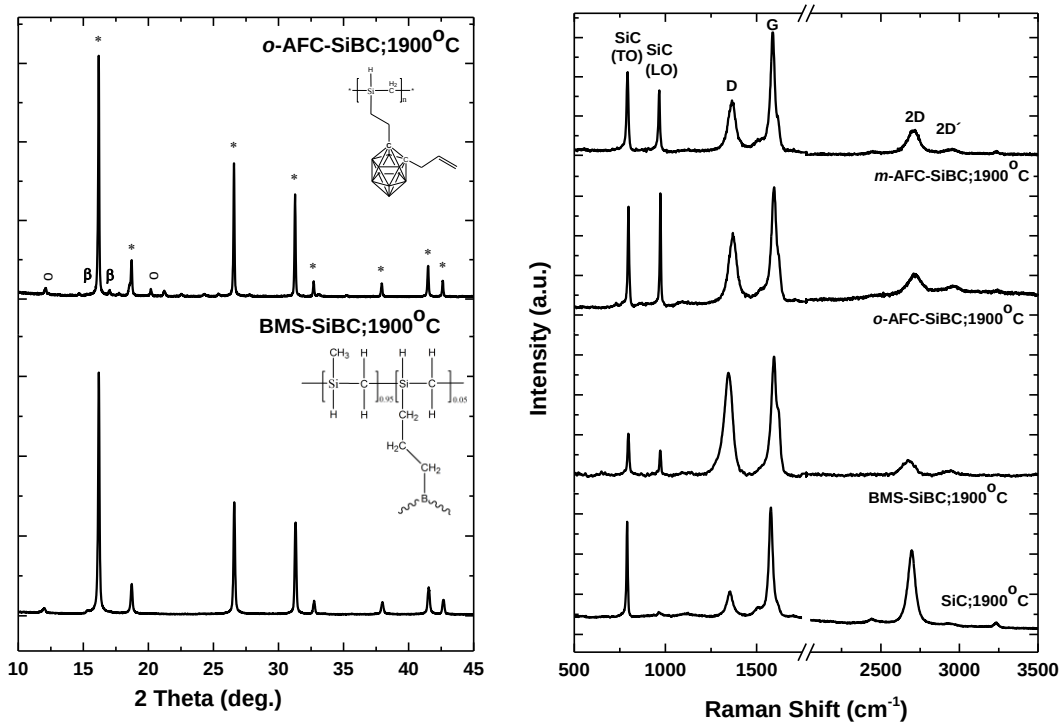

Figure 3-27. a) XRD patterns (°: carbon; β: $B_{10}C$; *: SiC) and b)Raman spectra of boron modified polymer-derived silicon carbide at high temperatures, obtained after modification with borane dimethylsulfide (BMS) and allyl-functionalized carboranes (AFC).

3.2.2.4. Summary

The results obtained during the present study indicate that novel single-source-precursors based on a polycarbosilane modified by allyl-functionalized carboranes (AFC) can be prepared. The as-prepared single-source-precursors were structurally characterized and investigated concerning their conversion into ceramic materials. Thus thermal treatment of the single-source-precursors in Ar atmosphere leads to X-ray amorphous SiBC-based materials. The SiBC material prepared from the AFC-SiBC shows a phase composition indicating the presence of a boron-rich boron carbide phase, which was not detected in the aforementioned BMS-SiBC derivatives.

3.3. Vanadium modified SiC-based ceramics

3.3.1. Vanadium-containing SSPs using vanadyl acetylacetonate

3.3.1.1. Characterization of obtained vanadium-containing SSPs

Figure 3-28 compares the ATR-FTIR spectrum of the as-received allyl-hydrido polycarbosilane (SMP-10), of the cross-linked SMP-10 at 250 °C and of the cross-linked vanadium-modified SMP-10 (referred to as V-SMP-10) at 250 °C. The absorption bands at around 1034 cm^{-1} (CH_2 bending in Si-CH_2-Si) and at 2900 cm^{-1} (C-H stretching in Si-CH-) are present in all samples, indicating the existence of the Si-CH_2-Si units in the backbone of polymer. The strong bands at ca. 2115 cm^{-1} and 928 cm^{-1} were assigned to Si-H groups and those 1625 and 3076 cm^{-1} to the allyl-groups in the as-received SMP-10 (low intensity, due to the low amount, i.e., 5 mol%). The absorption bands at 747 and 833 cm^{-1} are attributed to Si-C stretching and Si-CH_3 rocking.

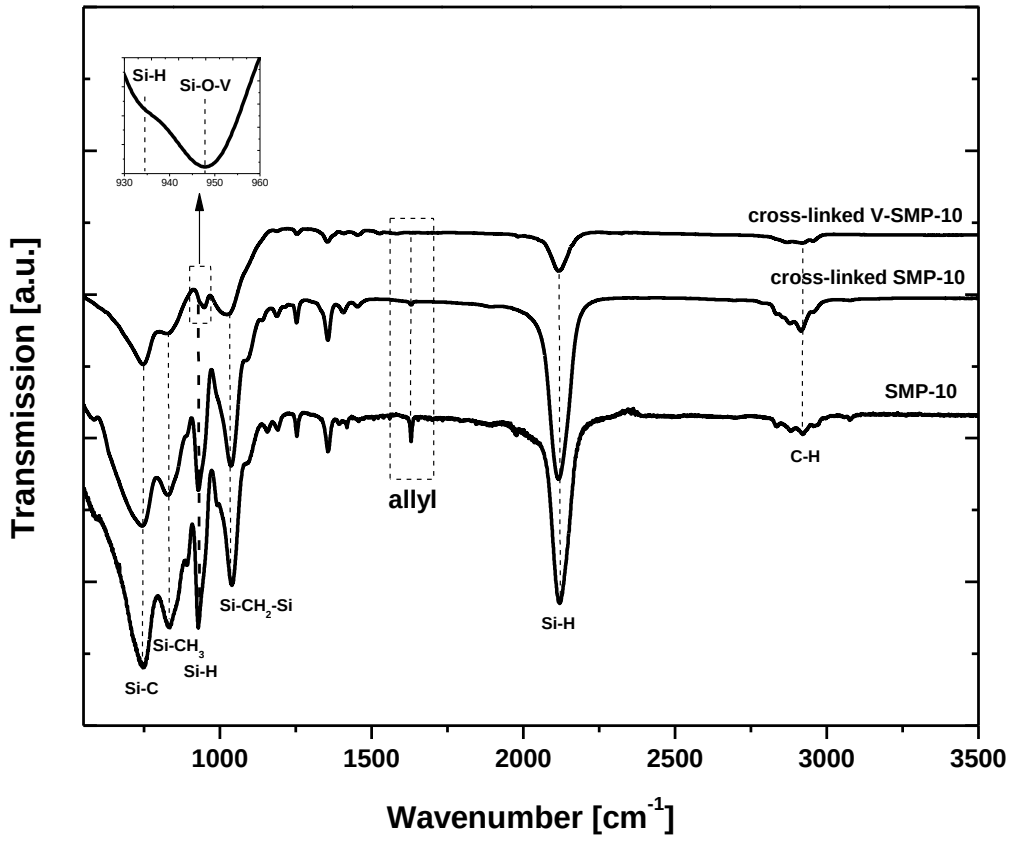

Figure 3-28. ATR-FTIR spectra of liquid SMP-10 as well as cross-linked SMP-10 and vanadium-modified SMP-10.

As the SMP-10 is thermally treated at high temperatures, the almost disappearance of the allyl bands indicates that hydrosilylation occurred under these conditions. There is a large excess of Si-H groups (if related to the amount of allyl-groups) present in the as-received SMP-10 as well as in the cross-linked SMP-10. While comparing the cross-linked SMP-10 with the cross-linked V-SMP-10, it is obvious that the absorption band related to the allyl groups (1625 cm^{-1}) completely disappeared and the bands related to Si-H (1625 and 3076 cm^{-1}) decreased in intensity. In the case of V-SMP-10, the new absorption band at 948 cm^{-1} is related to Si-O-V units [217, 218] which are generated upon the incorporation of vanadium in the polymer (Figure 3-29). Consequently, the modification of SMP-10 with the vanadyl acetylacetonate leads to a polymeric single-source-precursor.

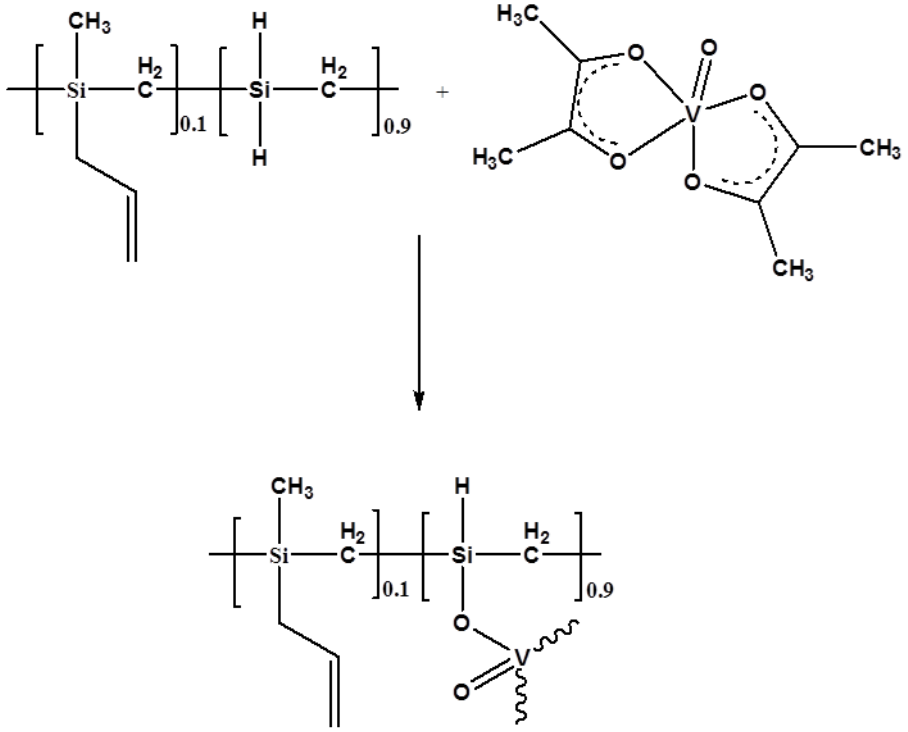

Figure 3-29. Possible reaction of SMP-10 with $VO(acac)_2$ upon formation of Si-O-V linkages.

3.3.1.2. Polymer-to-ceramic transformation

The thermal behavior/decomposition of as-received SMP-10 and of V-SMP-10 was studied by means of thermogravimetry analysis (TGA). For this study, the SMP-10 as well as V-SMP-10 (dried at 120 °C prior to TGA measurement) were heated up to 1400 °C in Ar atmosphere. In both cases, major weight loss takes place at temperatures up to 800 °C; whereas at higher temperatures no observable mass loss has been detected. As shown in Figure 3-30, the ceramic yield amounts ca. 77 wt% for the polycarbosilane (SMP-10) and ca. 90 wt% for vanadium-modified precursor. The reason behind the significant increase of the ceramic yield is that the chemical modification of SMP-10 with vanadyl acetylacetonate significantly increases its cross-linking degree.

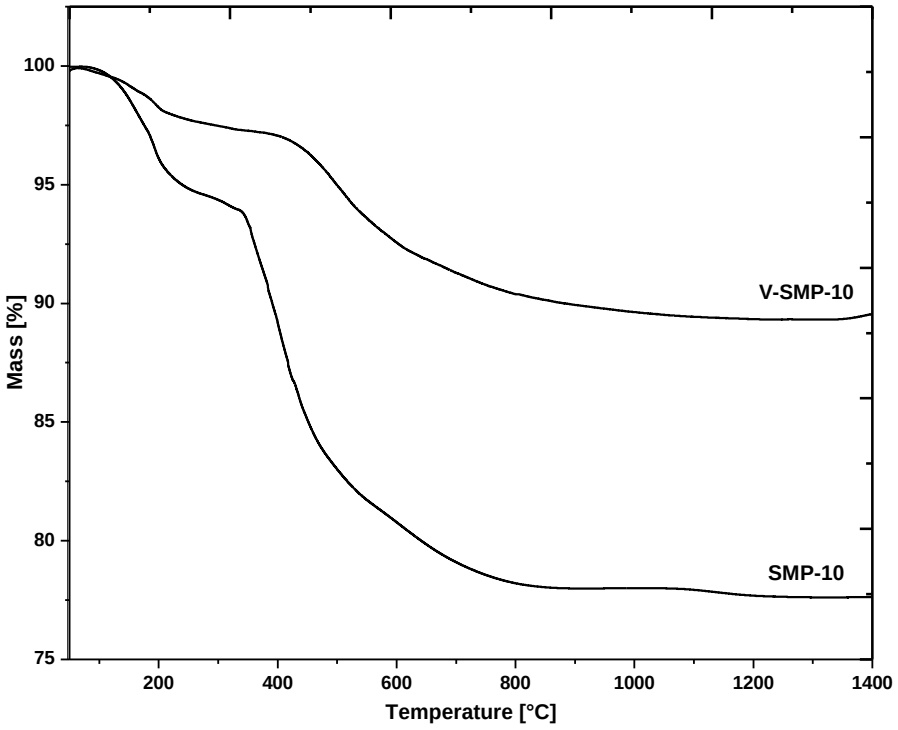

Figure 3-30. TG curves of the polymer-to-ceramic transformation for SMP-10 and V-SMP-10.

In situ infrared spectroscopy (IR) was done in order to elucidate the evolution of the gaseous species during the thermolysis under Ar atmosphere (Figure 3-31). In the case of V-SMP-10, following released gaseous species were detected: (i) The evolution of CH_4, which has been confirmed by two bands at 3019-3007 cm^{-1} and 1306-1301 cm^{-1}; (ii) Absorption bands at 2379-2294 cm^{-1} and 670-667 cm^{-1} confirms the evolution of CO_2; (iii) The release of alkenes which is associated with the band at 951-947 cm^{-1}. *In situ* mass spectrometry (MS) study supports the evolution of CH_4 (m/z=16) and CO_2

(m/z=44). Moreover, the evolution of H_2O (m/z=18) and C_2H_4O [219] (m/z=43) was also detected by MS. Interestingly, no H_2 evolution was detected by *in situ* MS.

EGA study of the ceramization behavior of SMP-10 (i.e., *in situ* mass spectrometry, MS; shown in Section 3.1.2) indicated that in the first main decomposition step (T < 250 °C) hydrogen (*m/z* = 2) and small polymer fragments evolve; whereas in the second major decomposition step (i.e., 400 - 850 °C), which represents the conversion of the preceramic polymer into an inorganic materials, H_2 (*m/z* = 2), SiH_4 (*m/z* = 32), and CH_3SiH_3 (*m/z* = 46) has were analyzed. Whereas during the ceramization of V-SMP-10, mainly the release of CO_2, C_2H_4, CH_4 and H_2O was detected (Figure 3-32).

By comparing the ceramization behavior of SMP-10 and vanadium-containing precursor, the effect of vanadium on the decomposition of the polycarbosilane is clear. The fact that hydrogen evolution during the first decomposition step of V-SMP-10 does not occur (at least it was not detected) indicates an increased cross-linking degree of the modified precursor as well as probably other cross-linking processes than dehydrocoupling (which has been shown to be the main cross-linking mechanism in SMP-10, see Section 3.1.1). Moreover, the lack of SiH_4 release during the ceramization of V-SMP-10 agrees very well with the improved ceramic yield observed during its thermal conversion as compared to that measured for SMP-10. At higher temperature (600-800 °C), the absence of hydrogen in decomposition gas can be explained due to the participation of hydrogen in the reduction of amorphous SiVCO matrix. This can be further confirmed by the appearance of the H_2O at the same temperature range.

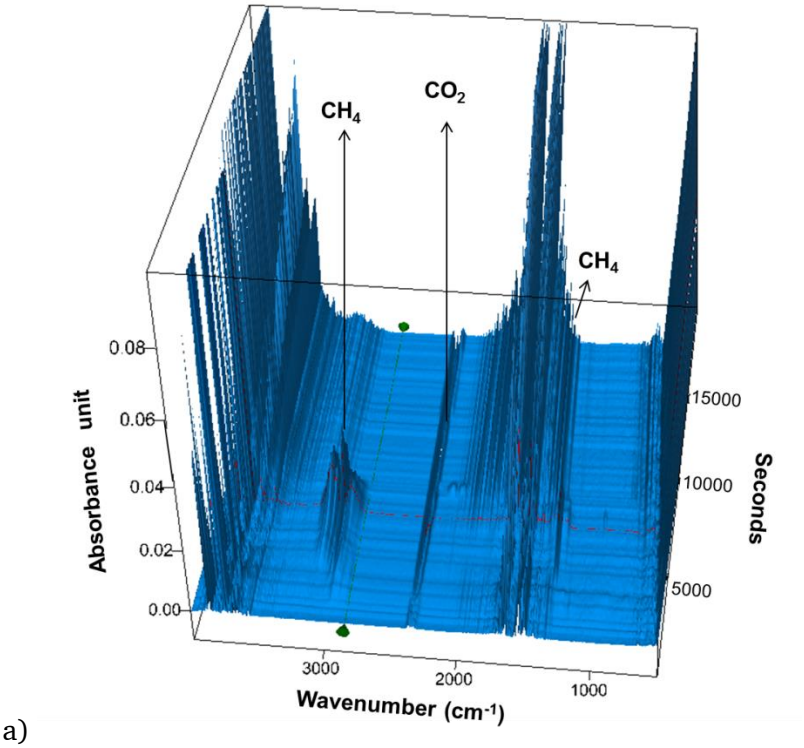

a)

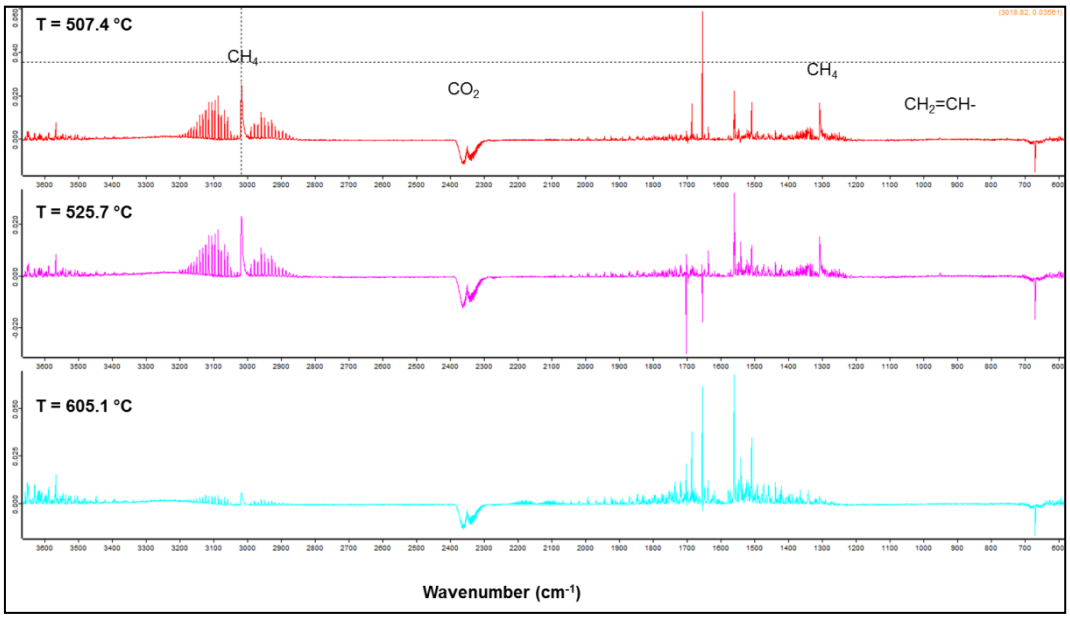

b)

Figure 3-31. *In situ* FTIR data recorded during the ceramization of V-SMP-10: a) Temperature/time-dependent FTIR spectra during the EGA; b) individual FTIR spectra recorded at different temperatures during the ceramization of V-SMP-10.

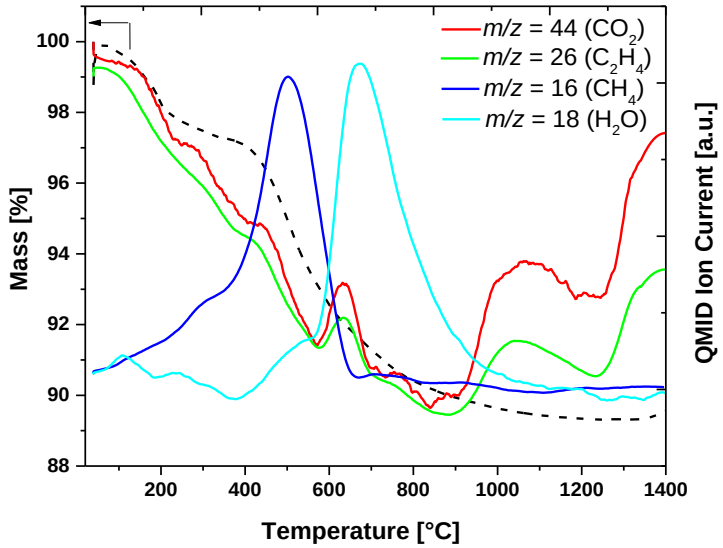

Figure 3-32. TG and QMID (quasi multiple ion detection) ion curves for the release of CO_2 (a), C_2H_4 (b), CH_4 (c), and H_2O (d) during the ceramization of V-SMP-10.

Figure 3-33 shows the XRD patterns of the samples annealed at different temperature under argon. The ceramic obtained upon heat treatment at 1100 °C for 2h was X-ray amorphous. The XRD data of the ceramic materials annealed at higher temperatures indicate the crystallization of V_8C_7 and β-SiC. Additionally, small amounts of α-SiC were identified. The crystallization of V_8C_7 occurs at temperatures from 1300 °C. Interestingly, the vanadium-free SiC prepared from SMP-10 did not show any significant crystallization up to temperatures as high as 1300 °C. Thus, the incorporation of V in SiC(O) is considered to enhance the crystallization of β-SiC as compared to the crystallization behavior of vanadium-free SiC.

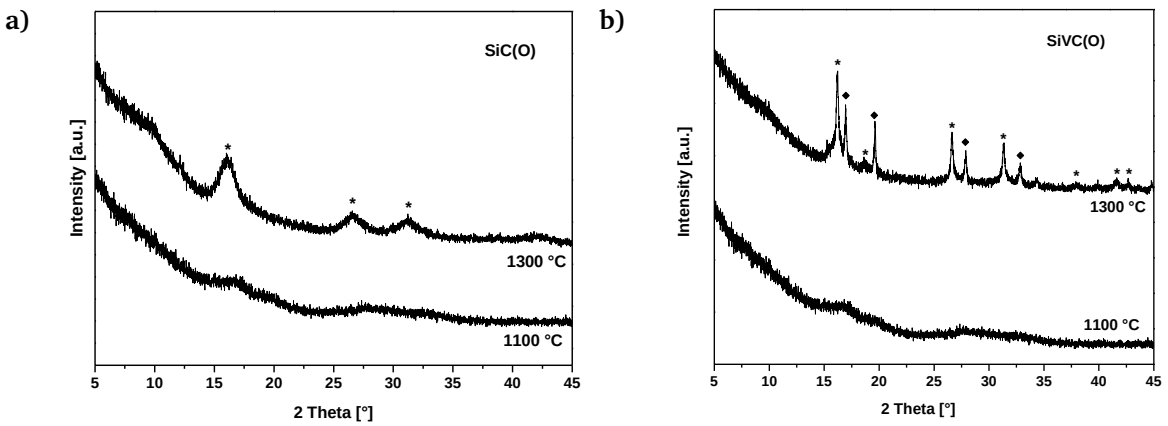

Figure 3-33. XRD patterns of vanadium-free SiC and SiVC(O) as prepared at 1100 and 1300 °C (* - β-SiC; ♦ - V_8C_7).

3.3.1.3. Electronic properties and microstructure analysis of SiVC(O)

The sample prepared upon pyrolysis of V-SMP-10 at 1300 °C was studied by photoelectron spectroscopy (XPS). The recorded spectrum and the V2p, O1s, Si2p, and C1s envelopes are shown in Figure 3-34 a. The deconvoluted V2p envelope (Figure 3-34 b) shows peaks centered at binding energies of 513.7, 516.3, 521.1 and 523.2 eV. The peaks at higher binding energies (i.e., 521.1 and 523.2 eV) were assigned to the $V2p_{3/2}$ and $V2p_{1/2}$ spin-orbit splitting. The peak at 513.7 eV was assigned to V-C bonds and agrees well with the XRD data which show the formation of the V_8C_7 phase at 1300 °C. The binding energy is in agreement to values reported in the literature for vanadium carbide-based materials. Thus, a binding energy of 513.1 eV was determined for stoichiometric VC single crystals as well as for VC powders [220]. The peak at 516.3 eV corresponds to V-O bonds and was unambiguously assigned to V^{4+}. For instance, the binding energy for the $V2p_{3/2}$ photoemission reported for metallic V is 512. 6 eV [221]; whereas for VO_2 and V_2O_5 binding energies of 515.9 and 517.1 eV [220, 222], respectively, were determined, indicating that the vanadium oxide phase present in our sample is most probably VO_2. As the characteristic photoemissions of the V2p photoelectron spectrum are slightly shifted to higher binding energies, it might indicate some bonding of the V_8C_7 and VO_2 phases with the SiC(O) matrix via V-O and V-C linkages, respectively. The opposite trend, i.e., the V2p peaks shifted to lower binding energies, was observed during the conversion of vanadium (IV) oxide to carbides (i.e., shift from 516.3 to 513.6 eV, respectively) [222, 223].

The deconvoluted O1s envelope (Figure 3-34 c) shows a low-intensity peak at 530.8 eV, which was assigned to vanadium oxide [220]. The high-intensity peak at 532.7 eV is assigned to Si-O bonds in the SiC(O) matrix [171]. As reported by earlier publication, silicon oxycarbide (SiC_xO_y) has lowered the binding energy (532.3 eV) [224]. An additional peak at ~ 533.7 eV, was is assigned either to O_2-Si (mostly silica phase) and/or O–C bonds in accordance with the study of nano-sized SiC powders [224].

The deconvoluted Si2p envelope from Figure 3-34 d shows three peaks, at 100.9, 101.6 and 103.4 eV. The peak at 100.9 eV corresponds to crystalline silicon carbide [225], whereas the signal at 101.6 eV was assigned to Si-C bonds in SiC(O) [226]. The peak at 103.4 eV was assigned to silica [171].

The deconvoluted C1s envelope evidences the presence of three contributions. The peak at 282.9 eV is assigned to carbidic carbon, while the most intensive peak at 284.3 eV

corresponds to C-C bonds and relates to the presence of segregated carbon in the sample [223]. The contribution at higher binding energy (285.4 eV) was ascribed to C-O bond [224].

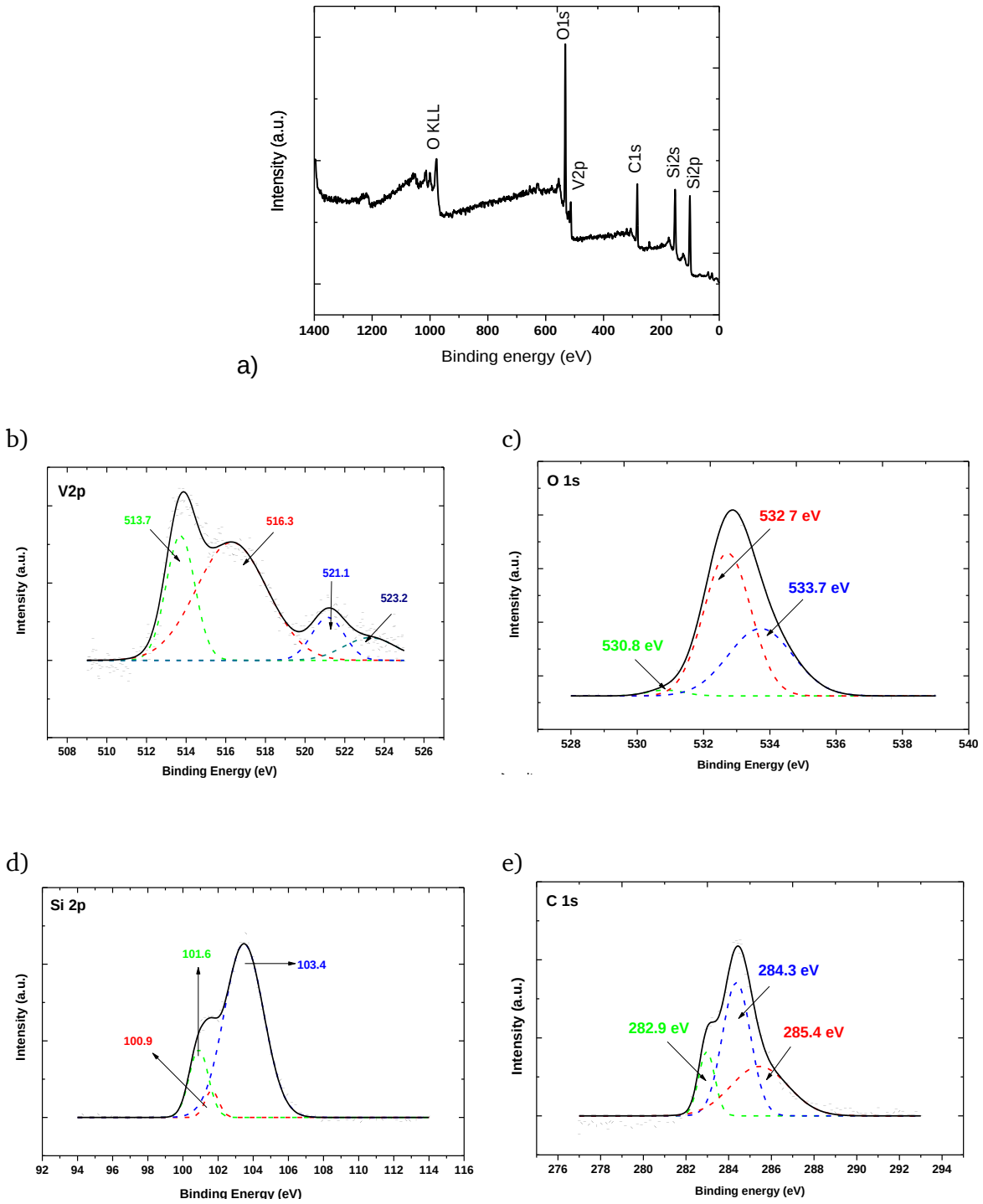

Figure 3-34. A typical survey of XPS spectra for the SiVC(O) sample prepared via pyrolysis of V-SMP-10 at 1300 °C (a). Deconvoluted XPS core level edges for V2p (b), O1s (c), Si2p (d), and C1s (e).

The SiVC(O) samples prepared from V-SMP-10 by thermal treatment in argon at 1100 and 1300 °C were also investigated by TEM. In Figure 3-35a, the microstructure of SiVC(O) obtained at 1100 °C is shown, indicating that the material is fully amorphous; whereas the micrograph of the sample synthesized at 1300 °C (Figure 3-35b) clearly show the crystallization of V_8C_7. The V_8C_7 precipitation are well faceted, showing a hexagonal shape and exhibit an average size of ca. 25 nm.

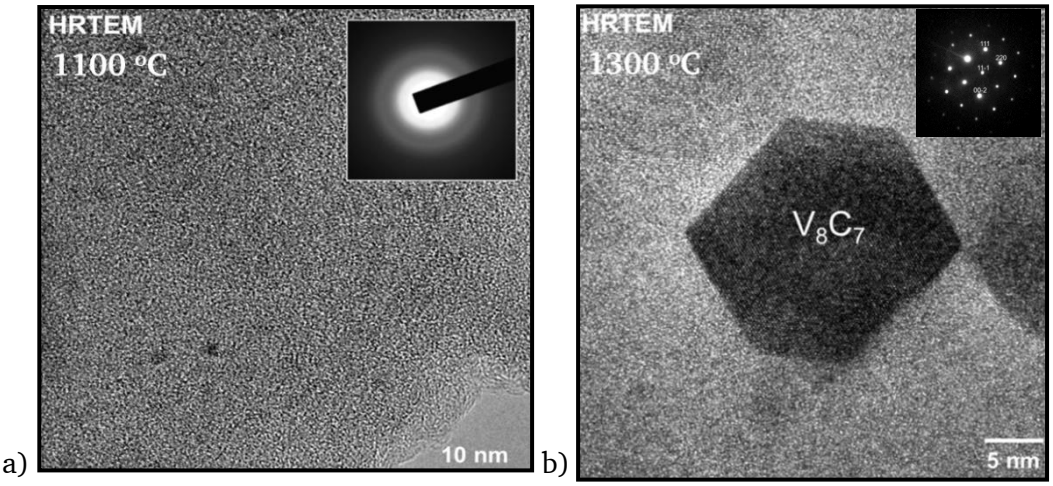

Figure 3-35. TEM micrographs of SiVC(O) samples as prepared at 1100 (a) and 1300 °C (b) in argon atmosphere.

3.3.1.4. Effect of temperature on the surface area of the sample

The specific surface area (SSA) values for the samples were determined from the Brunauer, Emmett and Teller (BET) adsorption isotherms. The total pore volume was calculated from the maximum amount of nitrogen gas adsorption at partial pressure (P/P0) = 0.999. The SSA of the vanadium modified ceramics was found to depend strongly on the preparation temperature. Thus, SSA significantly decreases from ca. 67 m^2/g to ca. 4 m^2/g upon increasing the pyrolysis temperature from 600 to 1300 °C (Figure 3-36). Thus, despite the presence of catalytically active V_8C_7 precipitations within the SiVC(O) sample prepared at 1300 °C, no significant catalytic activity with respect to ammonia decomposition is expected, as the surface area is too low.

However, the presence of oxygen within the SiC(O) matrix can be used to increase the porosity (and thus the SSA) upon annealing the material at high temperatures. Annealing at high temperatures will lead to a partial carbothermal decomposition of the matrix, which results in the generation of gaseous CO. A similar study was recently published, showing that the surface area and the porosity of carbon-rich C/SiCN systems can be

tuned by performing a controlled carbothermal decomposition of the materials which leads to the crystallization of β-SiC and nitrogen release, the latter being responsible for the increase of the SSA [227]. Accordingly, the SiVC(O) sample prepared at 1100 °C was annealed at high temperature in inert gas atmosphere. As expected, the oxygen content in the sample decreases from ca. 14 wt% (as for the SiVC(O) sample prepared at 1100 °C) to less than 1 wt% in the sample annealed at 1700 °C (Table 3-16). Interestingly, by comparing the phase composition of SiC(O) with that of SiVC(O), it is clear that the incorporation of V into silicon carbide has a significant effect on the content of the segregated carbon phase. Thus, the SiC(O) sample exhibit a volume fraction of ca. 1.2 % of segregated carbon; whereas the carbon content in the V-modified sample is as high as 7.6 vol%.

Table 3-16. Elemental analysis data and estimated phase composition of SiC(O) and SiVC(O) samples obtained from annealing at 1700 °C. The phase composition was estimated by assuming that the oxygen is present in the samples as silica (ρ = 2.196 g/cm^3 [228]), the remaining silicon is present as β-SiC (ρ = 3.21 g/cm^3 [229]) and the remaining carbon is present as segregated phase (ρ = 2.0–2.3 g/cm^3 [230]).

Sample	Elemental Analysis [wt%]				Empirical formula	Estimated phase composition (vol %)			
	Si	C	O	V		SiC	SiO_2	V_8C_7	C
SiC(O)	69.65	30.24	0.73	-	$SiC_{1.02}O_{0.01}$	97.68	1.07	-	1.23
SiVC(O)	50.76	30.36	0.33	18.55	$Si_1C_{1.40}V_{0.19}O_{0.01}$	78.10	0.81	13.49	7.59

In Figure 3-36, the evolution of the SSA in SiVC(O) as the pyrolysis temperature increases from 600 to 1700 °C is shown. Moreover, the SEM micrographs clearly show the presence of significant amounts of porosity in the samples annealed at high temperatures. Obviously, the temperature and the annealing time can be used to markedly increase the specific surface area of SiVC(O). Thus, annealing of SiVC(O) at 1700 °C for 6h induces a SSA of ca. 50 m^2/g, which is a reasonable value when intending to use the material for catalytic purposes (typical catalysts for ammonia decomposition reported in literature exhibited SSA of > 30 m^2/g [27].

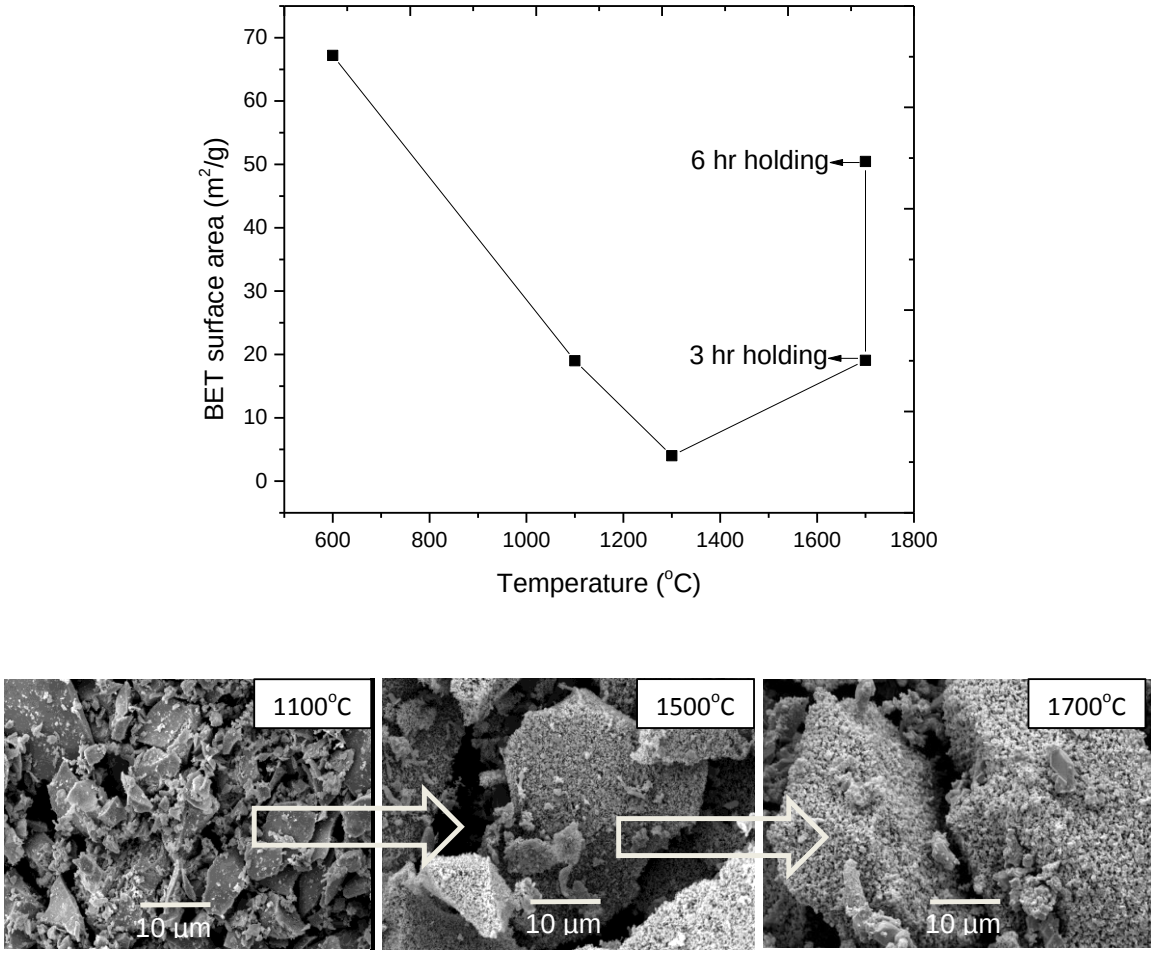

Figure 3-36. Effect of the preparation temperature on the specific surface area of the SiVC(O) samples.

3.3.1.5. Effect of experimental conditions on the phase composition

Figure 3-37 shows the XRD pattern of the sample annealed at 1700 °C for 6h under argon. The samples exhibit a specific surface area of 50 m^2/g and show high crystallinity as compared to the samples prepared at lower temperatures. Thus, β-SiC and V_8C_7 were identified as main crystalline phases, together with some small amounts of α-SiC and graphitic carbon. Upon using the Scherrer equation, the particle size of V_8C_7 was estimated to be ca. 25 nm and agreed well with the TEM data. Interestingly, the growth of V_8C_7 within the SiC matrix seems to be suppressed, as the grain size does not differ in the samples annealed at 1300 and at 1700 °C.

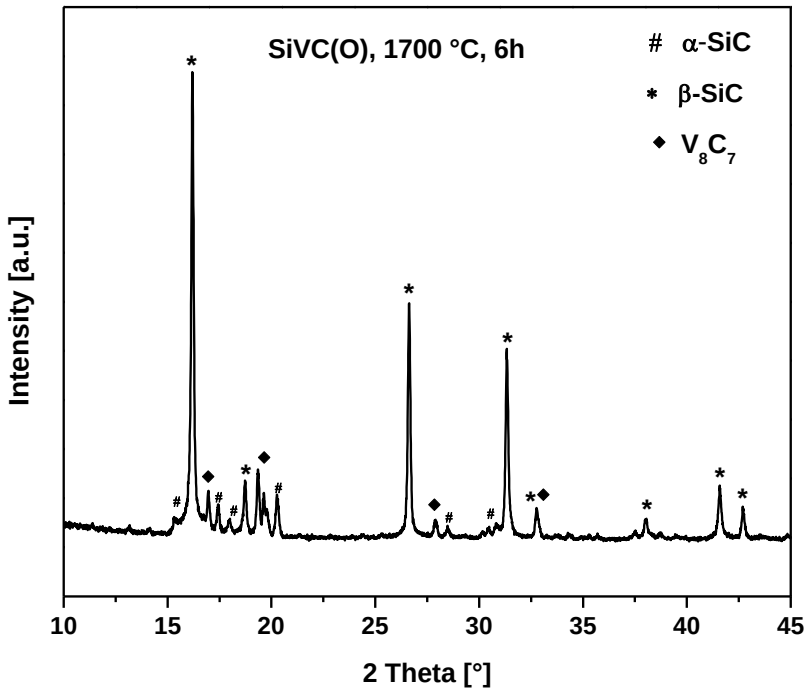

Figure 3-37. XRD pattern of SiVC(O) after annealing at 1700 °C for 6 h in a graphite furnance.

Interestingly, while performing the high-temperature annealing experiments, it was observed that small changes in the experimental conditions have a strong effect on the phase composition of the materials. Thus, while performing the experiments in a strong carburizing atmosphere (i.e., graphite crucible, graphite furnace), V_8C_7/SiC nanocomposites with low oxygen contents were obtained (see Table 3-16 and Figure 3-37). Furthermore, it was shown that the V_8C_7/SiC nanocomposite is stable at 1700 °C with respect to decomposition, as no change in the chemical and phase composition takes place even by using annealing time as high as 10 h. However, annealing of the samples under argon atmosphere at 1700 °C in an alumina tube furnace leads to the formation vanadium silicide (V_5Si_3) instead of V_8C_7 (Figure 3-38).

In the following, a rough thermodynamic rationalization of possible high temperature processes in the system Si-V-C-O is done in order to understand its high temperature evolution.

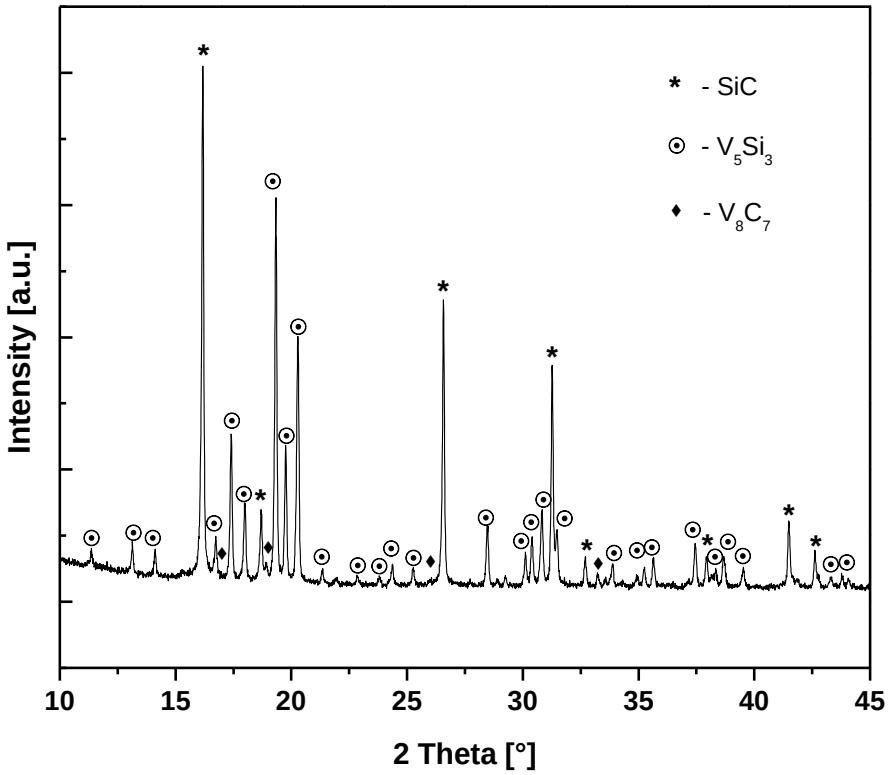

Figure 3-38. XRD pattern of SiVC(O) after annealing at 1700 °C in an alumina furnance.

As recently reported, the phase composition and crystallization in Si-M-O-C systems (M being a metal) is thermodynamically controlled [231]. Thus, it is assumed that the single-source-precursor (i.e., metal-modified polysiloxane or polycarbosilane) converts at moderate temperatures into a single-phase, glassy SiMOC material. Subsequently, MO_x precipitates upon annealing at higher temperatures, leading to nanocomposites consisting of metal oxide nanoparticles dispersed within a silicon (oxy)carbide matrix [232]. Since these systems are characterized by the fact that there is always some amount of segregated carbon, the evolution of the phase composition relies obviously on the thermodynamic stability of the metal oxide phase with respect to its carbothermal reduction (and probably subsequent reactions) [233]. As in our carbon-rich systems the oxygen fugacity is determined by $2\ C + O_2 = 2\ CO$, the evolution of the Si-V-C-O system at high temperatures was rationalized upon assessing the thermodynamic stability of VO_2, V_2O_3, and VO with respect to their carbothermal reduction (see the Ellingham diagram in Figure 3-39). At temperatures of 1100 °C-1300 °C, all three oxides seem to be stable against their carbothermal reduction. However, crystallization of V_8C_7 was observed by XRD in the samples prepared in this temperature range. This might be related to the increase activity of the nano-sized vanadium oxide precipitation. For instance, the

carbothermal reaction of vanadium oxides with nanoscaled carbon was reported in literature to take place at temperatures as low as 900 °C-1000 °C [231].

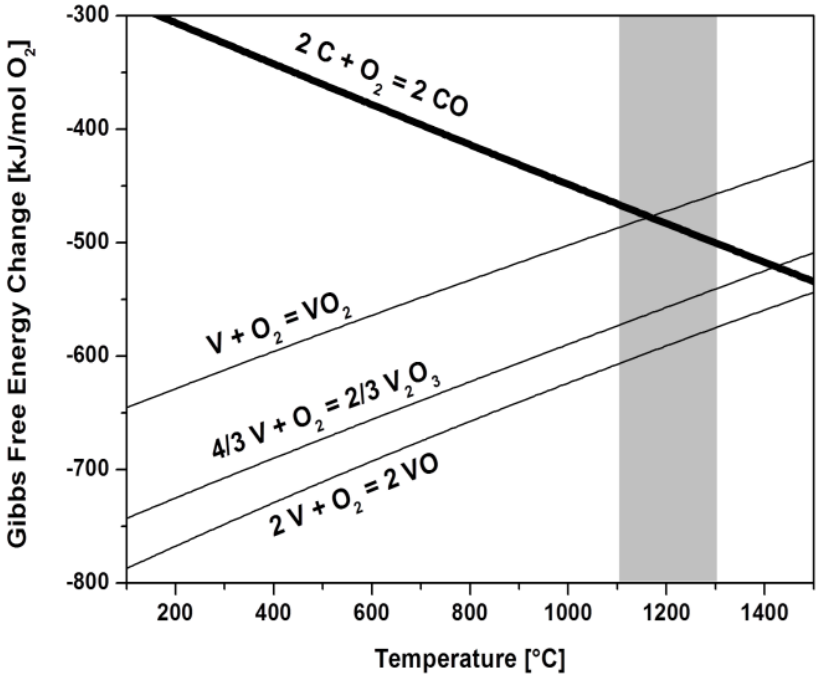

Figure 3-39. Ellingham diagrams showing the Gibbs free energy change of different oxides with respect to the system C–O [231].

In the present study, FTIR spectroscopy measurements (Figure 3-28) indicate that the reaction of the metal precursors with polycarbosilane leads to the formation of Si–O–V units (single-source-precursor). Pyrolysis of the vanadium-containing polycarbosilane in argon atmosphere at ≤ 1000 °C results in the formation of single-phase SiVC(O), which subsequently is considered to undergo partitioning and convert into a multi-phasic material consisting of V_8C_7, SiC(O) and segregated carbon (see also Table 3-16).

As there are strong carburizing conditions during the annealing of Si-V-C-O, we take into account the oxide with the lowest oxidation state at vanadium for our consideration (as shown in Figure 3-39, VO_2 and V_2O_3 can get reduced easily to lower vanadium oxides at temperatures beyond 1000 °C [234] by reducing species such as carbon, CO or H_2). Subsequently, the obtained lower vanadium oxide reacts with carbon leads to the formation of V_8C_7 (cf. VO + 15/8C = 1/8 V_8C_7 +CO). This is supported by the change in Gibbs free energy with respect to temperature which are strongly negative (-19.18 and -51.19 kJ/mol at 1100 °C and 1300 °C, respectively).

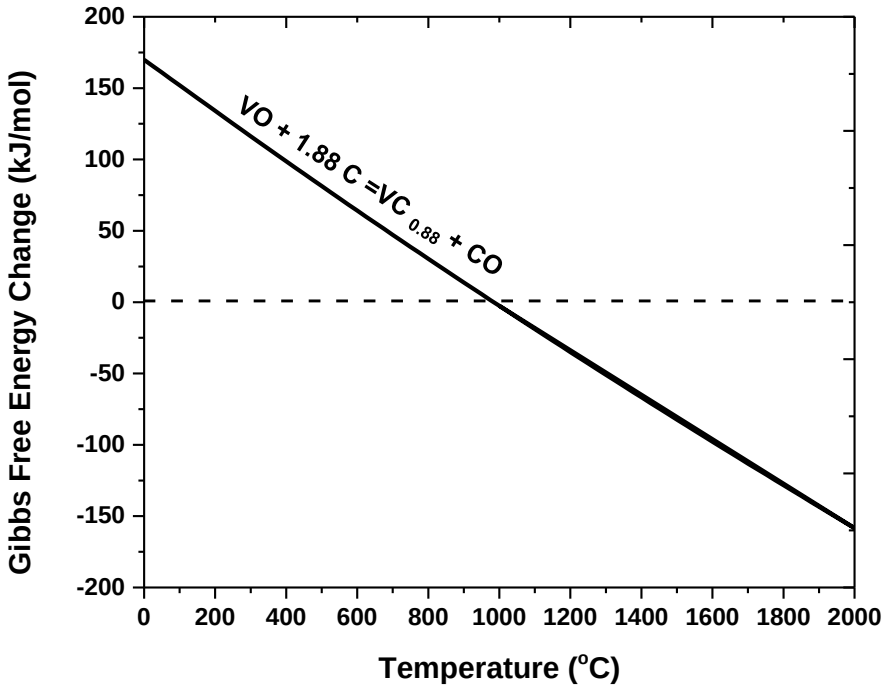

Figure 3-40. Plot of Gibbs free energy change of the reaction of VO with carbon with respect to the temperature.

Interestingly, while performing the high-temperature annealing of the samples under argon atmosphere at 1700 °C in an alumina tube furnace (not in graphite furnace) leads to the formation vanadium silicide (V_5Si_3) instead of V_8C_7 (Figure 3-38). This can be possibly explained by the reaction between V_8C_7 and SiC to yields V_5Si_3 and C. Free energy change became negative at high temperature region beyond 1900 °C. But in the present studies the crystallization has been occurred at lower temperature. This might be due to the existence of oxygen also confirmed by the XPS results which helps to reduce carbon activity and to lower the temperature of equilibrium.

Another possibility is the formation of metallic vanadium between the mechanism. As the obtained vanadium can react with the SiC(O) matrix (SiC + SiO_2) and thus V_5Si_3, this process is energetically possible (Figure 3-41b). The oxide of vanadium is quite stable for the carbothermal reduction to form metallic vanadium as also mentioned above (see the Ellingham diagram in Figure 3-39). But the formation of vanadium via reacting VO with V_8C_7 is energetically favorable is shown in the literature [234]. However, the Gibbs free energy of the formation of vanadium via the reaction of VO with V_8C_7 has large positive values (+171.672, +137.544 and +24.44 kJ/mol at 1100 °C, 1300 °C and 1900 °C, respectively). The oxygen content in the sample is relatively high (i.e., as for the case of high-temperature annealing in alumina furnace) as well as the presence of other reducing

species such as carbon, or CO, the reaction of VO with V_8C_7 to form metallic vanadium might get favorable.

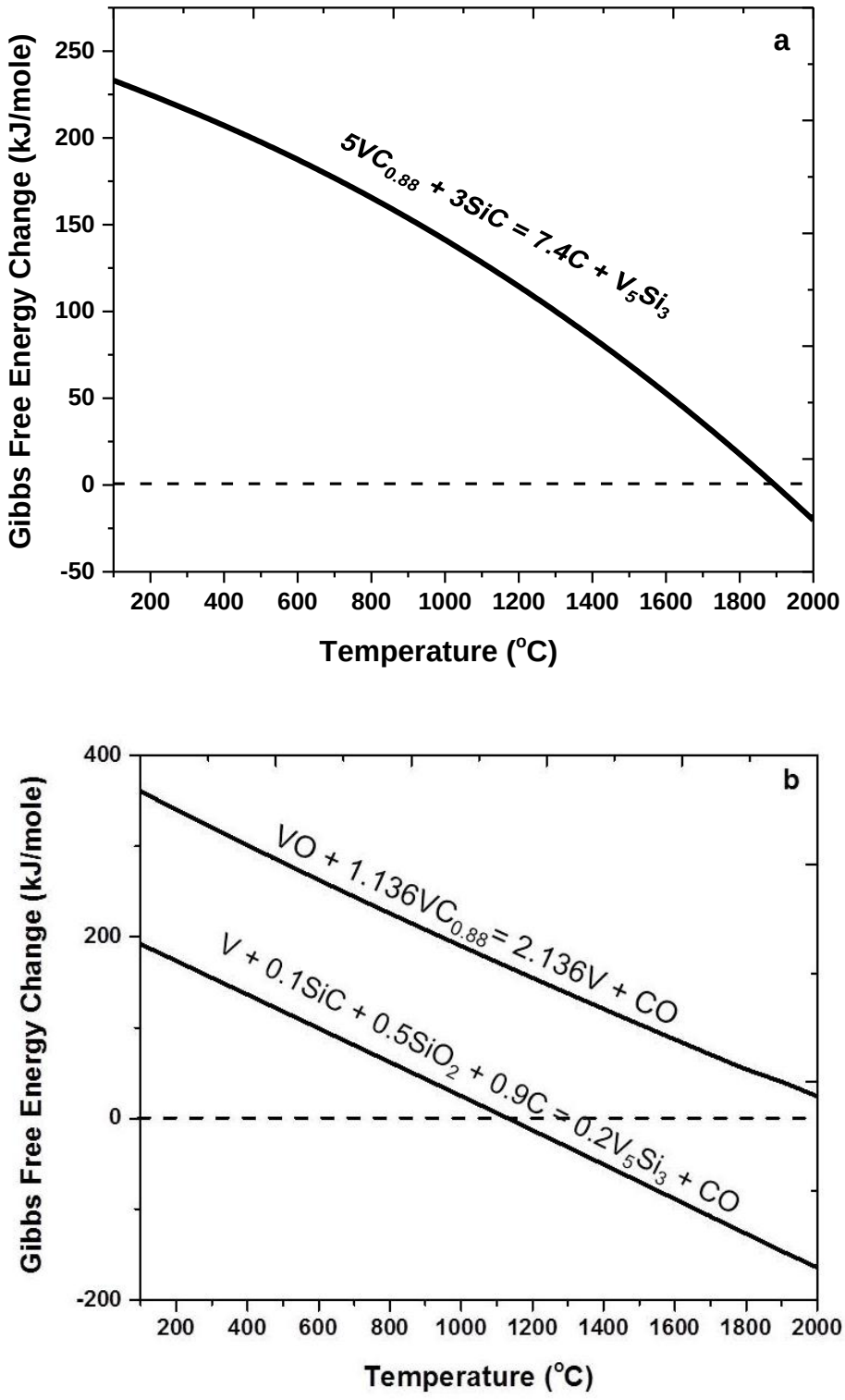

Figure 3-41. Plot of Gibbs free energy change of the different reaction with respect to the temperature.

3.3.1.6. Catalytic activity

The SiVC(O) sample prepared upon annealing at 1700 °C for 6h in strong carburizing atmosphere was chosen for the study of its catalytic activity with respect to ammonia decomposition, due to the fact that its specific surface area was relatively large (i.e., ca. 50 m^2/g) and the catalytically active phase V_8C_7 was well crystallized. The sample was heated in hydrogen environment in order to remove the surface oxygen prior to the catalytic test. The catalytic decomposition of ammonia over V_8C_7/SiC was performed at temperatures up to 1100 °C and the ammonia conversion efficiency was related to its decomposition *cf*. $NH_3 = N_2 + 1.5\ H_2$. Within this context the efficiency of the conversion of ammonia into hydrogen (η) has been defined as:

$$\eta = \frac{n_{H_2}}{1.5\ n_{NH_3}} . 100$$

with n_{H2} and n_{NH3} being the moles of produced H_2 and used NH_3, respectively, in the reaction chamber. The catalytic activity of the sample is shown in Figure 3-42. The maximum ammonia conversion efficiency was found to be 35 % at temperature of around 650 °C.

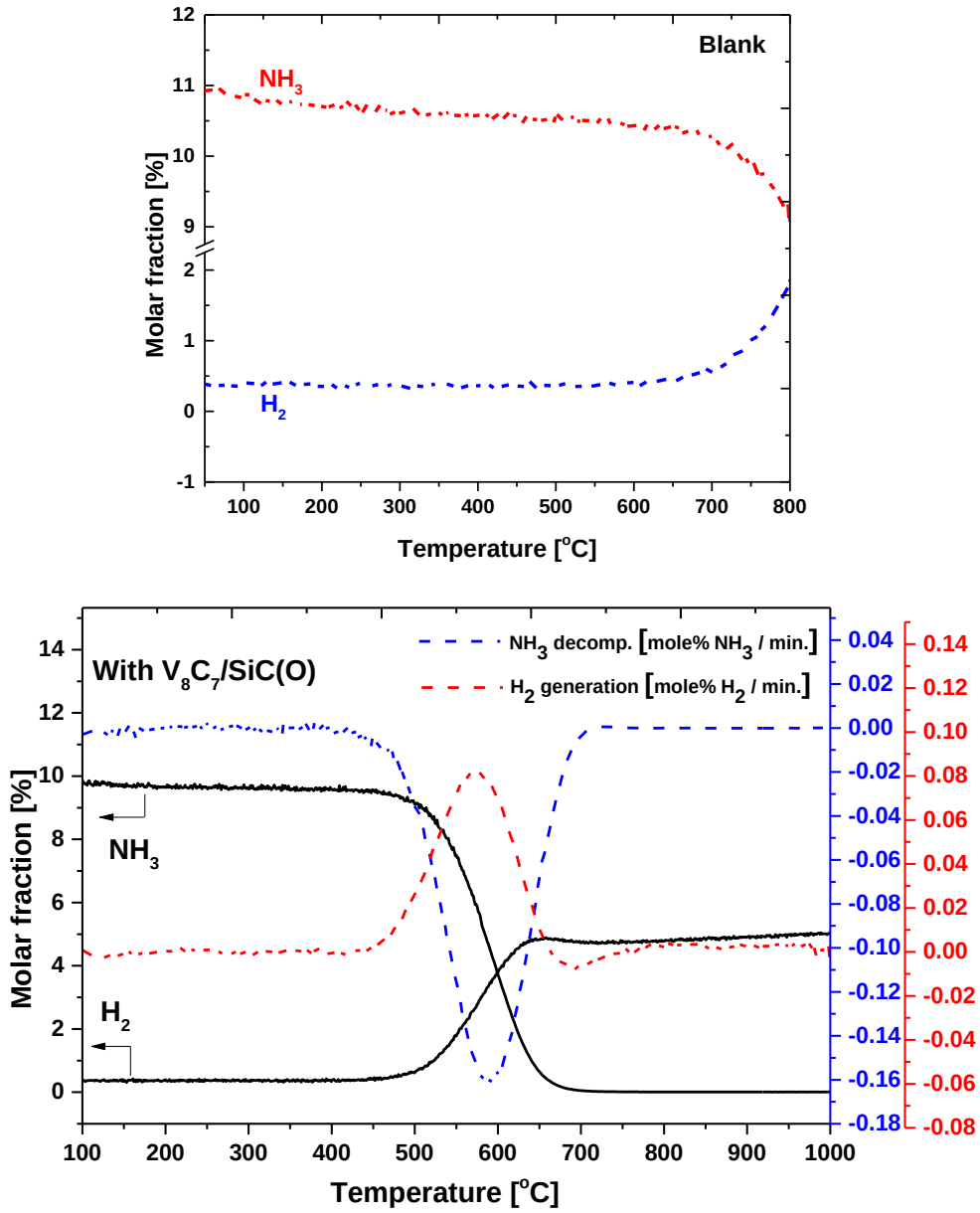

Figure 3-42. Comparison of catalytic activity of the V_8C_7/SiC(O) nanocomposites with the blank.

It is not easy to compare the performance of the present V_8C_7/SiC material with that of other catalysts, due to different conditions used in different studies. For instance, most studies report the activity of the catalysts in pure ammonia atmosphere; whereas in the present study a mixture of NH_3/He (10/90) was used.

Ruthenium is the most active metal for ammonia decomposition, and its activity varies with respect to the support materials used. Ru/CNT-based catalysts show 85 % of NH_3 conversion efficiency at 500 °C, which is obviously much higher than that of our V_8C_7/SiC nanocomposite (35%). However, the NH_3 conversion efficiency of the V_8C_7/SiC nanocomposite seems to be higher than that of pure vanadium carbide powder [27]. This

difference might rely on the fact that in V_8C_7/SiC the matrix prevents the agglomeration of the catalytically active V_8C_7 nanoparticles; whereas in the vanadium carbide powder agglomeration/sintering is considered to occur to a significant extent.

The relatively low efficiency of V_8C_7/SiC as compared to e.g. Ru/CNT might relate to the low surface area of V_8C_7/SiC as well as to the relatively low V_8C_7 content (and consequently low fraction of accessible V_8C_7 nanoparticles). Thus considering the volume fraction of V_8C_7 (i.e., ca. 14 vol%) and the specific surface area of the nanocomposite (i.e., ca. 50 m^2/g), only less amount of V_8C_7 nanoparticles are available at the surface for catalytical decomposition of ammonia. Hence, the efficiency of ca. 35 % concerning the decomposition of ammonia represents a rather good value.

3.3.1.7. Summary

The present study indicates that V_8C_7/SiC(O) nanocomposites can be prepared upon chemical modification of polycarbosilane (SMP-10; single-source-precursor) and subsequent pyrolysis. The nanocomposites obtained at 1300 °C were shown to be crystalline, with considerable amount of oxygen content on the surface, as confirmed by XPS results. The surface area of the obtained nanocomposites depends on the pyrolysis temperature and decreases up to 1300 °C as the network structure gradual collapse. At higher temperature the specific surface area again after starts to increase due to the carbothermal conversion of oxides into carbides and evolution of CO.

In situ synthesis by single-source-precursor of the vanadium carbide yields a homogeneously dispersed system and avoids the growth of the particle size even at elevated temperatures. The SiC matrix plays an important role to suppress the growth of V_8C_7 nanoparticles.

The preliminary results indicate that the system is active for the decomposition of ammonia with a conversion efficiency of 35% at 650 °C.

3.3.2. Vanadium-containing SSPs using vanadium oxytriisopropoxide

3.3.2.1. Characterization of obtained vanadium-containing SSPs

This part of the work involves the synthesis and processing of V_8C_7/SiC(O) nanocomposites using biomorphic and sacrificial technique. In biomorphic method, template (paper and wood) is infiltered by the precursor of ceramic and subsequently pyrolysis lead to the formation of desired nanocomposites. For this method liquid precursor is preferable and this is the main reason for using the vanadium oxytriisopropoxide (liquid in state) in place of vanadylacetonate (solid in state) for the processing.

In a typical preparation, SSPs have been synthesized from a reaction between vanadium oxytriisopropoxide (VISO) and allyl-hydridopolycarbosilane (SMP-10). The precursors obtained were investigated in detail by ATR-FTIR and NMR spectroscopy techniques. ATR-FTIR spectra of SMP-10, VISO, and VISO-modified SMP-10 with toluene (denoted as Vi-SMP-To) after reaction for 3 h, 1 day and 2 day respectively are presented in

Figure **3-43**. As obvious from the ATR-FTIR spectra, the band, at ca. ~ 2121 cm^{-1}, which is assigned to the Si-H groups in SMP-10, was still present even after 2 days of reaction. The characteristic bands of VISO framework are also observed at 1006 cm^{-1} for ν(V-O), 980 cm^{-1} for ν(V=O) [235, 236] and 1051 cm^{-1} for ν(C-O) [235].

Furthermore, the observable changes starts to appear after 1 day of mixing. The band assigned to the V=O bonding starts to diminish in the precursor and the relative intensity of the Si-H band is found to be decreasing with increasing reaction time. Instead of it a new band at 950 cm^{-1} starts to appear. This new band at 950 cm^{-1} was assigned to Si-O-V, [217, 218] indicating the formation of vanadium-containing single-source-precursor. No considerable changes has been observed with respect to allyl-band (1650 cm^{-1}) indicating that it is not participating in the reaction of the starting materials. It also confirms that the crosslinking of the SSPs is not yet started.

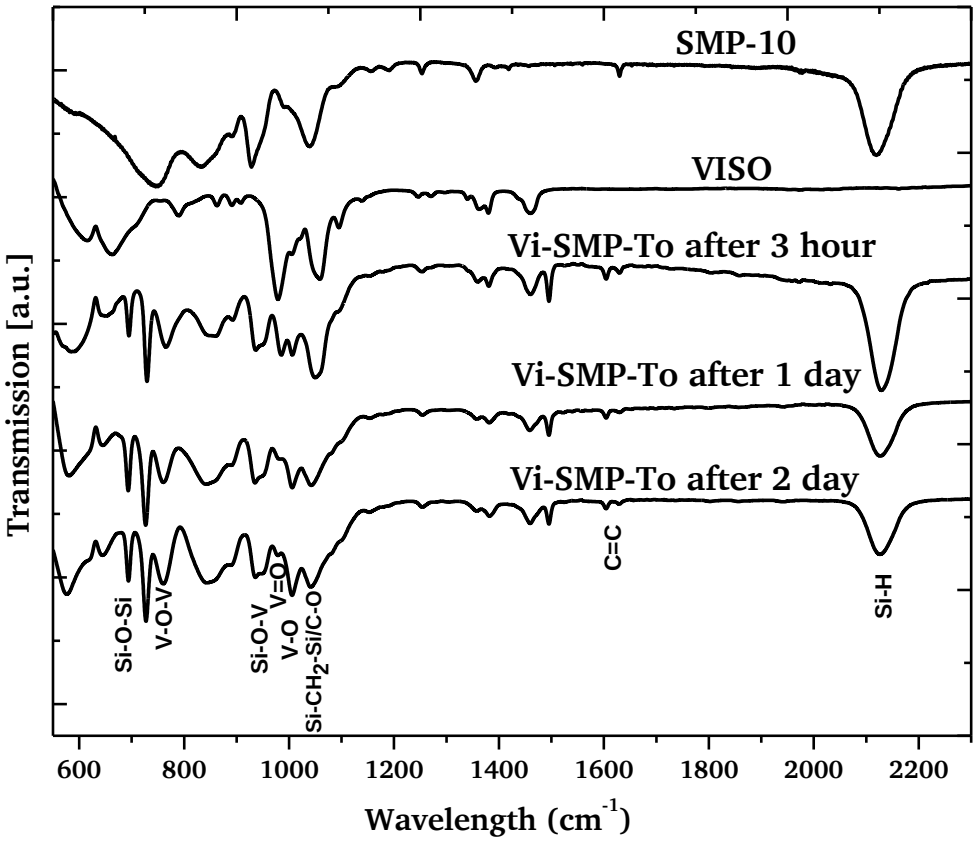

Figure 3-43. ATR-FTIR spectra of the SMP-10, of VISO and of VISO-modified SMP-10 (Vi-SMP-To) after reaction for 3 hours, one day and two days.

The ^{29}Si NMR results (Figure 3-44) further supports the ATR-FTIR results. The group of peaks between -8 ppm and -20 ppm are assigned to C_3SiH. Several resolved singlets ranging from -61 ppm to -67 ppm are also originating from the silicon in $CSiH_3$ units [78, 81, 237] whereas those appear between -31 and -39 ppm are assigned to the C_2SiH_2 units in SMP-10. When compared with pure SMP-10, the integral of the peaks in the case of vanadium modified samples clearly shows that the amount of $CSiH_3$ units is decreased. This indicates the structural changes of SMP-10 which consumes Si-H bonds. Another noticable change has been seen with a change in chemical shift towards low field which confirms the formation of Si-O bonds. This results confirms that the formation of Si-O-V by using Si-H bond and supports the ATR-FTIR for the formation of SSP.

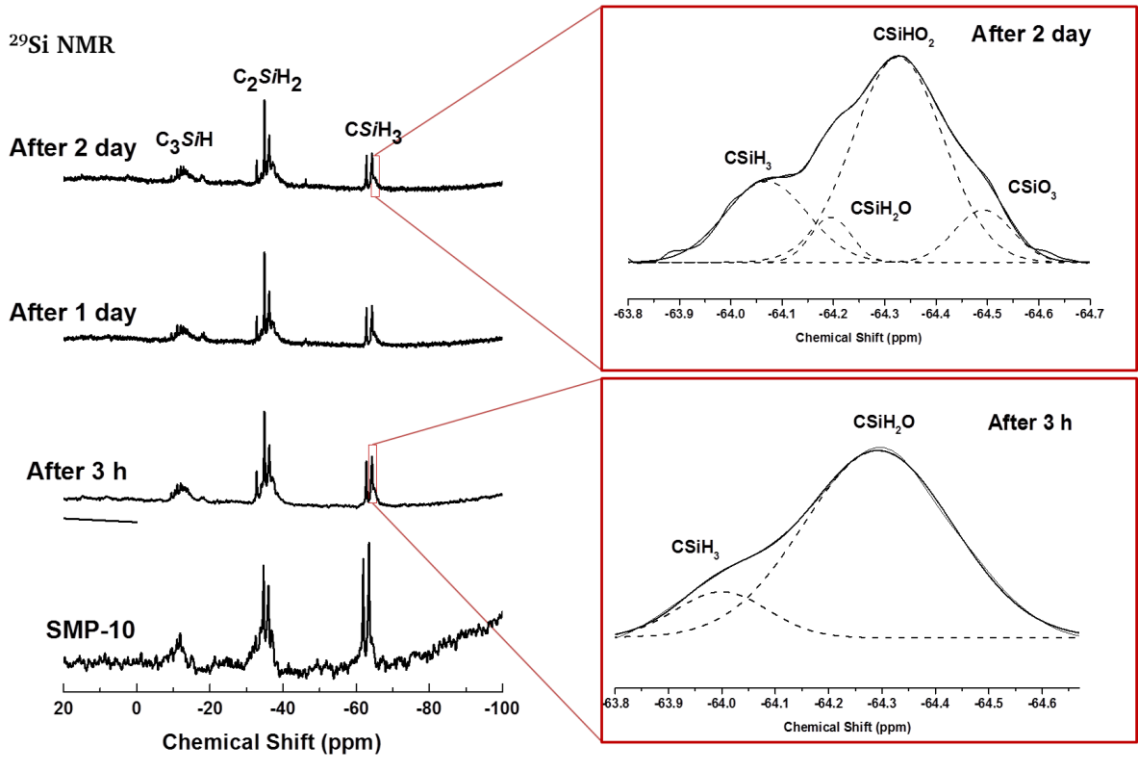

Figure 3-44. ^{29}Si NMR spectra of the single-source-precursor solution after reaction for 3 h, 1 day and 2 day.

Toluene (solvent) was removed at room temperature with the aid of vacuum from the obtained SSPs (Vi-SMP). It was found that the liquid precursor is converted into solid precursor. The obtained sample was characterized by ATR-FTIR (Figure 3-45). The bands related to the allyl-group were not found in the resulting spectra. The disappearance of the allyl-bands and relative decrease in the intensity of the Si-H band confirms the crosslinking of the SSPs via hydrosilylation reaction starts after the removal of solvent.

It has already been reported in the literatures that neutral oxovanadium complexes have great potential for using in the process of catalysis [238]. Here the complex of VISO is expected to act as a catalyst for the hydrosilylation reaction. The disappearance of -ν(V=O) (980 cm^{-1}) and appearance of the Si-O-V [217, 218] at 950 cm^{-1} is more pronounced with respect to the precursor obtained before removal of toluene (Vi-SMP-To) and supports the formation of single-source-precursor. At the same time it also confirms that the crosslinking within the SSPs starts at room temperature after removal of toluene. The probable proposed reaction mechanism is shown in Figure 3-46.

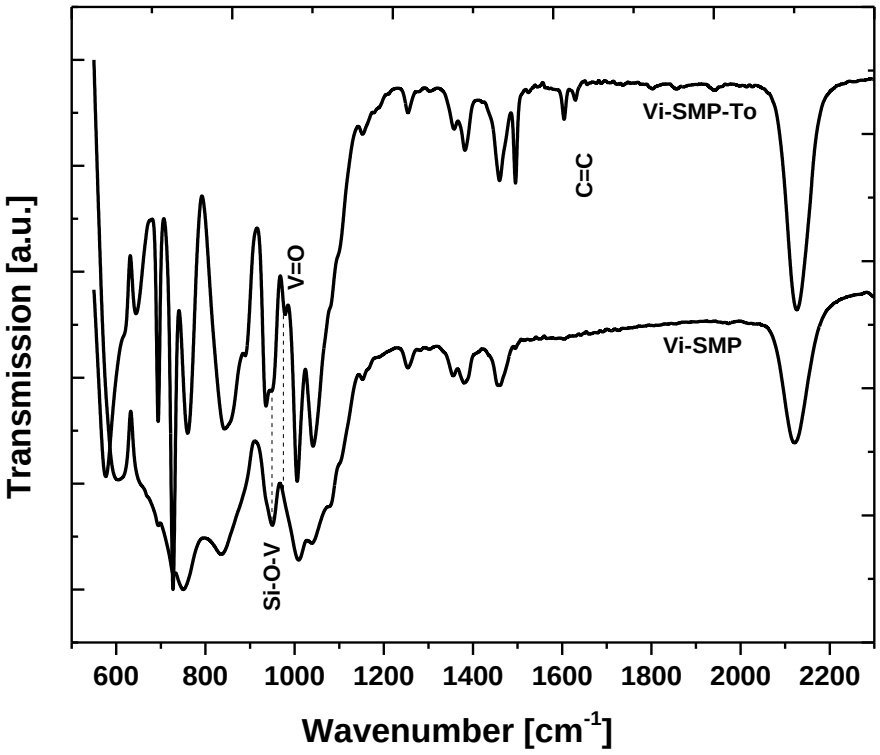

Figure 3-45. ATR-FTIR spectra of the VISO-modified SMP-10 with toluene (Vi-SMP-To) and after removal of toluene (Vi-SMP).

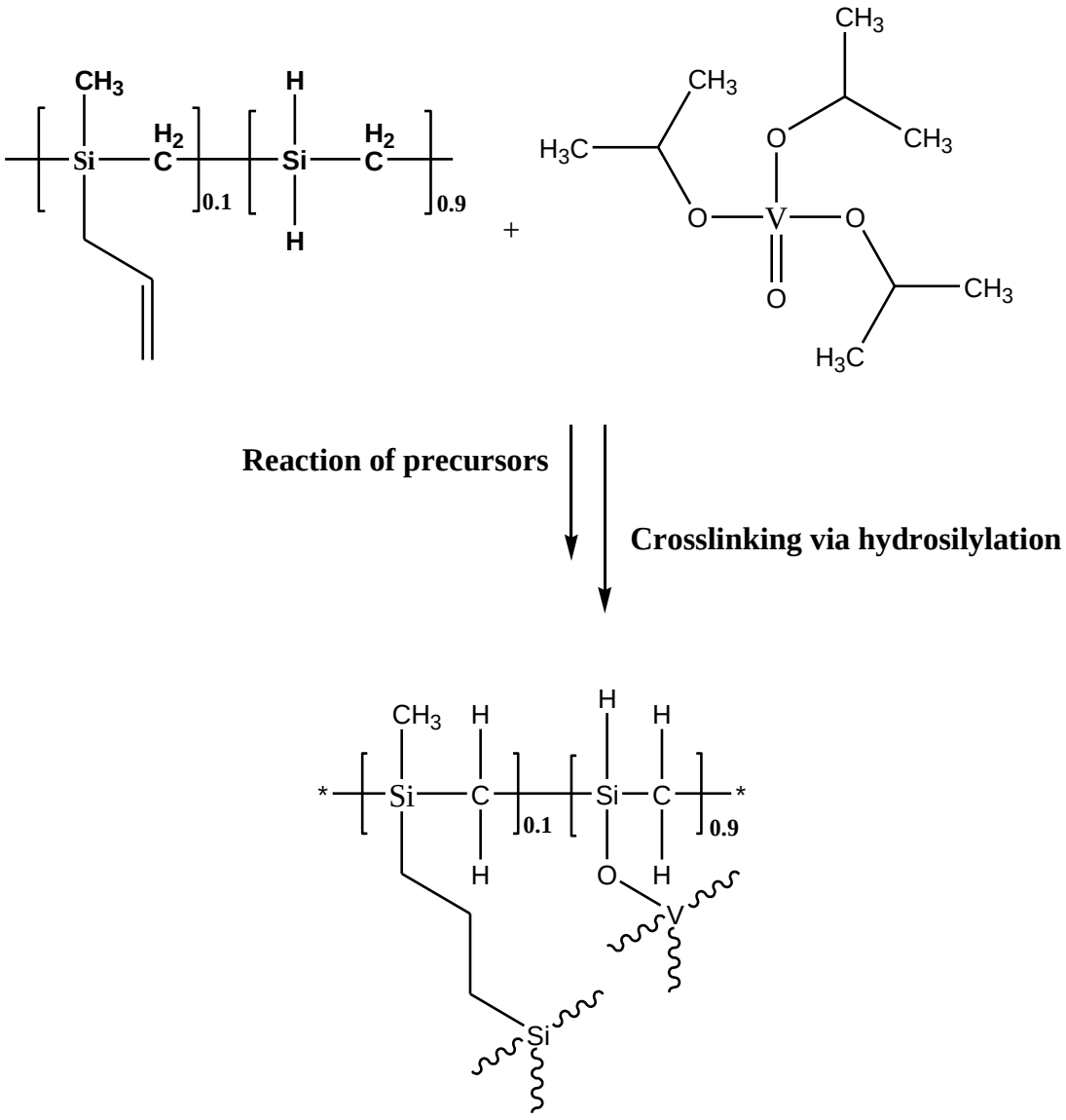

Figure 3-46. Possible reaction of SMP-10 with VISO upon formation of Si-O-V linkages.

3.3.2.2. Polymer-to-ceramic transformation

The polymer-to-ceramic conversion of the vanadium modified SSP was studied by means of TGA analysis. Major mass loss (around 27 wt%) has been observed in the temperature range of 200-600 °C and no further mass changes were observed at temperatures beyond 800-850 °C. Thus, it is concluded that the polymer-to-ceramic transformation is completed at temperatures up to 800-850 °C. The final ceramic yield amounts ca. 69 wt%. *In situ* infrared spectroscopy coupled with TGA (IR-TGA) is done in order to elucidate the evolution of the gaseous species during the thermolysis under Ar atmosphere. Oligomers, CH_4, CO_2, C_2H_4 and C_3H_7 are the main gaseous species detected by IR-TGA.

1. The fragments of oligomers results from the decomposition of the SSP are detected by the IR-TGA at temperature 273 and 465 °C with evolution pattern ~995-951, 1079-1030, 1277-1182, 2910-2865, 2995-2929 cm^{-1}.

2. The evolution of CH_4 has been confirmed by the three maxima at 295, 493 and 638 °C (3019 -3007 cm^{-1} and 1306-1301 cm^{-1}). The condensation of Si–CH_2–Si and/or terminal Si–CH_3 bonds results in the formation of CH_4.

3. The composite with four maxima at 282, 425, 872 and 1100 °C is expected due to the evolution of CO_2 (2379 -2294 cm^{-1} and 670-667 cm^{-1}). The formation of CO_2 at low temperatures leads to the formation of amorphous metal oxycarbides (SiVOC). In addition, the evolution of CO_2 at higher temperature is ascribed to the reaction of vanadium oxide and silicon oxycarbide with carbon resulting in the formation of metal carbide composites (V_8C_7/SiC).

4. The release of alkenes is associated with two maxima at ~280 and ~480 °C (952-946 cm^{-1}). The formation of alkenes is related to the rearrangement reactions, leading to the combination of -CH_2- linkages of carbosilane bonds (Si-CH_2-Si).

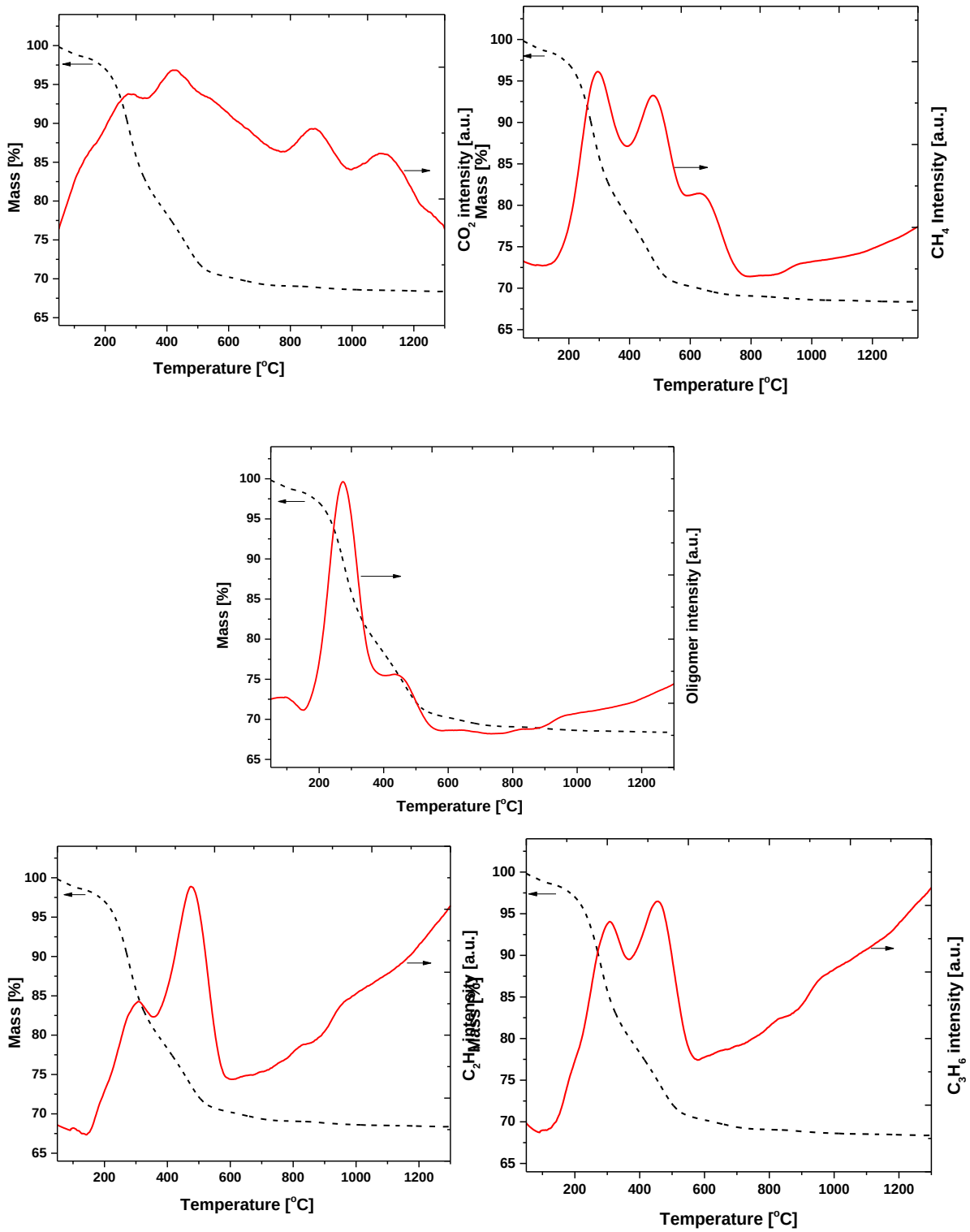

Figure 3-47. IR-TGA measurements of the VISO-modified SMP-10 after removal of toluene (Vi-SMP) (dashed lines, TG and solid line are selected evolution pattern of respective gaseous species).

3.3.2.3. Processing of SiVC-based monoliths

In order to process the sample using the biotemplate method, VISO-modified SMP-10 with toluene (Vi-SMP-To) was used. After removal of toluene, the precursor converts into solid as already discussed in section 3.3.2.1 and is difficult to be processed further. This is the reason for selecting Vi-SMP-To for the processing. The templates used for this study were paper and wood. Samples were prepared from coniferous pine wood. Pine was chosen because of its relatively homogeneous tracheidal pore structure and exhibits an uniform morphology of 90-95 vol%. [239].

The processing of paper templates involves the impregnation of templates with the precursor solution (Vi-SMP-To). In order to obtained properly replicated templates, several experiments were done using different composition of Vi-SMP-To. The processing starts with the composition of 1:1:1 (VISO:SMP-10:toluene). This composition is found to be higly viscous and not able to be processed further. Than the viscosity of the precursor is adjusted by the amount of the toluene. And the optimal ratio for the starting precursor solution found to be 1:1:4. By the use of this ratio, the fibrous structure of the paper template retained. Further optimization of the process condition has been done by changing infiltration cycle and drying time (for removal of toluene at ambient temperature and pressure).

Table 3-17. Optimization of the composition and conditions to process VISO-modified SMP-10 with toluene using paper as a template

S.No.	Sample composition SMP-10:Viso:Toluene	Infiltration cycles	Drying at amb. condition
1	**1:1:2**	1	3 hour
2	-	4	3 hour
3	**1:1:4**	1	3 hour
4	-	-	6 days
5	-	4	3 hour
6	-	-	6 days

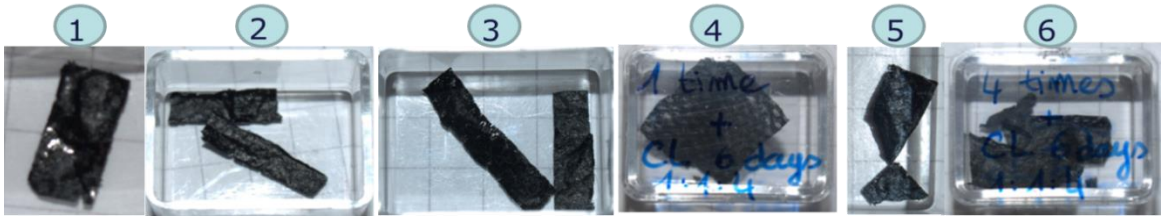

Finally the obtained samples are subjected to heat treatment at different temperature (800, 1300 and 1700 °C) and further characterized in order to understand clearly their microstructure and geometrical surface area using different characterization techniques.

In case of wood the processing consists of two step. The first step is the pyrolysis of the wood to get carbon preform, to increase the porosity and reduce the chances of contamination and the second step is infiltration of this carbon preform with the SSP. The obtained samples are subjected to heat treatment at 1700 °C.

3.3.2.4. Microstructure and surface area analysis

Scanning electron microscopy (SEM) images helps to understand the replication of the microstructure of templates after processing using different parameters. SEM images of the templates used within the present study (i.e., paper and carbonized wood) are shown in Figure 3-48. It can be seen that the paper template has randomly oriented cellulose fibrillar microstructure. The single fibers possesses strip or strap structure with size of 7-24 μm in radial direction and the spaces between these fibres correspond to the pores of these materials. The carbonized wood template shows a tubular structure with size of 13-15 μm in the vertical direction.

a) b)

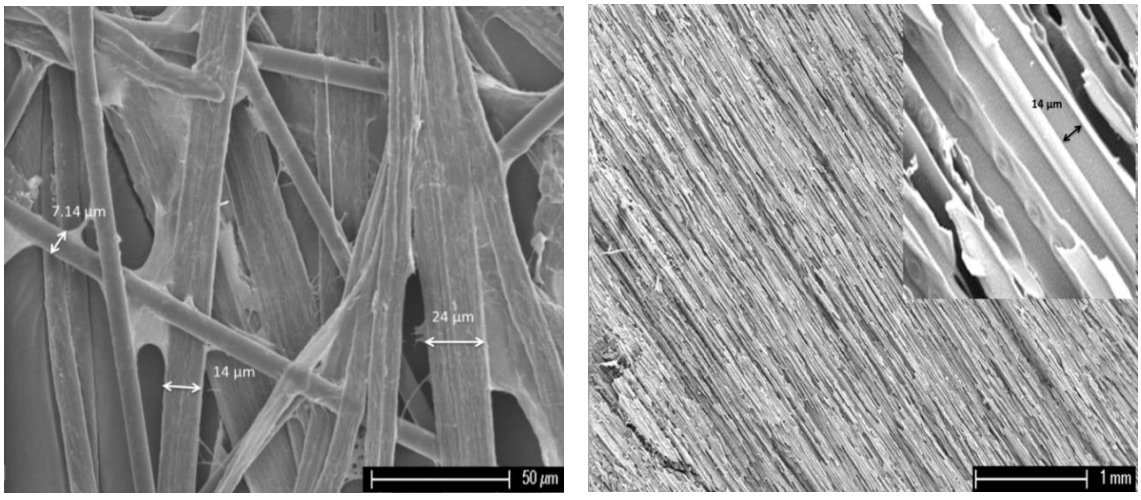

Figure 3-48. SEM image of paper (a) and of the cross section of carbonized wood (b).

Figure 3-49 shows the SEM images of papers infiltrated in a solution of 1:1:4 compositions by weight, with different number of infiltration cycles (1 time and 4 times) and pyrolysed at 800 °C after respective drying procedures for 3 hours and 6 days. The SEM images clearly shows the effect of the number of infiltration cycle and drying hours

on the replication of the fibrous structure of paper. The best results obtained with one infiltration cycle and 6 days of the drying.

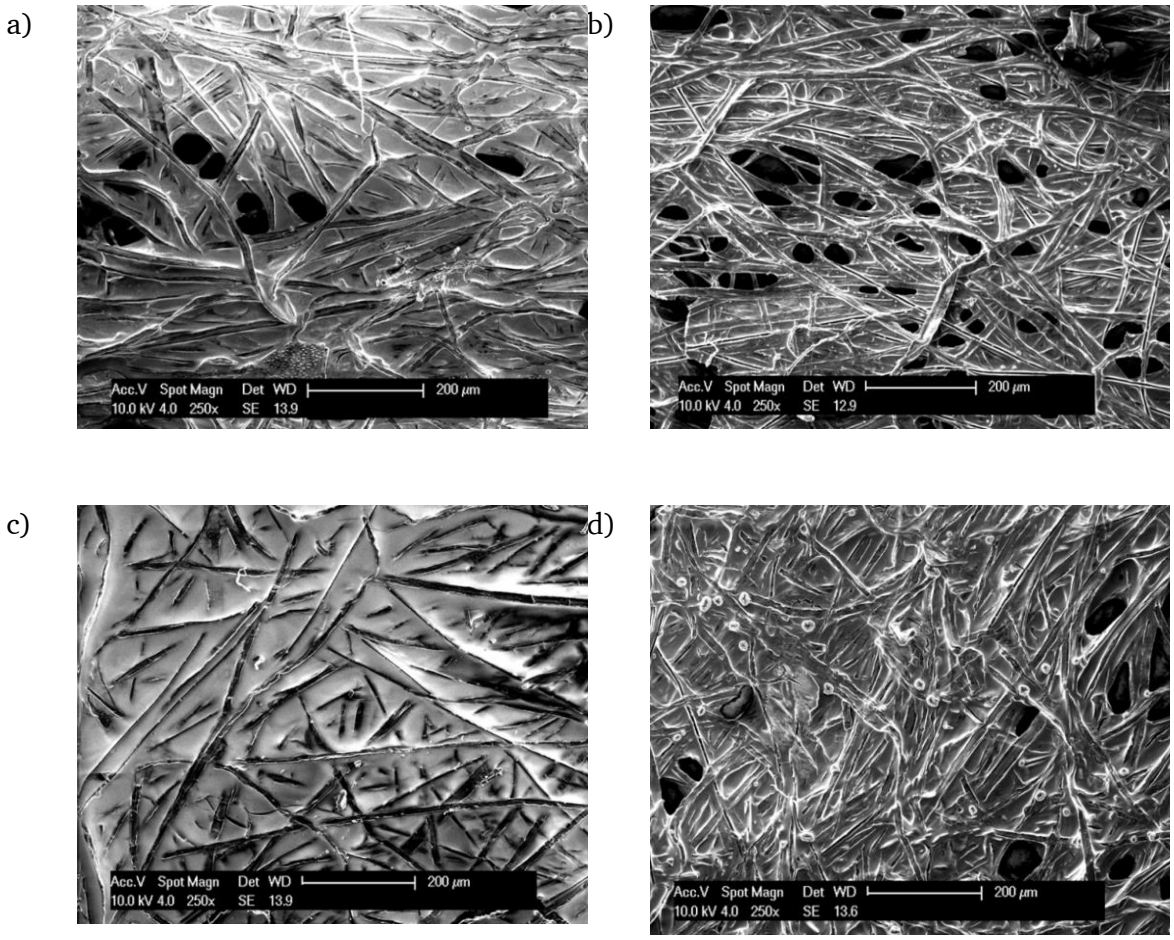

Figure 3-49. 1) SEM images of paper infiltrated with the Vi-SMP-To one time and pyrolysed at 800 °C after 3 hours (a) and 6 days (b), 2) SEM images of paper infiltrated four times and pyrolysed at 800 °C after 3 hours (c) and 6 days (d).

As the pyrolysis temperature is not sufficient high for the crystallization of ceramic nanocomposites. The optimized pyrolyzed sample (1:1:4 compositions by weight, 1 infiltration cycles, and 6 days drying) is annealed at 1300 °C and 1700 °C for 3h. Figure 3-50 shows the SEM image of the sample pyrolyzed at 800 °C and 1300 °C for 3h respectively. The image shows that the replication of the fibrous structure of paper is now more pronounced and apparent than the sample pyrolyzed at 800 °C. In general it is hard to comment on the diameter of the fiber as it is in wide range of 5-24 μm. Unfortunately, the infiltered paper template sintered at 1700 °C was not able to recover during the process.

a) b)

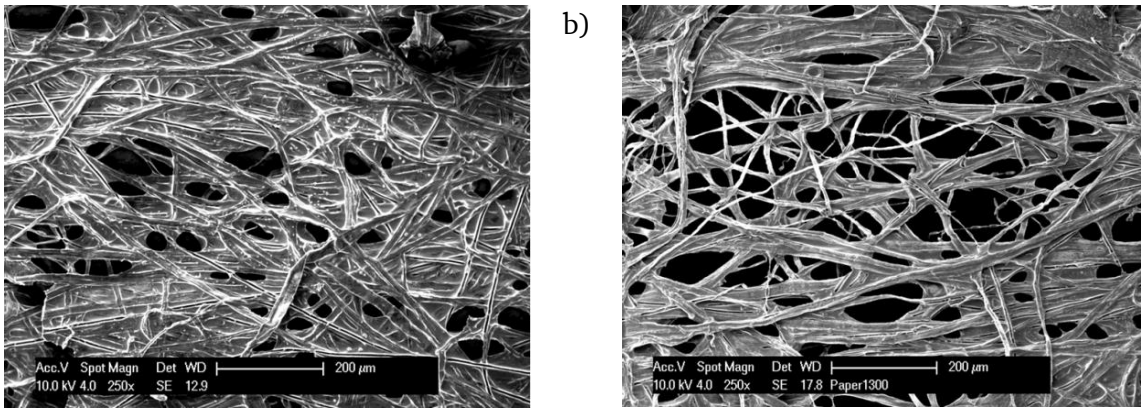

Figure 3-50. SEM images of paper infiltrated with the Vi-SMP-To for one time at temperature of 800 °C (a), and high temperature treatment at 1300 °C (b).

The results obtained from the study discussed above showed that the best parameter for the replication of the structure is: 1:1:4 compositions combined with 1 infiltration cycle and 6 days of drying. The same parameter has been used for the processing of wood template. The infiltered wood sample was also pyrolyzed at 800 °C and further sintered at 1700 °C. The obtained sample was mechanically stable, unlike paper based template and further characterized by SEM.

Figure 3-51 represents the SEM images coupled with EDX of infiltrated carbonized wood template pyrolyzed at 1700 °C for 6h. In general, these images confirm the fact that the composites replicate the structure of the wood. In case of wood, the main challenge was related to the complete infiltration of the Vi-SMP-To. EDX coupled with SEM demonstrated the successful infiltration of precursor. The results shows that the vanadium is present also in the inner part of the sample.

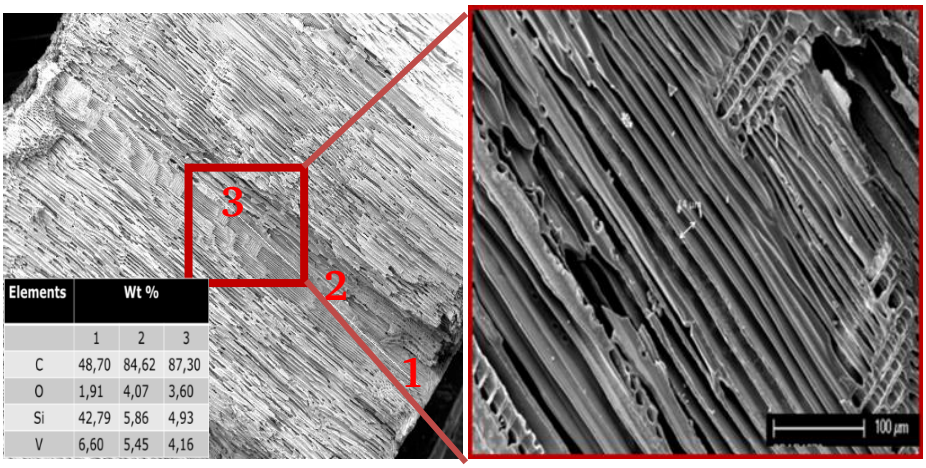

Elements	Wt %		
	1	2	3
C	48,70	84,62	87,30
O	1,91	4,07	3,60
Si	42,79	5,86	4,93
V	6,60	5,45	4,16

Figure 3-51. SEM images coupled with EDX of carbonized wood infiltrated with the Vi-SMP-To pyrolyzed at 1700 °C.

The pore sizes of monoliths obtained by wood template assisted methods are too large (13-15 μm) to obtain a reliable value for the specific surface area using the N_2 physisorption. The challenge in the fabrication of the monoliths in the high temperature fuel reforming is to get high geometric surface area per unit volume with stable pore structure with respect to temperature. Reforming of higher hydrocarbon fuels requires geometric surface areas per unit volume of the order of 105-108 m^2 per m^3 . In this regard the geometric surface area (GSA) as per volume is calculated. The geometrical surface area is calculated using following equation.

$$SA = \pi d\left(h + \frac{d}{2}\right) \qquad (1)$$

$$V = \pi \frac{d^2}{4} h \qquad (2)$$

$$GSA = \frac{SA}{V} = \frac{2(2h+d)}{dh} \qquad (3)$$

The obtained geometric surface area per unit volume is of the order of 10^2 - 10^3 m^2 per m^3 (4 mm tall cylindrical monolith with 8 mm of diameter). The advantage of wood template is tailored made structure to get desired geometrical surface area as per the application.

The last technique which is going to discuss here is sacrificial, in this type of system it will be the inverse replication of the structure as the template is decompose at high temperature and leave the pores behind. Figure 3-52 shows the microstructure of the

porous specimen pyrolyzed at different temperature. The average cell size of the sample pyrolyzed at 1400 °C is 5.12 μm (ranging from 1.36 μm to 10.76 μm). The sample pyrolyzed at higher temperature was mechanical unstable with shrinkage. The surface areas of powdered vanadium modified ceramics obtained by self-sacrificial technique at 1700 °C for 6h is 19 m^2/g.

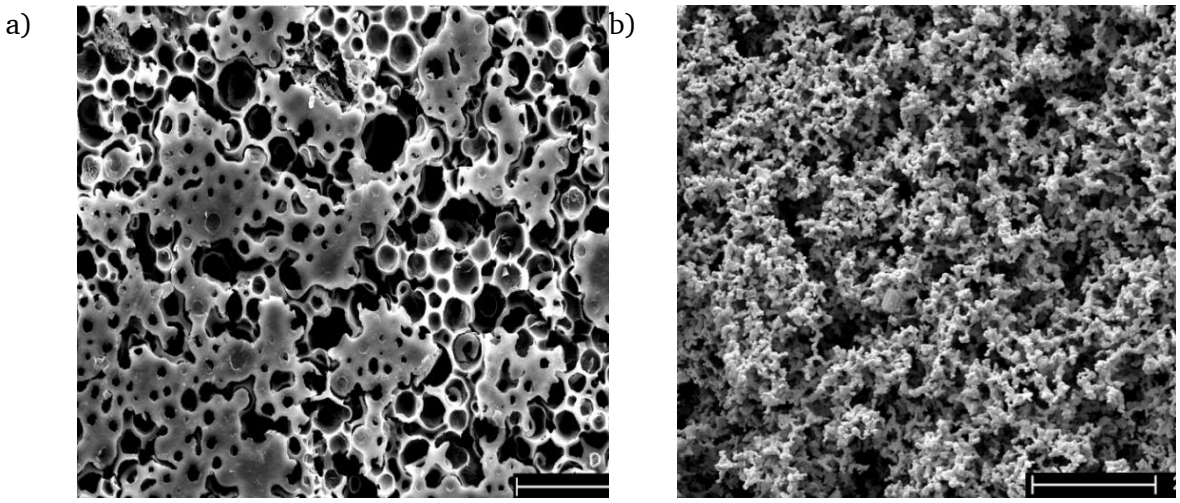

Figure 3-52. SEM images of ceramic obtained by self-sacrificial template pyrolyzed at 1700 °C.

The XRD pattern of all the samples annealed at different temperature under controlled argon atmosphere is shown in Figure 3-53. The XRD results indicate the crystallization of respective β-SiC and V_8C_7 phases.

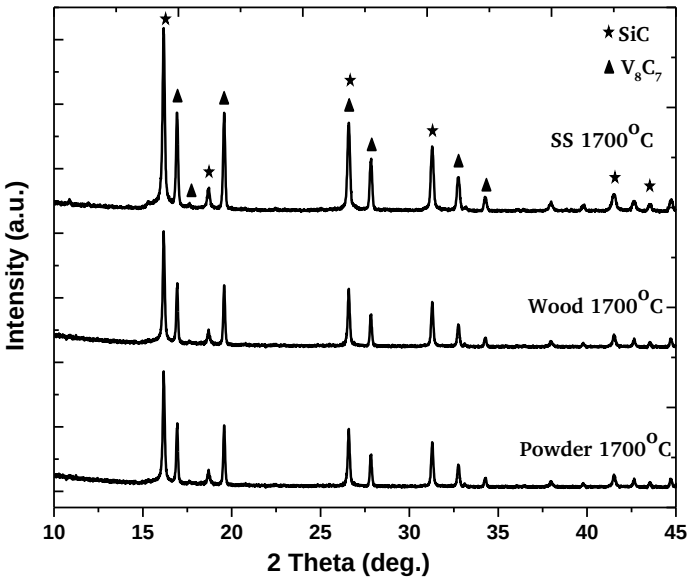

Figure 3-53. XRD pattern of the pyrolyzed samples (SS denotes for the sample obtained using Sacrificial template)

3.3.2.5. Catalytic activity

The wood assisted SiVC(O) sample prepared upon annealing at 1700 °C for 6h was selected for the study of its catalytical activity with respect to ammonia decomposition, due to the fact that it has considerably good geometrical surface area, mechanical stability, and nanocomposite was well crystallized. The preliminary investigations performed with and without catalyst indicates that the system is active for the decomposition of ammonia. The sample was preheated in hydrogen environment to get rid of surface oxygen.

The catalytic decomposition of ammonia over wood assisted V_8C_7/SiC was performed with respect to temperature (250-720 °C) and the ammonia conversion efficiency was related to its decomposition *cf*. $NH_3 = N_2 + 1.5\ H_2$. Within this context the efficiency of the conversion of ammonia into hydrogen (η) has been defined as:

$$\eta = \frac{n_{H_2}}{1.5\ n_{NH_3}} . 100$$

with n_{H2} and n_{NH3} being the moles of produced H_2 and used NH_3, respectively, in the reaction chamber. The results shows that the formation of the hydrogen increases with respect to the temperature. Comparison of the results with the blank points that till 525 °C the catalyst activity is nil and after this a sharp increase in the catalytic activity is observed.

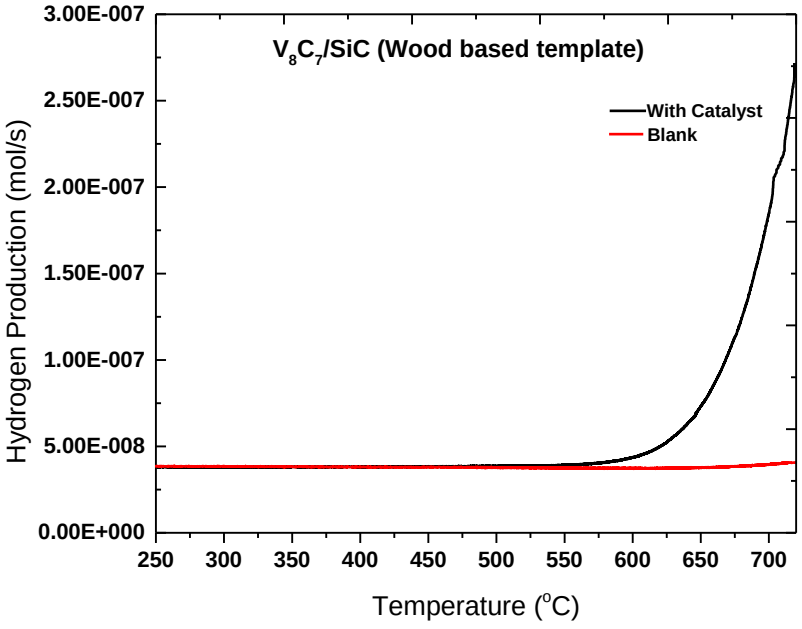

Figure 3-54. Comparison of Hydrogen production with wood based nanocomposites and blank

The efficiency for ammonia conversion is found to be 18 % at 720 °C which is higher than the pure vanadium carbide reported in the literatures (13 %). The reaction rates reported in the literatures for the decomposition of the ammonia hints that the reaction rates for vanadium carbide are temperature sensitive. The rate for the hydrogen generation in our case is found to be around 40 μmol/g(catalyst)/s which is much higher than the rates reported for vanadium carbides in literatures (12.9 μmol/g/s). Preliminary results show that the obtained SiVC(O) system is promising candidate for the decomposition of ammonia. The relatively low efficiency of V_8C_7/SiC might relate to the relatively low V_8C_7 content (i.e., ca. 5 vol%).

While looking catalytic activity of the sample obtained by vanadyl acetylacetonate (volume fraction of V_8C_7, ca. 14 vol% and efficiency 35% at 650 °C) with the sample obtained by vanadium oxytriisopropoxide (volume fraction of V_8C_7, ca. 5 vol% and efficiency 18% at 720 °C). The results give an impression that the catalytic activity get might improved by increasing of the volume fraction of the catalytically active V_8C_7 nanoparticles. At the same time it also provide the possibility that it also affects the conversion temperature. So the catalytic activity of V_8C_7/SiC material has been worth to investigate in detail with respect to increasing the volume fraction of the catalytically active V_8C_7 nanoparticles. The another factor which is also needed to investigate further is the measurement of the activity of the catalysts in pure ammonia atmosphere; as in the present studies a mixture of NH_3/He was used.

3.3.2.6. Summary

In the present study, template-assisted V_8C_7/SiC nanocomposites were prepared via impregnation of templates with the precursor solution (Vi-SMP-To). The optimum composition and conditions for the fabrication of templates found to be 1:1:4 compositions with 1 infitratrion cycle and 6 days of drying. The SEM results confirms that the method is helpful for the replication of the template structure (paper and wood). Corroborated spectroscopic and diffraction studies indicate that the single-source-precursor converts at high temperatures into an amorphous, single-phase SiVOC ceramic, which subsequently partitions and crystallizes to deliver V_8C_7/SiC nanocomposites. The V_8C_7/SiC nanocomposites were shown to exhibit promising catalytic activity concerning ammonia decomposition, which can be further improved upon increasing their specific surface area as well as by increasing the volume fraction of the catalytically active V_8C_7 nanoparticles.

4. Conclusion

Within the present work, it has been shown that the single-source-precursor (SSP) technique is feasible for the synthesis of Si-M-C-based ceramic nanocomposites. The phase composition and the microstructure of the SiC-based ceramic nanocomposites can be tailored by using this technique. Furthermore, selected case studies are presented, which reveals the applicability of this preparative technique for the processing of samples with tunable density/porosity.

Silicon-containing SSPs were successfully synthesized by the chemical modification of allyl-hydrido polycarbosilane (SMP-10) with molecular metal precursors. The obtained silicon-containing SSPs were identified as promising precursor for the synthesis and processing of ceramic nanocomposites with tailored phase compositions and microstructure. It has been demonstrated that the thermal decomposition of SSPs occurs via two steps:1) formation of amorphous single-phase ceramic (Si-M-C); 2) crystallization of the single-phase ceramic to furnish respective ceramic nanocoposites.

The first part of the work deals with the processing of crack-free and dense silicon carbide monoliths, which can be prepared by pressureless cross-linking and pyrolysis of green body obtained from SMP-10 followed by PIP treatment. The obtained monoliths were shown to be crack-free even upon annealing at high temperatures, despite of a large volume shrinkage occurring upon pyrolysis. Elemental analysis data revealed that at low annealing temperatures some excess carbon is present within the ceramic monoliths; additionally, oxygen has also been found to be present (several wt%). Both, the carbon and the oxygen contents decrease upon increasing the annealing temperature; thus, at temperatures beyond 1500 °C near-stoichiometric SiC can be produced. The bulk density of the formed SiC ceramics (2.63-2.69 gm/cm^3) was rather low as compared to taditionally processed SiC-based ceramics, due to the presence of some excess carbon and porosity in the monoliths. Thus, the produced ceramic monoliths have been shown to exhibit residual porosities of 15-25 vol%, which however can further be reduced to less than 1 vol% by using the PIP method to obtain crack-free and dense SiC-based bulk ceramics.

In order to promote densification, boron-containing SiC has been synthesized. It was succesfully synthesized by the chemical modification of SMP-10 with borane dimethylsulfide (BMS). The pressureless fabrication of low-porosity SiBC monolithic

samples confirms the beneficial effect of boron on the sintering behavior of silicon carbide. Crack-free and nearly dense boron-modified silicon carbide monoliths can be prepared by a boron modified single-source precursor (0.9 wt% B) using pressureless synthesis technique with subsequent pyrolysis at relatively low temperatures. The open porosity of the monoliths is analysed to be 4.6 vol% at 1100 °C and kept almost constant up to high temperature (3.7 vol% at 1900 °C).

Furthermore, X-ray diffraction data, corroborated with XPS, FTIR, and Raman spectroscopic results confirms the fate of the boron in the formed SiBC ceramic which has not been clear so far in the literature. It indicated that in the polymer-derived SiBC material prepared from the BMS-modified SMP-10 (BMS-SiBC), boron preferentially is found in the free carbon phase and does not get incorporated into the SiC lattice (at least not in significant amounts). Interestingly, the incorporation of boron into the structure of polycarbosilane induces an increase in the amount of segregated carbon in the resulting ceramics. Moreover, the resulting segregated carbon in the SiBC samples is shown to be markedly less graphitized than that in boron-free SMP-10-derived SiC. Additionally, despite the rather large amount of boron present in the segregated carbon (i.e., 9 to 19 at%), no crystallization thereof to furnish boron carbide was found.

Additionally, boron-containing SiC was also successfully synthesized by the chemical modification of SMP-10 with allyl-functionalized *o*- and *m*-carboranes (AFC). The as-prepared single-source-precursors were structurally characterized and investigated concerning their conversion within ceramic materials. Thus thermal treatment of the single-source-precursors in argon atmosphere leads to X-ray amorphous SiBC-based materials. The XRD data of the ceramic materials annealed at high temperatures indicates the crystallization of boron-rich boron carbide phase, which was not detected in BMS-SiBC. The modification of SMP-10 with diallyl-*m*-carborane was shown to increase the ceramic yield, as it increases the cross-linking degree of the polymeric backbone of the single-source-precursor. The results confirm the crucial effect of the molecular architecture and chemism of the single-source-precursors on the phase composition and consequently properties of the resulting ceramic materials.

The second part of the work reports on the successful synthesis and processing of V_8C_7/SiC(O) nanocomposites for functional applications. It involves the formation of V_8C_7/SiC(O) nanocomposites upon chemical modification of SMP-10 with a molecular vanadium compound and subsequently pyrolysis. Corroborated spectroscopic and

diffraction studies indicate that the single-source-precursor converts at high temperatures into an amorphous, single-phase SiVOC ceramic, which subsequently partitions and crystallizes to deliver nanocomposites consisting of well faceted V_8C_7 nano precipitates homogeneously dispersed within β-SiC matrix. The XPS results confirms the presence of considerable amount of oxygen content on the surface. The surface area of the obtained nanocomposites is dependent on the pyrolysis temperature. It has been observed that upto 1300 °C, the specific surface area decreases as the structure gradual collapses but at higher temperatures it again starts to increase due to the carbothermal conversion of oxides to carbides and evolution of CO. *In situ* synthesis by single-source-precursor of the vanadium carbide helps to get homogeneously dispersed systems and avoid the growth of the particles even at elevated temperatures. The SiC matrix plays an important role to suppress the growth of the V_8C_7 nanoparticles. Moreover, they exhibit promising catalytic activity concerning ammonia decomposition in order for the production of hydrogen with 35% of conversion efficiency, which can be further improved upon increasing their specific surface area as well as by increasing the volume fraction of the catalytically active V_8C_7 nanoparticles.

The present study indicates that polymer processing of ceramics is a versatile technique to prepare dense SiC-based ceramic parts with tailor-made phase compositions, microstructures and property profiles. Their high potential in applications for next generation nuclear energy will be emphasized. Preliminary results on the catalytic activity show that the obtained SiVC system is promising candidate for the production of hydrogen via decomposition of ammonia.

References

1. Ledoux M J, Hantzer S, Huu C P, Guille J, Desaneaux M-P. New synthesis and uses of high-specific-surface SiC as a catalytic support that is chemically inert and has high thermal resistance. Journal of Catalysis 1988;114:176-85.

2. Yang W, Araki H, Tang C, Thaveethavorn S, Kohyama A, Suzuki H, Noda T. Single-Crystal SiC Nanowires with a Thin Carbon Coating for Stronger and Tougher Ceramic Composites. Advanced Materials 2005;17:1519-23.

3. Wong E W, Sheehan P E, Lieber C M. Nanobeam Mechanics: Elasticity, Strength, and Toughness of Nanorods and Nanotubes. Science 1997;277:1971-5.

4. Cui Y, Lieber C M. Functional Nanoscale Electronic Devices Assembled Using Silicon Nanowire Building Blocks. Science 2001;291:851-3.

5. Harris C I, Savage S, Konstantinov A, Bakowski M, Ericsson P. Progress towards SiC products. Applied Surface Science 2001;184:393-8.

6. Klimczyk P, SiC-Based Composites Sintered with High Pressure Method, in Silicon Carbide - Materials, Processing and Applications in Electronic Devices, Mukherjee M, Editor. 2011: p. 309-34.

7. Keller N, Vieira R, Nhut J-M, Pham-Huu C, Ledoux M J. New catalysts based on silicon carbide support for improvements in the sulfur recovery. Silicon carbide as support for the selective H2S oxidation. Journal of the Brazilian Chemical Society 2005;16:202-9.

8. Hepel M, Composite Films of Nickel / Silicon Carbide, in MRS Proceedings, Arkles B, Beach D N, Hepp A F, Kumta P N, Sullivan J J, Editors. 2011, 495.

9. Hu J Q, Bando Y, Zhan J H, Golberg D. Fabrication of ZnS/SiC nanocables, SiC-shelled ZnS nanoribbons (and sheets), and SiC nanotubes (and tubes). Applied Physics Letters 2004;85:2932-4.

10. Ledoux M, Pham-Huu C. Silicon Carbide: A Novel Catalyst Support for Heterogeneous Catalysis. CATTECH 2001;5:226-46.

11. Prochazka S, Scanlan R M. Effect of Boron and Carbon on Sintering of SiC. Journal of the American Ceramic Society 1975;58:72-3.

12. Ionescu E, Polymer Derived Ceramics, in Ceramics Science and Technology 3: Synthesis and Processing, Riedel R, Chen I-W, Editors. 2012, 3: p. 457-500.

13. Ionescu E, Riedel R, Polymer Processing of Ceramics, in Ceramics and Composites Processing Methods, Bansal N P, Boccaccini A R, Editors. 2012: p. 235-70.

14. Riedel R, Passing G, Schönfelder H, Brook R J. Synthesis of dense silicon-based ceramics at low temperatures. Nature 1992;355:714 - 7.

15. Martínez-Crespiera S, Ionescu E, Kleebe H-J, Riedel R. Pressureless synthesis of fully dense and crack-free SiOC bulk ceramics via photo-crosslinking and pyrolysis of a polysiloxane. Journal of the European Ceramic Society 2011;31:913-9.

16. Janakiraman N, Aldinger F. Fabrication and characterization of fully dense Si–C–N ceramics from a poly(ureamethylvinyl)silazane precursor. Journal of the European Ceramic Society 2009;29:163-73.

17. Esfehanian M, Oberacker R, Fett T, Hoffmann M J. Development of Dense Filler-Free Polymer-Derived SiOC Ceramics by Field-Assisted Sintering. Journal of the American Ceramic Society 2008;91:3803-5.

18. Shah S R, Raj R. Mechanical properties of a fully dense polymer derived ceramic made by a novel pressure casting process. Acta Materialia 2002;50.

19. Ishihara S, Gu H, Bill J, Aldinger F, Wakai F. Densification of Precursor-Derived Si-C-N Ceramics by High-Pressure Hot Isostatic Pressing. Journal of the American Ceramic Society 2002;85: 1706-12

20. Colombo P, Paulson T E, Pantano C G. Synthesis of Silicon Carbide Thin Films with Polycarbosilane (PCS). Journal of the American Ceramic Society 1997;80:2333-40.

21. Su Z, Tang M, Wang Z, Zhang L, Chen L. Processing of Silicon Carbide Fibers from Polycarbosilane with Polypropylene as the Additive. Journal of the American Ceramic Society 2010;93:679-85.

22. Jang Y-S, Zollfrank C, Jank M, Greil P. Fabrication of Silicon Carbide Micropillar Arrays from Polycarbosilanes. Journal of the American Ceramic Society 2010;93:3929-34.

23. Liu H A, Balkus K J. Electrospinning of beta silicon carbide nanofibers. Materials Letters 2009;63:2361-4.

24. Yao R, Feng Z, Yu Y, Li S, Chen L, Zhang Y. Synthesis and characterization of continuous freestanding silicon carbide films with polycarbosilane (PCS). Journal of the European Ceramic Society 2009;29:2079-85.

25. Koga K, Mizuta S, Nagano S, Nakayama M. Method of producing dense sintered silicon carbide body from polycarbosilanes. United states patent 4374793 A 1983.

26. Kaur S, Riedel R, Ionescu E. Pressureless fabrication of dense monolithic SiC ceramics from a polycarbosilane. Journal of the European Ceramic Society 2014;34:3571-8.

27. Choi J-G. Ammonia Decomposition over Vanadium Carbide Catalysts. Journal of Catalysis 1999;182:104-16.

28. Nicholas G. Wright A B H. Silicon Carbide: The Return of an Old Friend. Material Matters 4:1-5.

29. Izhevskyi V A, Genova L A, Bressiani J C, Bressiani A H A. Review article: silicon carbide. Structure, properties and processing. Cerâmica 2000;46:4-13.

30. Wu L, Chen Y, Jiang Y, Lu Y, Huang Z, Liquid Phase Sintering of Silicon Carbide with AlN-Re_2O_3 Additives, in Properties and Applications of Silicon Carbide, Gerhardt R, Editor. 2011.

31. Abderrazak H, Hmida E S B H, Silicon Carbide: Synthesis and Properties, in Properties and Applications of Silicon Carbide, Gerhardt R, Editor. 2011: p. 351-88.

32. Rahmana. Bulk and nano-scale characterization of polymer derived silicon carbide and comparison with sintered silicon carbide. Master Thesis 2009.

33. Yu. G, M.E. L, S.L R, Silicon Carbide (SiC), in Properties of Advanced Semiconductor Materials: GaN, AIN, InN, BN, SiC, SiGe, Levinshtein M E, Rumyantsev S L, Shur M S, Editors. 2001.

34. Guichelaar P, Acheson Process, in Carbide, Nitride and Boride Materials Synthesis and Processing, Weimer A, Editor. 1997: p. 115-29.

35. Satapathy L N, Ramesh P D, Agrawal D, Roy R. Microwave synthesis of phase-pure, fine silicon carbide powder. Materials Research Bulletin 2005;40:1871-82.

36. Changhong D, Xianpeng Z, Jinsong Z, Yongjin Y, Lihua C, Fei X. The synthesis of ultrafine SiC powder by the microwave heating technique. Journal of Materials Science 1997;32:2469-72.

37. Carassiti L, Jones A, Harrison P, Dobson P S, Kingman S, Maclaren I, Gregory D H. Ultra-rapid, sustainable and selective synthesis of silicon carbide powders and nanomaterials via microwave heating. Energy & Environmental Science 2011;4:1503-10.

38. Moshtaghioun B M, Poyato R, Cumbrera F L, De Bernardi-Martin S, Monshi A, Abbasi M H, Karimzadeh F, Dominguez-Rodriguez A. Rapid carbothermic synthesis of silicon carbide nano powders by using microwave heating. Journal of the European Ceramic Society 2012;32:1787-94.

39. Mukasyan A S, Combustion Synthesis of Silicon Carbide in Properties and Applications of Silicon Carbide, Gerhardt R, Editor. 2011: p. 389-410.

40. Narayan J, Raghunathan R, Chowdhury R, Jagannadham K. Mechanism of combustion synthesis of silicon carbide. Journal of Applied Physics 1994;75:7252-7.

41. Yamada O, Miyamoto Y, Koizumi M. Self-propagating high-temperature synthesis of the SiC. Journal of materials research 1986;1:275-9.

42. Zurnachyan A R, Kharatyan S L, Khachatryan H L, Kirakosyan A G. Self-propagating high temperature synthesis of SiC–Cu and SiC–Al cermets: Role of chemical activation. International Journal of Refractory Metals and Hard Materials 2011;29:250-5.

43. Dimitar D. Radev, Uzunov I. Nanosized Silicon Carbide Obtained from Rice Husks. Solid State Phenomena 2010;159:153-6.

44. Niyomwas S. Synthesis and Characterization of Silicon-Silicon Carbide Composites from Rice Husk Ash via Self-Propagating High Temperature Synthesis Journal of Metals, Materials and Minerals 2009;19:21-5.

45. Li B, Zhang C, Hu H, Qi G. Preparation of nanosized silicon carbide powders by chemical vapor deposition at low temperatures. Front. Mater. Sci. China 2007;1:309-11.

46. Adrien Reau, Benoit Guizard, Cyrille Mengeot, Loic Boulanger, Ténégal F. Large Scale Production of Nanoparticles by Laser Pyrolysis. Materials Science Forum 2007;534 - 536:85-8.

47. Martin H-P, Ecke R, Müller E. Synthesis of nanocrystalline silicon carbide powder by carbothermal reduction. Journal of the European Ceramic Society 1998;18:1737-42.

48. Yang G Z, Cui H, Sun Y, Gong L, Chen J, Jiang D, Wang C X. Simple Catalyst-Free Method to the Synthesis of β-SiC Nanowires and Their Field Emission Properties. The Journal of Physical Chemistry C 2009;113:15969-73.

49. Ye J, Zhang S, Lee W E. Novel low temperature synthesis and characterisation of hollow silicon carbide spheres. Microporous and Mesoporous Materials 2012;152:25-30.

50. Xi G, Peng Y, Wan S, Li T, Yu W, Qian Y. Lithium-Assisted Synthesis and Characterization of Crystalline 3C−SiC Nanobelts. The Journal of Physical Chemistry B 2004;108:20102-4.

51. Pan Z, Lai H L, Au F C K, Duan X, Zhou W, Shi W, Wang N, Lee C S, Wong N B, Lee S T, Xie S. Oriented Silicon Carbide Nanowires: Synthesis and Field Emission Properties. Advanced Materials 2000;12:1186-90.

52. Li J, Shirai T, Fuji M. Rapid carbothermal synthesis of nanostructured silicon carbide particles and whiskers from rice husk by microwave heating method. Advanced Powder Technology 2013;24:838-43.

53. Kavecký Š, Janeková B, Madejová J, ŠajgalíK P. Silicon carbide powder synthesis by chemical vapour deposition from silane/acetylene reaction system. Journal of the European Ceramic Society 2000;20:1939-46.

54. Hench L L, West J K. The sol-gel process. Chemical Reviews 1990;90:33-72.

55. Brinker C J. Hydrolysis and condensation of silicates: Effects on structure. Journal of Non-Crystalline Solids 1988;100:31-50.

56. Yajima S, Okamura K, Hayashi J, Omori M. Synthesis of Continuous Sic Fibers with High Tensile Strength. Journal of the American Ceramic Society 1976;59:324-7.

57. Riedel R, Ionescu E, Chen I W, Modern Trends in Advanced Ceramics, in Ceramics Science and Technology, Riedel R, Chen I-W, Editors. 2008, 1: p. 1-38.

58. Riedel R, Gurlo A, Ionescu E. Synthesemethoden für keramische Materialien. Hochtechnologiewerkstoffe. Chemie in unserer Zeit 2010;44:208-27.

59. Ionescu E, Kleebe H J, Riedel R. Silicon-containing polymer-derived ceramic nanocomposites (PDC-NCs): preparative approaches and properties. Chemical Society reviews 2012;41:5032-52.

60. Mera G, Gallei M, Bernard S, Ionescu E. Ceramic Nanocomposites from Tailor-Made Preceramic Polymers. Nanomaterials 2015;5:468.

61. Widgeon S, Mera G, Gao Y, Sen S, Navrotsky A, Riedel R. Effect of Precursor on Speciation and Nanostructure of SiBCN Polymer-Derived Ceramics. Journal of the American Ceramic Society 2013;96:1651-9.

62. Puerta A R, Remsen E E, Bradley M G, Sherwood W, Sneddon L G. Synthesis and Ceramic Conversion Reactions of 9-BBN-Modified Allylhydridopolycarbosilane: A New Single-Source Precursor to Boron-Modified Silicon Carbide. Chemistry of Materials 2003;15:478-85.

63. Wang K, Ma B, Li X, Wang Y, An L. Structural Evolutions in Polymer-Derived Carbon-Rich Amorphous Silicon Carbide. The Journal of Physical Chemistry A 2015;119:552-8.

64. Riedel R, Mera G, Hauser R, Klonczynski A. Silicon-Based Polymer-Derived Ceramics Synthesis Properties and Applications-A Review. Journal of ceramic society Japan 2006;114:425-44.

65. Colombo P, Mera G, Riedel R, Sorarù G D. Polymer-Derived Ceramics: 40 Years of Research and Innovation in Advanced Ceramics. Journal of the American Ceramic Society 2010;93:1805-37.

66. Systems S. StarPCSTM SMP-10. Silicon Carbide Matrix Precursor, Technical Data Sheet by Starfire Systems.

67. Representative list of KDT polymer applications. KiON Defense Technologies Database.

68. Liew L A, Raj Rs. Micro-glow plug and method of making same field of the invention. United States Patent 20030085214 A1. 2003.

69. Ishikawa T, Kohtoku Y, Kumagawa K. Production mechanism of polyzirconocarbo-silane using zirconium(IV)acetylacetonate and its conversion of the polymer into inorganic materials. Journal of Materials Science 1998;33:161-6.

70. Ishikawa T, Shibuya M, Yamamura T. The conversion process from polydimethylsilane to polycarbosilane in the presence of polyborodiphenylsiloxane. Journal of Materials Science 1990;25:2809-14.

71. Yajima S, Hasegawa Y, Okamura K, Matsuzawa T. Development of high tensile strength silicon carbide fibre using an organosilicon polymer precursor. Nature 1978;273:525-7.

72. Yajima S, Hayashi J, Omori M. Continuous Silicon carbide fiber of high tensile strength. Chemistry letter 1975;9:931-4.

73. Yajima S, Hasegawa Y, Hayashi J, Iimura M. Synthesis of continuous silicon carbide fibre with high tensile strength and high Young's modulus. Journal of Materials Science 1978;13:2569-76.

74. Bouillon E, Langlais F, Pailler R, Naslain R, Cruege F, Huong P V, Sarthou J C, Delpuech A, Laffon C, Lagarde P, Monthioux M, Oberlin A. Conversion

mechanisms of a polycarbosilane precursor into an SiC-based ceramic material. Journal of Materials Science 1991;26:1333-45.

75. Zheng C-M, Li X-D, Wang H, Zhu B. Thermal stability and curing kinetics of polycarbosilane fibers. Transactions of Nonferrous Metals Society of China 2006;16:44-8.

76. Moraes K V, Interrante L V. Processing, Fracture Toughness, and Vickers Hardness of Allylhydridopolycarbosilane-Derived Silicon Carbide. Journal of American ceramic society. 2003;86:342-6.

77. Yu Z, Zhan J, Huang M, Li R, Zhou C, He G, Xia H. Preparation of a hyperbranched polycarbosilane precursor to SiC ceramics following an efficient room-temperature cross-linking process. Journal of Materials Science 2010;45:6151-8.

78. Whitmarsh C K, Interrante L V. Synthesis and structure of a highly branched polycarbosilane derived from (chloromethyl)trichlorosilane. Organometallics 1991;10:1336-44.

79. Lee R. Carbosilanes: Reactions & Mechanisms of SMP-10 Pre-Ceramic Polymers Marshall Space Flight Center Jacobs ESTS Group / ICRC 2009;1-23.

80. Interrante L V, Whitmarsh C W, Sherwood W, Wu H-J, Lewis R, Maciel G, High Yield Polycarbosilane Precursors to Stoichiometric SiC. Synthesis, Pyrolysis and Application, in MRS Online Proceedings Library, Sanchez C, Mecartney M L, Brinker C J, Cheetham A, Editors. 1994, 346.

81. Yu Z, Fang Y, Huang M, Li R, Zhan J, Zhou C, He G, Xia H. Preparation of a liquid boron-modified polycarbosilane and its ceramic conversion to dense SiC ceramics. Polymers for Advanced Technologies 2011;22:2409-14.

82. Kaur S, Gallei M, Ionescu E, Polymer–Ceramic Nanohybrid Materials, in Organic-Inorganic Hybrid Nanomaterials, Kalia S, Haldorai Y, Editors. 2015, 267: p. 143-85.

83. Paine R T, Janik J F, Fan M. Some recent developments in precursor routes to ceramic nanocomposites. Polyhedron 1994;13:1225-32.

84. Kockrick E, Krawiec P, Petasch U, Martin H-P, Herrmann M, Kaskel S. Porous CeOX/SiC Nanocomposites Prepared from Reverse Polycarbosilane-Based Microemulsions. Chemistry of Materials 2007;20:77-83.

85. Czekaj C L, Hackney M L J, Hurley W J, Interrante L V, Sigel G A, Schields P J, Slack G A. Preparation of Silicon Carbide/Aluminum Nitride Ceramics Using Organometallic Precursors. Journal of the American Ceramic Society 1990;73:352-7.

86. Aldinger F, Bill J, Kienzle A, Riedel Rs. Production of ceramic materials by the hydroboration of silylcarbodiimides. WO1996006813 A1. 1996.

87. Singh G, Bhandavat Rs. Boron-modified silazanes for synthesis of SiBCN ceramics. United States Patent 20150030856 A1. 2013.

88. Chen Z-Y, Li X-D, Wang J, Li W-F. Preparation of continuous Si-Fe-C-O functional ceramic fibers. Transactions of Nonferrous Metals Society of China 2007;17:987-91.

89. Chen X, Su Z, Zhang L, Tang M, Yu Y, Zhang L, Chen L. Iron Nanoparticle-Containing Silicon Carbide Fibers Prepared by Pyrolysis of Fe(CO)5-Doped Polycarbosilane Fibers. Journal of the American Ceramic Society 2010;93:89-95.

90. Yu Z, Yang L, Min H, Zhang P, Zhou C, Riedel R. Single-source-precursor synthesis of high temperature stable SiC/C/Fe nanocomposites from a processable hyperbranched polyferrocenylcarbosilane with high ceramic yield. Journal of Materials Chemistry C 2014;2:1057-67.

91. Alliegro R A, Coffin L B, Tinklepaugh J R. Pressure-Sintered Silicon Carbide. Journal of the American Ceramic Society 1956;39:386-9.

92. Omori M, Takei H. Pressureless Sintering of SiC. Journal of the American Ceramic Society 1982;65:c92-c9292.

93. Omori M, Takei H. Preparation of pressureless-sintered SiC-Y_2O_3-Al_2O_3. Journal of Materials Science 1988;23:3744-9.

94. Van Dijen F K, Mayer E. Liquid phase sintering of silicon carbide. Journal of the European Ceramic Society 1996;16:413-20.

95. Strecker K, Ribeiro S, Camargo D, Silva R, Vieira J, Oliveira F. Liquid phase sintering of silicon carbide with AlN/Y_2O_3, Al_2O_3/Y_2O_3 and SiO_2/Y_2O_3 additions. Materials Research 1999;2:249-54.

96. Izhevskyi V A, Bressiani A H A, Bressiani J C. Effect of Liquid Phase Sintering on Microstructure and Mechanical Properties of Yb_2O_3-AlN Containing SiC-Based Ceramics. Journal of the American Ceramic Society 2005;88:1115-21.

97. Prochazka S, Dondalski W Js. Hot pressed silicon carbide. United states Patent 3,853,566. 1974.

98. Passing G, Riedel R, Petzow G. Influence of Pyridine-Borane on the Sintering Behavior and Properties of alpha-Silicon Carbide. Journal of the American Ceramic Society 1991;74:642-5.

99. Prochazka S, Sintering of Silicon Carbide, in Mass Transport Phenomena in Ceramics, Cooper A R, Heuer A H, Editors. 1975, 9: p. 421-31.

100. Wroblewska G H, Nold E, Thummler F. The Role of Boron and Carbon Additions on the Microstructural Development of Pressureless Sintered Silicon-Carbide. Ceramics International 1990;16:201-9.

101. Nadeau J S. Very High Pressure Hot Pressing of Silicon Carbide. Am Ceram Soc Bull 1973;52:170-4.

102. Lee D-H, Kim H-E, Cho S-J. Microstructure and Fracture Toughness of Hot-Pressed Silicon Carbide Reinforced with Silicon Carbide Whiskers. Journal of American ceramic society. 1994;77:3270-2.

103. Omori M, Takei H. Pressureless Sintering of Sic. Communications of the American Ceramic Society 1982;C-92.

104. Omori M, Takei H. Preparation of pressureless-sintered SiC-Y_20_3-AI_20_3. Journal of Materials Science 1988;23:3744-9.

105. Gao Y. Nanodomain Structure and Energetics of Carbon Rich SiCN and SiBCN Polymer-Derived Ceramics. Thesis 2013.

106. Harshe R, Balan C, Riedel R. Amorphous Si(Al)OC ceramic from polysiloxanes: bulk ceramic processing, crystallization behavior and applications. Journal of the European Ceramic Society 2004;24:3471-82.

107. Konetschny C, Galusek D, Reschke S, Fasel C, Riedel R. Dense silicon carbonitride ceramics by pyrolysis of cross-linked and warm pressed polysilazane powders. Journal of the European Ceramic Society 1999;19:2789-96.

108. Koumoto K, Shimohigoshi M, Takeda S, Yanagida H. Thermoelectric energy conversion by porous SiC ceramics. Journal of Materials Science Letters 1987;6:1453-5.

109. Vogt U F, Györfy L, Herzog A, Graule T, Plesch G. Macroporous silicon carbide foams for porous burner applications and catalyst supports. Journal of Physics and Chemistry of Solids 2007;68:1234-8.

110. Wood S, Harris A T. Porous burners for lean-burn applications. Progress in Energy and Combustion Science 2008;34:667-84.

111. Ortona A, Pusterla S, Fino P, Mach F R A, Delgado A, Biamino S. Aging of reticulated Si-SiC foams in porous burners. Advances in Applied Ceramics 2010;109:246-51.

112. Adler J. Ceramic Diesel Particulate Filters. International Journal of Applied Ceramic Technology 2005;2:429-39.

113. Pyzik A J, Li C G. New Design of a Ceramic Filter for Diesel Emission Control Applications. International Journal of Applied Ceramic Technology 2005;2:440-51.

114. Keller N, Pham-Huu C, Roy S, Ledoux M J, Estournes C, Guille J. Influence of the preparation conditions on the synthesis of high surface area SiC for use as a heterogeneous catalyst support. Journal of Materials Science 1999;34:3189-202.

115. Zampieri A, Sieber H, Selvam T, Mabande G T P, Schwieger W, Scheffler F, Scheffler M, Greil P. Biomorphic Cellular SiSiC/Zeolite Ceramic Composites: From Rattan Palm to Bioinspired Structured Monoliths for Catalysis and Sorption. Advanced Materials 2005;17:344-9.

116. Lu A-H, Schmidt W, Kiefer W, Schüth F. High surface area mesoporous SiC synthesized via nanocasting and carbothermal reduction process. Journal of Materials Science 2005;40:5091-3.

117. Krawiec P, Kaskel S. Thermal stability of high surface area silicon carbide materials. Journal of Solid State Chemistry 2006;179:2281-9.

118. Suwanmethanond V, Goo E, Liu P K T, Johnston G, Sahimi M, Tsotsis T T. Porous Silicon Carbide Sintered Substrates for High-Temperature Membranes. Industrial & Engineering Chemistry Research 2000;39:3264-71.

119. Suda H, Yamauchi H, Uchimaru Y, Fujiwara I, Haraya K. Preparation and gas permeation properties of silicon carbide-based inorganic membranes for hydrogen separation. Desalination 2006;193:252-5.

120. Fukushima M, Zhou Y, Miyazaki H, Yoshizawa Y-I, Hirao K, Iwamoto Y, Yamazaki S, Nagano T. Microstructural Characterization of Porous Silicon Carbide Membrane Support With and Without Alumina Additive. Journal of the American Ceramic Society 2006;89:1523-9.

121. Konstantinov A O, Harris C I, Henry A, Janzén E. Fabrication and properties of high-resistivity porous silicon carbide for SiC power device passivation. Materials Science and Engineering: B 1995;29:114-7.

122. M. Dröschel, Michael J. Hoffmann, Rainer Oberacker, H.V. Both W S, Yu Ying Yang, Munz D. SiC-Ceramics with Tailored Porosity Gradients for Combustion Chambers. Key Engineering Materials 1999;175-175:149-62.

123. Wilkes T E, Young M L, Sepulveda R E, Dunand D C, Faber K T. Composites by aluminum infiltration of porous silicon carbide derived from wood precursors. Scripta Materialia 2006;55:1083-6.

124. Eom J-H, Kim Y-W, Raju S. Processing and properties of macroporous silicon carbide ceramics: A review. Journal of Asian Ceramic Societies 2013;1:220-42.

125. Lin P K, Tsai D S. Preparation and analysis of a silicon carbide composite membrane. Journal of the American Ceramic Society 1997;80:365-72.

126. Ohji T, Fukushima M. Macro-porous ceramics: processing and properties. Int Mater Rev 2012;57:115-31.

127. F. Sánchez Rojas C B O, J. M. Cano Pavón. Microwave Assisted Acid Digestion of Biomorphic Ceramic Obtained from Beech Wood Infiltrated with Nickel Oxide: Factorial Design. American Journal of Chemistry 2012;2:83-8.

128. Greil P, Lifka T, Kaindl A. Biomorphic Cellular Silicon Carbide Ceramics from Wood: I. Processing and Microstructure. Journal of the European Ceramic Society 1998;18:1961-73.

129. Qian J, Wang J, Jin Z. Preparation of biomorphic SiC ceramic by carbothermal reduction of oak wood charcoal. Materials Science and Engineering: A 2004;371:229-35.

130. Jinhong L I, Hongwen M A, Zhenqing C H I. Preparation of Biomorphic SiC/C Ceramics from Pine Wood via Supercritical Ethanol Infiltration. Acta Geologica Sinica - English Edition 2007;81:674-9.

131. Ota T, Takahashi M, Hibi T, Ozawa M, Suzuki S, Hikichi Y, Suzuki H. Biomimetic Process for Producing SiC “Wood”. Journal of the American Ceramic Society 1995;78:3409-11.

132. Maity A, Kalita D, Kayal N, Goswami T, Chakrabarti O, Rao P G. Synthesis of biomorphic SiC ceramics from coir fibreboard preform. Ceramics International 2012;38:6873-81.

133. Streitwieser D A, Popovska N, Gerhard H, Emig G. Application of the chemical vapor infiltration and reaction (CVI-R) technique for the preparation of highly porous biomorphic SiC ceramics derived from paper. Journal of the European Ceramic Society 2005;25:817-28.

134. Hammel E C, Ighodaro O L R, Okoli O I. Processing and properties of advanced porous ceramics: An application based review. Ceramics International 2014;40:15351-70.

135. Studart A R, Gonzenbach U T, Tervoort E, Gauckler L J. Processing Routes to Macroporous Ceramics: A Review. Journal of the American Ceramic Society 2006;89:1771-89.

136. Yoon T-H, Hong L-Y, Kim D-P, Fabrication of SiC-based Ceramic Microstructures from Preceramic Polymers with Sacrificial Templates and Softlithography Techniques, in Lithography, Wang M, Editor. 2010.

137. Ding S, Zhu S, Zeng Y, Jiang D. Effect of Y_2O_3 addition on the properties of reaction-bonded porous SiC ceramics. Ceramics International 2006;32:461-6.

138. Demirbas A. Potential applications of renewable energy sources, biomass combustion problems in boiler power systems and combustion related environmental issues. Progress in Energy and Combustion Science 2005;31:171-92.

139. W. Luther S H. Application of nanotechnologies in the energy sector. Aktionlinie hessen nanotech of the hessian ministry of economy, transport, urban and regional development 9.

140. Bragg-Sitton S, Barrett K, Rooyen I V, Hurley D, Khafizov M. Studying silicon carbide for nuclear fuel cladding. News Letter in Nuclear Engineering International 2013.

141. New Nuclear Fuel-rod Cladding Could Lead to Safer Power Plants Released by Massachusetts Institute of Technology. 2013;in Science Newsline Physics and Chemistry.

142. Vladimir D. Krstić M D V, R.A. Verrall. Silicon Carbide Ceramics for Nuclear Application. Key Engineering Materials 122-124:387-98.

143. Katoh Y, Snead L L, Henager Jr C H, Hasegawa A, Kohyama A, Riccardi B, Hegeman H. Current status and critical issues for development of SiC composites for fusion applications. Journal of Nuclear Materials 2007;367–370, Part A:659-71.

144. Hudson L K, Misra C, Perrotta A J, Wefers K, Williams F S, Aluminum Oxide, in Ullmann's Encyclopedia of Industrial Chemistry. 2000.

145. Sun W-Z, Jin G-Q, Guo X-Y. Partial oxidation of methane to syngas over Ni/SiC catalysts. Catalysis Communications 2005;6:135-9.

146. Akande A J, Idem R O, Dalai A K. Synthesis, characterization and performance evaluation of Ni/Al2O3 catalysts for reforming of crude ethanol for hydrogen production. Applied Catalysis A: General 2005;287:159-75.

147. Moene R, Makkee M, Moulijn J A. High surface area silicon carbide as catalyst support characterization and stability. Applied Catalysis A: General 1998;167:321-30.

148. Riis T, Hagen E F, Preben J. S. Vie, Ulleberg Ø. Hydrogen production and storage. published by International Energy Agency 2006;1-38.

149. Cheddie D, Ammonia as a Hydrogen Source for Fuel Cells: A Review, in Hydrogen Energy - Challenges and Perspectives, Minic D, Editor. 2012: p. 333-62.

150. Schuth F, Palkovits R, Schlogl R, Su D S. Ammonia as a possible element in an energy infrastructure: catalysts for ammonia decomposition. Energy & Environmental Science 2012;5:6278-89.

151. Yin S-F, Xu B-Q, Ng C-F, Au C-T. Nano Ru/CNTs: a highly active and stable catalyst for the generation of COx-free hydrogen in ammonia decomposition. Applied Catalysis B: Environmental 2004;48:237-41.

152. Neylon M K, Choi S, Kwon H, Curry K E, Thompson L T. Catalytic properties of early transition metal nitrides and carbides: n-butane hydrogenolysis, dehydrogenation and isomerization. Applied Catalysis A: General 1999;183:253-63.

153. Kwon H, Thompson L T, Eng Jr J, Chen J G. n-Butane Dehydrogenation over Vanadium Carbides: Correlating Catalytic and Electronic Properties. Journal of Catalysis 2000;190:60-8.

154. Choi J-G, Ha J, Hong J-W. Synthesis and catalytic properties of vanadium interstitial compounds. Applied Catalysis A: General 1998;168:47-56.

155. RodríGuez P, Brito J N L, Albornoz A, Labadí M, Pfaff C, Marrero S, Moronta D N, Betancourt P. Comparison of vanadium carbide and nitride catalysts for hydrotreating. Catalysis Communications 2004;5:79-82.

156. Gonzalez-Campo A, Nunez R, Vinas C, Boury B. Synthetic approaches to the preparation of hybrid network materials incorporating carborane clusters. New Journal of Chemistry 2006;30:546-53.

157. Zunjarrao S C, Rahman A, Singh R P, Reidel R. Characterization of the Evolution and Properties of Silicon Carbide Derived From a Preceramic Polymer Precursor. Journal of the American Ceramic Society 2013;96:1869-76.

158. Laine R M, Babonneau F. Preceramic Polymer Routes to Silicon Carbide. Chem. Mater. 1993;5:260-79.

159. Gao Y, Mera G, Nguyen H, Morita K, Kleebe H-J, Riedel R. Processing route dramatically influencing the nanostructure of carbon-rich SiCN and SiBCN polymer-derived ceramics. Part I: Low temperature thermal transformation. Journal of the European Ceramic Society 2012;32:1857-66.

160. Interrante L V, Whitmarsh C W, Sherwood W, Fabrication of Sic Matrix Composites by Liquid Phase Infiltration with a Polymeric Precursor, in MRS Online Proceedings Library, Chawla K K, DiPietro S G, Ferber M K, Hellmann J R, Lowden R A, Editors. 1994, 365.

161. Zheng J, Kramer M J, Akinc M. In-situ Growth of SiC Whisker in Pyrolyzed Monolithic Mixture of AHPCS and SiC. Journal of American ceramic society. 2000;83:2961-6.

162. Soraru G D, Babonneau F, Mackenzie J D. Structural evolutions from polycarbosilane to SiC ceramic. Journal of Materials Science 1990;25:3886-93.

163. Tu W-C, Lange F F. Liquid Precursor Infiltration Processing of Powder Compacts: II, Fracture Toughness and Strength. Journal of the American Ceramic Society 2005;78:3283–9.

164. Namazu T, Hasegawa Y. Influence of polymer infiltration and pyrolysis process on mechanical strength of polycarbosilane-derived silicon carbide ceramics. Journal of Materials Science 2010;46:3046-51.

165. Yu Z, Huang M, Fang Y, Li R, Zhan J, Zeng B, He G, Xia H, Zhang L. Modification of a liquid polycarbosilane with 9-BBN as a high-ceramic-yield precursor for SiC. Reactive and Functional Polymers 2010;70:334-9.

166. Sreeja R, Swaminathan B, Painuly A, Sebastian T V, Packirisamy S. Allylhydridopolycarbosilane (AHPCS) as matrix resin for C/SiC ceramic matrix composites. Materials Science and Engineering: B 2010;168:204-7.

167. Greskovich C, Rosolowski J H. Sintering of Covalent Solids. Journal of the American Ceramic Society 1976;59:336-43.

168. Swann G E A, Patwardhan S V. Application of Fourier Transform Infrared Spectroscopy (FTIR) for assessing biogenic silica sample purity in geochemical analyses and palaeoenvironmental research. Clim. Past 2011;7:65-74.

169. Rodil S E, Ferrari A C, Robertson J, Muhl S. Infrared spectra of carbon nitride films. Thin Solid Films 2002;420:122-31.

170. Werheit H, Au T, Schmechel R, Shalamberidze S O, Kalandadze G I, Eristavi A M. IR-Active Phonons and Structure Elements of Isotope-Enriched Boron Carbide. Journal of Solid State Chemistry 2000;154:79-86.

171. Gross T, Ramm M, Sonntag H, Unger W, Weijers H M, Adem E H. An Xps Analysis of Different Sio2 Modifications Employing a C 1s as Well as an Au 4f7/2 Static Charge Reference. Surf Interface Anal 1992;18:59-64.

172. Jackson S T, Nuzzo R G. Determining hybridization differences for amorphous carbon from the XPS C 1s envelope. Applied Surface Science 1995;90:195-203.

173. Shirasaki T, Derré A, Ménétrier M, Tressaud A, Flandrois S. Synthesis and characterization of boron-substituted carbons. Carbon 2000;38:1461-7.

174. Fang Y, Huang M, Yu Z, Xia H, Chen L, Zhang Y, Zhang L. Synthesis, Characterization, and Pyrolytic Conversion of a Novel Liquid Polycarbosilane. Journal of the American Ceramic Society 2008;91:3298-302.

175. Zhang H, Ding W, He K, Li M. Synthesis and Characterization of Crystalline Silicon Carbide Nanoribbons. Nanoscale research letters 2010;5:1264-71.

176. Li Z, Zhou W, Su X, Luo F, Huang Y, Wang C. Effect of boron doping on microwave dielectric properties of SiC powder synthesized by combustion synthesis. Journal of Alloys and Compounds 2011;509:973-6.

177. M. Gadzira G G, O. Mykhaylyk, O. Andreyev. Synthesis and structural peculiarities of nonstoichiometric β-SiC. Diamond and Related Materials 1998;7: 1466–70.

178. Li Y, Yin J, Wu H, Lu P, Yan Y, Liu X, Huang Z, Jiang D. High thermal conductivity in pressureless densified SiC ceramics with ultra-low contents of additives derived from novel boron–carbon sources. Journal of the European Ceramic Society 2014;34:2591-5.

179. Murty H N, Biederman D L, Heintz E A. Apparent Catalysis of Graphitization .3. Effect of Boron. Fuel 1977;56:305-12.

180. Burgess J S, Acharya C K, Lizarazo J, Yancey N, Flowers B, Kwon G, Klein T, Weaver M, Lane A M, Heath Turner C, Street S. Boron-doped carbon powders formed at 1000°C and one atmosphere. Carbon 2008;46:1711-7.

181. Hamada T, Suzuki K, Kohno T, Sugiura T. Structure of coke powder heat-treated with boron. Carbon 2002;40:1203-10.

182. Hennig G. Diffusion of Boron in Graphite. The Journal of Chemical Physics 1965;42:1167-72.

183. Hagio T, Nakamizo M, Kobayashi K. Studies on X-ray diffraction and Raman spectra of B-doped natural graphite. Carbon 1989;27:259-63.

184. Oya A, Yamashita R, Otani S. Catalytic Graphitization of Carbons by Borons. Fuel 1979;58:495-500.

185. Turnbull J A, Stagg M S, Eeles W T. Annealing studies of boron-doped graphite by Electron Microscopy and X-ray Diffraction. Carbon 1966;3:387-92.

186. Way B M, Dahn J R, Tiedje T, Myrtle K, Kasrai M. Preparation and Characterization of Bxc1-X Thin-Films with the Graphite Structure. Phys Rev B 1992;46:1697-702.

187. Hishiyama Y, Inagaki M. Lattice parameter changes in graphite with boron doping. Carbon 2001;39:150-2.

188. Hach C T, Jones L E, Crossland C, Thrower P A. An investigation of vapor deposited boron rich carbon - a novel graphite-like material - part I: the structure of BCx (C6B) thin films. Carbon 1999;37:221-30.

189. Lowell C E. Solid Solution of Boron in Graphite. Journal of the American Ceramic Society 1967;50:142-4.

190. Kouvetakis J, Kaner R B, Sattler M L, Bartlett N. A Novel Graphite-Like Material of Composition Bc3, and Nitrogen-Carbon Graphites. J Chem Soc Chem Comm 1986;1758-9.

191. Aselage T L, Tissot R G. Lattice-Constants of Boron Carbides. Journal of the American Ceramic Society 1992;75:2207-12.

192. Bouchacourt M, Thevenot F. The Properties and Structure of the Boron-Carbide Phase. J Less-Common Met 1981;82:227-35.

193. Matkovich V I. Extension of the boron-carbon homogeneity range. Journal of the Less Common Metals 1976;47:39-42.

194. Modena S, Soraru G D, Blum Y, Raj R. Passive oxidation of an effluent system: The case of polymer-derived SiCO. Journal of the American Ceramic Society 2005;88:339-45.

195. Wieligor M, Wang Y, Zerda T W. Raman spectra of silicon carbide small particles and nanowires. Journal of Physics: Condensed Matter 2005;17:2387-95.

196. Wang C, Huang F, Jiang Y, Zhou Y, Du L, Mera G. A novel oxidation resistant SiC/B_4C/C nanocomposite derived from a carborane-containing conjugated polycarbosilane. Journal of the American Ceramic Society 2012;95:71-4.

197. Domnich V, Reynaud S, Haber R A, Chhowalla M. Boron Carbide: Structure, Properties, and Stability under Stress. Journal of the American Ceramic Society 2011;94:3605-28.

198. Ferrari A C, Robertson J. Interpretation of Raman spectra of disordered and amorphous carbon. Phys Rev B 2000;61:14095-107.

199. Zickler G A, Smarsly B, Gierlinger N, Peterlik H, Paris O. A reconsideration of the relationship between the crystallite size L-a of carbons determined by X-ray diffraction and Raman spectroscopy. Carbon 2006;44:3239-46.

200. Larouche N, Stansfield B L. Classifying nanostructured carbons using graphitic indices derived from Raman spectra. Carbon 2010;48:620-9.

201. Tuinstra F, Koenig J L. Raman Spectrum of Graphite. The Journal of Chemical Physics 1970;53:1126-30.

202. Lucchese M M, Stavale F, Ferreira E H M, Vilani C, Moutinho M V O, Capaz R B, Achete C A, Jorio A. Quantifying ion-induced defects and Raman relaxation length in graphene. Carbon 2010;48:1592-7.

203. Ferreira E H M, Moutinho M V O, Stavale F, Lucchese M M, Capaz R B, Achete C A, Jorio A. Evolution of the Raman spectra from single-, few-, and many-layer graphene with increasing disorder. Phys Rev B 2010;82.

204. Schwan J, Ulrich S, Batori V, Ehrhardt H, Silva S R P. Raman spectroscopy on amorphous carbon films. J Appl Phys 1996;80:440-7.

205. Ferrari A C, Robertson J. Raman spectroscopy of amorphous, nanostructured, diamond-like carbon, and nanodiamond. Philos T R Soc A 2004;362:2477-512.

206. Mcguire K, Gothard N, Gai P L, Dresselhaus M S, Sumanasekera G, Rao A M. Synthesis and Raman characterization of boron-doped single-walled carbon nanotubes. Carbon 2005;43:219-27.

207. Wang B, Ostrikov K, Van Der Laan T, Shao R, Li L. Structure and photoluminescence of boron-doped carbon nanoflakes grown by hot filament chemical vapour deposition. Journal of Materials Chemistry C 2015;3:1106-12.

208. Coppola J A, Smoak R Hs. Method of producing high density silicon carbide product United States Patent 4080415 A. 1978.

209. Narushima T, Goto T, Maruyama M, Arashi H, Iguchi Y. Oxidation of Boron Carbide-Silicon Carbide Composite at 1073 to 1773 K. Materials Transactions 2003;44:401-6.

210. González-Campo A, Viñas C, Teixidor F, Núñez R, Sillanpää R, Kivekäs R. Modular Construction of Neutral and Anionic Carboranyl-Containing Carbosilane-Based Dendrimers. Macromolecules 2007;40:5644-52.

211. Ferrer-Ugalde A, Juárez-Pérez E J, Teixidor F, Viñas C, Sillanpää R, Pérez-Inestrosa E, Núñez R. Synthesis and Characterization of New Fluorescent Styrene-Containing Carborane Derivatives: The Singular Quenching Role of a Phenyl Substituent. Chemistry – A European Journal 2012;18:544-53.

212. Mirabelli M G L, Sneddon L G. Transition-metal-promoted reactions of boron hydrides. 9. Cp*Ir-catalyzed reactions of polyhedral boranes and acetylenes. Journal of the American Chemical Society 1988;110:449-53.

213. Qiu Z. Recent advances in transition metal-mediated functionalization of o-carboranes. Tetrahedron Letters 2015;56:963-71.

214. Bazarjani M S, Muller M M, Kleebe H-J, Fasel C, Riedel R, Gurlo A. In situ formation of tungsten oxycarbide, tungsten carbide and tungsten nitride nanoparticles in micro- and mesoporous polymer-derived ceramics. Journal of Materials Chemistry A 2014;2:10454-64.

215. Vast N, Sjakste J, Betranhandy E. Boron carbides from first principles. Journal of Physics: Conference Series 2009;176:012002.

216. Morgan D A, Sloan J, Green M L H. Direct imaging of o-carborane molecules within single walled carbon nanotubes. Chemical communications 2002;2442-3.

217. Barbosa G N, Lassali T a F, Oliveira H P. Electrochemical study of vanadia–silica xerogel film. Solid State Ionics 2004;169:15-20.

218. Wildberger M D, Mallat T, Göbel U, Baiker A. Oxidation of butane and butadiene to furan over vanadia–silica mixed oxides. Applied Catalysis A: General 1998;168:69-80.

219. Tureček F, Hanuš V. Mass spectra of ethenol and its deutero analogues. Organic Mass Spectrometry 1984;19:423-7.

220. Rodriguez J A, Liu P, Gomes J, Nakamura K, Viñes F, Sousa C, Illas F. Interaction of oxygen with ZrC(001) and VC(001): Photoemission and first-principles studies. Physical Review B 2005;72:075427.

221. Groenenboom C J, Sawatzky G, De Liefde Meijer H J, Jellinek F. Electron spectroscopy of some cyclopentadienylcycloheptatrienylmetal compounds. Journal of Organometallic Chemistry 1974;76:C4-C6.

222. Choi J-G. The surface properties of vanadium compounds by X-ray photoelectron spectroscopy. Applied Surface Science 1999;148:64-72.

223. Zhao Z, Liu Y, Cao H, Zheng H, Ye J, Gao S, Tu M. A novel method to synthesize vanadium carbide (V_8C_7) nanopowders by thermal processing NH_4VO_3, $C_6H_{12}O_6$ and urea. Journal of Alloys and Compounds 2009;468:58-63.

224. Shimoda K, Park J-S, Hinoki T, Kohyama A. Influence of surface structure of SiC nano-sized powder analyzed by X-ray photoelectron spectroscopy on basic powder characteristics. Applied Surface Science 2007;253:9450-6.

225. Virojanadara C, Johansson L I. Photoemission study of Si-rich 4H-SiC surfaces and initial SiO2/SiC interface formation. Phys Rev B 2005;71.

226. Taylor T N. The Surface-Composition of Silicon-Carbide Powders and Whiskers - an Xps Study. J Mater Res 1989;4:189-203.

227. Prasad R M, Mera G, Morita K, Müller M, Kleebe H-J, Gurlo A, Fasel C, Riedel R. Thermal decomposition of carbon-rich polymer-derived silicon carbonitrides leading to ceramics with high specific surface area and tunable micro- and mesoporosity. Journal of the European Ceramic Society 2012;32:477-84.

228. Estella J, Echeverría J, Laguna M, Garrido J. Effect of supercritical drying conditions in ethanol on the structural and textural properties of silica aerogels. J Porous Mater 2008;15:705-13.

229. Winterer M. Nanocrystalline Ceramics: Synthesis and Structure: Springer Berlin Heidelberg; 2013.

230. Iwaki M. Estimation of the atomic density of amorphous carbon using ion implantation, SIMS and RBS. Surface and Coatings Technology 2002;158–159:377-81.

231. Ionescu E, Terzioglu C, Linck C, Kaspar J, Navrotsky A, Riedel R. Thermodynamic Control of Phase Composition and Crystallization of Metal-Modified Silicon Oxycarbides. Journal of the American Ceramic Society 2013;96:1899-903.

232. Ionescu E, Papendorf B, Kleebe H J, Poli F, Muller K, Riedel R. Polymer-Derived Silicon Oxycarbide/Hafnia Ceramic Nanocomposites. Part I: Phase and Microstructure Evolution During the Ceramization Process. Journal of the American Ceramic Society 2010;93:1774-82.

233. E. Ionescu, C. Terzioglu, C. Linck, J. Kaspar, A. Navrotsky, R. Riedel. Thermodynamic Control of Phase Composition and Crystallization of Metal-Modified Silicon Oxycarbides. J. Am. Ceram. Soc. 2013;96:1899-903.

234. Bauer G, Güther V, Hess H, Otto A, Roidl O, Roller H, Sattelberger S, Vanadium and Vanadium Compounds, in Ullmann's Encyclopedia of Industrial Chemistry. 2000.

235. Atal M, Dhayal V, Nagar M, Bohra R, Rathore K, Saxena N. Synthesis and characterization of glycol-modified vanadium(V) oxoisopropoxide and their oximato derivatives: sol–gel transformations of [VO(OPr i)3], [VO{OCH2CH2OCH2CH2O}{OPr i }] and [VO{OCH2CH2OCH2CH2O}{ON=C(CH3)(C4H3S-2)}] to vanadia. Journal of Sol-Gel Science and Technology 2010;53:67-78.

236. Rajak K K, Mondal S, Rath S P. Synthesis, structure and properties of mononuclear oxovanadium(V) alkoxides incorporating chelated ethane-1,2-diol and propane-1,3-diol. Polyhedron 2000;19:931-6.

237. Li H, Zhang L, Cheng L, Wang Y, Yu Z, Huang M, Tu H, Xia H. Polymer–ceramic conversion of a highly branched liquid polycarbosilane for SiC-based ceramics. Journal of Materials Science 2008;43:2806-11.

238. Jiang F, Anderson O P, Miller S M, Chen J, Mahroof-Tahir M, Crans D C. Stepwise Cluster Assembly Using VO2(acac) as a Precursor: cis-[VO(OCH(CH3)2)(acac)2], [V2O2(μ-OCH3)2(acac)2(OCH3)2], [V3O3{μ,μ-(OCH2)3CCH3}2(acac)2(OC2H5)], and [V4O4(μ-O)2(μ-OCH3)2(μ3-OCH3)2(acac)2(OCH3)2]·2CH3CN1. Inorganic Chemistry 1998;37:5439-51.

239. Greil P, Vogli E, Fey T, Bezold A, Popovska N, Gerhard H, Sieber H. Effect of microstructure on the fracture behavior of biomorphous silicon carbide ceramics. Journal of the European Ceramic Society 2002;22:2697-707.

List of Abbreviations:

Allyl-hydridopolycarbosilane	:	SMP-10
Attenuated-total-reflectance	:	ATR
Allyl-functionalized carboranes	:	AFC
Borane dimethyl sulfide complex	:	BMS
Brunauer, Emmett and Teller	:	BET
Polymer derived ceramics	:	PDCs
Polymer derived ceramic Nano-composites	:	PDC-NCs
Polymer Infiltration pyrolysis	:	PIP
Single-source-precursors	:	SSPs
Thermogravimetric analysis	:	TGA
Vanadyl acetylacetonate	:	VAA
Vanadium oxytriisopropoxide	:	VISO
X-ray photoelectron spectroscopy	:	XPS

CURRICULUM VITAE

PERSONAL INFORMATION

Date/Place of Birth : 2. February 1982/Umaria, Bhopal (India)

Citizenship : Indian

Residence Permit : Europe (Schengen Area)

MAIN RESEARCH FIELDS

Sol-gel synthesis.
Materials chemistry and characterization.
Polymer-derived ceramics/nanocomposites.
Processing of ceramics with tailored porosity.
Geopolymer and Geopolymeric materials.

PROFESSIONAL EXPERIENCES

10/2011 – 12/2015 **PhD in Materials Science**

Technische Universität (TU) Darmstadt - Department of Material Science.

Anticipated degree: **Dr. rer. nat. Material Science**

Title of PhD thesis: Single-Source-Precursor Synthesis of SiC-Based Ceramic Nanocomposites for Energy-Related Applications.

Main focus: Materials for (Ultra)high temperatures, harsh environments and as catalyst for production of Hydrogen.

Supervision: Lab courses: Polymer-derived SiOC and Si_3N_4 ceramic and **Advanced Research Labcourses** for Master and Bachelor students at TU Darmstadt: Synthesis of 1) SiYtC, 2) Ni/βSiC 3) SiLiMnOC and 4) $BaSrAlSiO_4$-based ceramic nanocomposites. Biomorphic preparation of high-surface-area V_8C_7/SiC nanocomposites.

Research Assistant

10/2011 – 12/2013 Cooperation with **Xycarb Ceramic and SGL carbon** industrial partners at TU Darmstadt. Polymer-derived route for preparing dense SiC monoliths (**Xycarb Ceramic**); High-temperature annealing and characterization of SiC-based ceramic fibers (**SGL Group**).

02/2009 – 03/2011 **Project Assistant** in **Advanced materials and processes research institute, Bhopal.** Development of lead free shielding materials for gamma and neutron radiation using conventional and advance ceramic route.

07/2008 – 01/2009 Principal of Educational Academy (Real English Medium School).

07/2005 – 03/2008 Post Graduate Teacher (Science and Chemistry)

ACADEMIC CREDENTIALS

07/2003 – 05/2005 **Master of Science (Chemistry)**
Sarojini Naidu Girls P.G. College, Barkatullah University, Madhya Pradesh, India. **Subjects:** Organic, Inorganic, Physical, Biophysical, Bioinorganic and Bioorganic Environmental, Polymer, Organo-transitional metal, Medical and Analytical chemistry, Application of spectroscopy.
Training program on **Advanced Instrumental Methods** at M.P. council of science and technology.
State level seminar on **Applied aspect of biological sciences.**

07/2000 – 05/2003 **Bachelor of Science (Botany, Zoology and Chemistry)**
Sarojini Naidu Girls P.G. College, Barkatullah University, Madhya Pradesh, India.

07/2006 – 05/2007 **Bachelor of Education**
Chitransh Amulya Dutta College, Barkatullah University, Madhya Pradesh, India.

AWARDS AND ACHIEVEMENTS

2009 First prize during Second Young Researcher's Poster Competition at AMPRI, Bhopal.

2010 First prize in Young Scientist Presentation Competition during Construction Materials Vision 2030 National Conference at CRRI, New Delhi.

2011 Research scholarship granted by the Technical University of Darmstadt, Germany. **Novel hybrid precursors derived advanced "Silicoborocarbonitrides".**

2014 Research scholarship by EU cost project under Short-term scientific missions. **Synthesis of Carborane-based polymeric precursors for ultrahigh-temperature stable SiBC ceramics**

EXTRA CURRICULUM ACTIVITIES

State and National played in Chess (1994-2003)
Second postion in 1994, first in 1999 (state level chess tournaments)
Stood 4th in Inter college chess tournament

State played in Badminton (1996-2003)
Member of TSG Wixhausen, Darmstadt (Badminton)

Darmstadt, 27. Juli 2016

Sarabjeet Kaur

PUBLICATIONS (PEER-REVIEWED JOURNALS)

1. Sarabjeet Kaur, R. Riedel, E. Ionescu, "Pressureless Fabrication of Dense Monolithic SiC Ceramics from a Polycarbosilane" J. Eur. Ceram. Soc., 34(15) (2014) 3571-3578.
2. Sarabjeet Kaur, M. Gallei, E. Ionescu, "Polymer-Ceramic Nanohybrid Materials" in Organic-Inorganic Hybrid Nanomaterials, Editors: Kalia, Susheel, Haldorai, Yuvaraj. Springer Berlin Heidelberg, July 2014.
3. Sarabjeet Kaur, G. Mera, R. Riedel, E. Ionescu, "Effect of Boron Incorporation on the Phase Composition and High-Temperature Behavior of Polymer-Derived Silicon Carbide", 2015, J. Eur. Ceram. Soc, 36(4) (2016) 967–977.
4. Sarabjeet Kaur, G. Cherkashinin, C. Fasel, R. Riedel, H-J. Kleebe, E. Ionescu, Single-Source-Precursor Synthesis of Novel V_8C_7/SiC(O)-based Ceramic Nanocomposites, accepted J. Eur. Ceram. Soc..
5. A. Anshul, S. S. Amritphale, R. Yadav, Sarabjeet Kaur, N. Chandra, A. K. Gupta, "Wide- Range Colossal Magnetoresistance in $La_{0.7}A_{0.3}MnO_3$ (A = Sr, Ag) thin films", Int. J. Appl. Ceram. Technol. 2012, 9, 214-220.
6. A. Anshul, S. S. Amritphale, R. Yadav, Sarabjeet Kaur, R. Hada, "Wide Range Magnetoresistance through grain size variation in Ag doped Lanthanum Manganite", Mater. Res. Innov. 2011, 15, 274-278.
7. A. Anshul, S. S. Amritphale, Sarabjeet Kaur, R. Hada, "Nanomaterials synthesis and effect of granular disorders on electrical behavior of Lanthanum Manganites", J. Mater. Sci. Technol. 2011, 27, 691-695.

CONFERENCE CONTRIBUTIONS

1. Sarabjeet Kaur, R. Nunez, C. Vinas, R. Riedel, E. Ionescu, 2nd European Conference on Smart Inorganic Polymers 2015, "Effect of the single-source precursor on the phase composition of SiBC-based ceramic nanocomposites" (oral presentation).
2. Sarabjeet Kaur, S. P. Munagala, E. Ionescu, Materials science engineering 2014, "Synthesis of metal-modified silicon carbide-based ceramic nanocomposites from single-source precursors" (oral presentation).
3. Sarabjeet Kaur, E. Poix, M. Biesalski, R. Riedel, E. Ionescu, Materials science engineering 2014, "Biomorphic preparation of high-surface-area V8C7/SiC nanocomposites using paper- and wood-based templates" (Poster presentation).

4. Sarabjeet Kaur, E. Poix, M. Biesalski, R. Riedel, E. Ionescu, Junior Euromat 2014, “Template-assisted preparation of high-surface-area V8C7/SiC nanocomposites from single-source precursors” (Oral Poster).
5. Sarabjeet Kaur, Q. Wen, R. Riedel, E. Ionescu, International Conference on High-Performance Ceramics, Single-Source-Precursor 2013, “Synthesis and Processing of Dense Metal-Modified Silicon Carbide Monoliths and Their Behavior in Ultraharsh Environments” (Oral presentation).
6. Sarabjeet Kaur, O. Genschka, H.-J. Kleebe, R. Riedel, E. Ionescu, WiFo Conference of GDCh, Darmstadt 2013, "Single-source-precursor synthesis of novel V8C7/SiC(O)- based ceramic nanocomposites" (Poster presentation).
7. Sarabjeet Kaur, S. S. Amritphale, A. Anshul, J. Khan, R. Hada, N. Chandra, 3rd International Conference on Advanced Materials and Systems – ICAMS 2010, Bucharest 2010, "Synthesis and characterization of aluminium oxide borate whisker powder" (Poster presentation).
8. R. Hada, S. S. Amritphale, J. Khan, Sarabjeet Kaur, N. Chandra, National Conference on Nanomaterials and Nanotechnology, VNIT Nagpur 2010, "Synthesis of TiO2 nanoparticles by simple EG route" (Oral presentation).
9. R. Hada, M. Sharma, S. S. Amritphale, A. Anshul, J. Khan, Sarabjeet Kaur, N. Chandra, National Conference on Recent Trends in Materials and Devices (RTMD) 2010, "Synthesis of TiO2 Nanaparticles by a New Solvent System through Sol-Gel Route" (Poster presentation).
10. J. Khan, S. S. Amritphale, A. Anshul, Sarabjeet Kaur, R. Hada, N. Chandra, Construction Materials Vision 2030, New Delhi 2010, "Development of green cement using Fly ash", (Oral presentation).
11. Sarabjeet Kaur, S. S. Amritphale, J. Khan, R. Hada, N. Chandra, Bhartiya Vigyan Sammelan Conference, Indore 2009, "Development of green cement using industrial waste" (Poster presentation).
12. R. Hada, S. S. Amritphale, J. Khan, Sarabjeet Kaur, N. Chandra, Indo-RussianWorkshop and Conference on Nanotechnology and Laser Induced Plasma 2009 (IRNANO-2009), New Delhi 2009, "Synthesis of BaSO4 nanoparticles through reverse microemulsion route" (Poster presentation).
13. R. Hada, S. S. Amritphale, J. Khan, Sarabjeet Kaur, N. Chandra, Indo-Russian Workshop and Conference on Nanotechnology and Laser Induced Plasma 2009 (IRNANO 2009), New Delhi 2009, "Synthesis of NiO nanoparticles through homogeneous precipitation" (Poster presentation).

Eidesstattliche Erklärung

Hiermit erkläre ich an Eides statt, dass ich die vorliegende Dissertation selbständig und nur mit den angegebenen Hilfsmiteln angefertigt habe. Von mir wurde weder an der Technischen Universität Darmstadt noch einer anderen Hochschule ein Promotionsversuch unternommen.

Darmstadt, den 27. Juli 2016